Investigating the Role of Descending Neurons in Freely flying *Drosophila melanogaster*

Doctoral thesis

to obtain a doctorate (PhD)

from the Faculty of Medicine

of the University of Bonn

Elhanan Buchsbaum, née Ben-Yishay

from Afula, Israel

2025

Written with authorization of

the Faculty of Medicine of the University of Bonn

First reviewer: Dr. Bettina Schnell

Second reviewer: Prof. Dr. Heinz Beck

Day of oral examination: 22.07.2025

From the Max Planck Institute for Neurobiology of Behavior – caesar

Table of Contents

List of Abbreviations

AD	Activation domain
AHN	Ascending histaminergic neurons
AMMC	Antennal mechanosensory and motor centre
AN	Ascending neurons
ATR	All-trans-retinal
CDIN	Contralateral descending interneurons
CNS	Central nervous system
CRG	Cerebral ganglia
DBD	DNA-binding domain
DCMD	Descending contralateral movement detector
DLM	Dorsal longitudinal muscle
DN	Descending neuron
DPE	Days post-eclosion
DVM	Dorsoventral muscles
EM	Electron microscopy
FAFB	Female adult fly brain
FANC	Female adult nerve cord
FLP	Flippase
FRT	Flippase Recognition Target
GF	Giant fiber
GFP	Green fluorescent protein
GNG	Gnathal ganglia
HS	Horizontal system
IDIN	Ipsilateral descending interneurons
IPS	Inferior posterior slope
LAL	Lateral accessory lobe
LC	Lobula columnar
LPLC	Lobula plate-lobula columnar
LPTC	Lobula plate tangential cells
MANC	Male adult nerve cord
MDN	Moonwalker descending neuron

MTD-II	Mediodorsal tract II
N-syb	Neuronal synaptobrevin
NGS	Normal goat serum
PBS	Phosphate-buffered saline
PRW	Prow
ReaChR	Red-activated channelrhodopsin
SAD	Saddle
SEZ	Subesophageal zone
SGU	Saccade generating unit
SLEAP	Social LEAP Estimates Animal Poses
SNARE	SNAP REceptors
SPARC	Sparse Predictive Activity through Recombinase Competition
SPS	Superior posterior slope
TeTxLC	Tetanus toxin light chain
TSDN	Target-selective descending neurons
Tx	Triton X-100
UAS	Upstream Activating Sequence
VAC	Ventral association center
VNC	Ventral nerve cord
VPN	Visual projection neuron
VS	Vertical system
w-CHIN	Wing contralateral haltere interneurons

1. Introduction

Understanding how neural circuits generate complex behaviors remains a fundamental challenge in neuroscience. *Drosophila melanogaster* has emerged as an invaluable model organism for addressing this challenge, offering a unique combination of experimental advantages: a rapid life cycle, genetic tractability, and a relatively simple nervous system of approximately 140,000 neurons compared to the human brain's 86 billion (Bellen, Tong, and Tsuda 2010; Hales et al. 2015). These characteristics, coupled with the fly's sophisticated behavioral repertoire, make *Drosophila* particularly well-suited for investigating the neural basis of behavior.

Among the most striking examples of *Drosophila*'s behavioral capabilities is its extraordinary flight control. During flight, flies alternate between periods of straight flight and rapid turns known as body saccades—a strategy that minimizes motion blur and maintains visual acuity. These saccadic maneuvers showcase remarkable precision, with flies capable of rotating their bodies approximately 90° within just 50 milliseconds, achieving angular velocities exceeding 1000 degrees per second (Muijres et al. 2015). Such maneuvers can occur either spontaneously, driven by internal processes that optimize search patterns, or in response to specific environmental triggers such as potential threats (Maye et al. 2007; Muijres et al. 2014).

The neural basis of these flight maneuvers lies largely in the descending neurons (DNs), which form the critical bridge between the brain and motor circuits in the ventral nerve cord (VNC). These DNs play an essential role in the control of flight maneuvers by transmitting and integrating signals from sensory and decision-making centers in the brain to the locomotor circuits that generate coordinated motor output. Recent connectomic analyses have identified approximately 1,300 DNs that originate from various higher brain centers and project to the VNC (Namiki et al. 2018; Stürner et al. 2024). Of particular significance in flight control are the DNs that project to the tectulum, a region in the dorsal VNC. This anatomical organization is functionally relevant because the tectulum houses motor neurons that innervate the wings and halteres. The spatial proximity between these DNs and flight-related motor neurons suggests a direct synaptic pathway for rapid transmission of steering commands, enabling precise control of flight maneuvers. (Azevedo et al. 2024).

Despite significant advances in mapping DN connectivity and understanding their general role in motor control, crucial questions remain regarding how these neurons coordinate natural flight behaviors, particularly saccadic maneuvers. Previous studies have primarily relied on tethered flight preparations, which, while valuable for detailed neural recording and manipulation, do not fully capture the dynamics of natural flight behavior.

The present thesis aims to bridge this knowledge gap by developing and implementing a novel experimental approach that combines precise manipulation of DN activity with quantitative analysis of natural, unrestrained flight behavior. By constructing a free-flight arena with real-time tracking capabilities and closed-loop optogenetic control, I investigated how specific DNs contribute to the generation and control of flight maneuvers. Particular focus was placed on several DNs implicated in saccade initiation and control, with the goal of determining whether activation of individual DNs is sufficient to elicit complete saccadic responses or if coordinated activity across multiple DNs is required for full behavioral execution.

1.1. Flight Behavior of *Drosophila melanogaster*

The flight behavior of *Drosophila melanogaster* represents a remarkable example of sensorimotor integration, characterized by two distinct flight modes: straight flight segments, and rapid turns known as *saccades*. During straight flight, flies maintain course stability through the optomotor response, a fundamental visual-motor reflex that enables them to adjust their wing movements in response to perceived patterns of large-field visual motion (Borst, Haag, and Reiff 2010). This response helps to stabilize the flight path against external perturbations and to maintain a consistent flight speed relative to the visual environment (Cellini and Mongeau 2020b).

Interspersed within these periods of straight flight are rapid, stereotyped turns called saccades. These maneuvers typically involve sharp changes in heading of approximately 90° executed within 40-60 milliseconds, achieving angular velocities exceeding 1000 degrees per second (Muijres et al. 2015). Saccades serve a dual purpose: they allow flies to quickly reorient toward salient features in their environment while minimizing the duration of motion blur that would otherwise compromise visual acuity during turning (Muijres et al. 2014). This strategy effectively divides flight into discrete segments of stable vision, interrupted by brief periods of rapid reorientation.

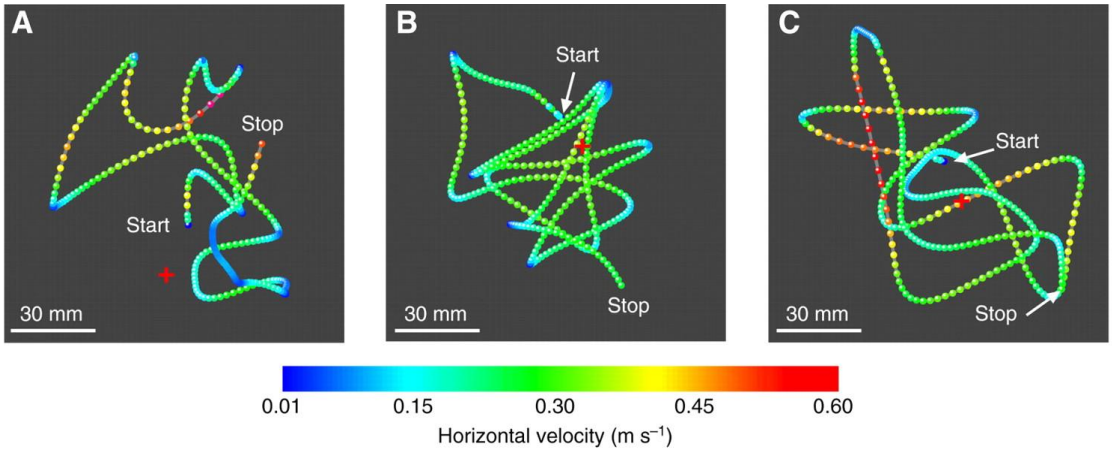

Figure 1. Example of flight trajectories from freely flying flies. Adapted from Mronz and Lehmann (2008).

Saccades can be categorized into two main types based on their initiation mechanism. Spontaneous saccades appear to be driven by internal stochastic processes and optimize the fly's search patterns within its environment (Reynolds and Frye 2007). These turns are highly stereotyped, consisting of banked turns that maintain flight control while minimizing retinal slip (Maye et al. 2007; Mongeau and Frye 2017; Cellini and Mongeau 2020a). In contrast, escape saccades are triggered by specific visual cues, particularly expanding visual patterns that might indicate an approaching obstacle or predator. These defensive maneuvers prioritize rapid heading changes over flight stability, resulting in faster but potentially less controlled turns (Dickinson and Muijres 2016).

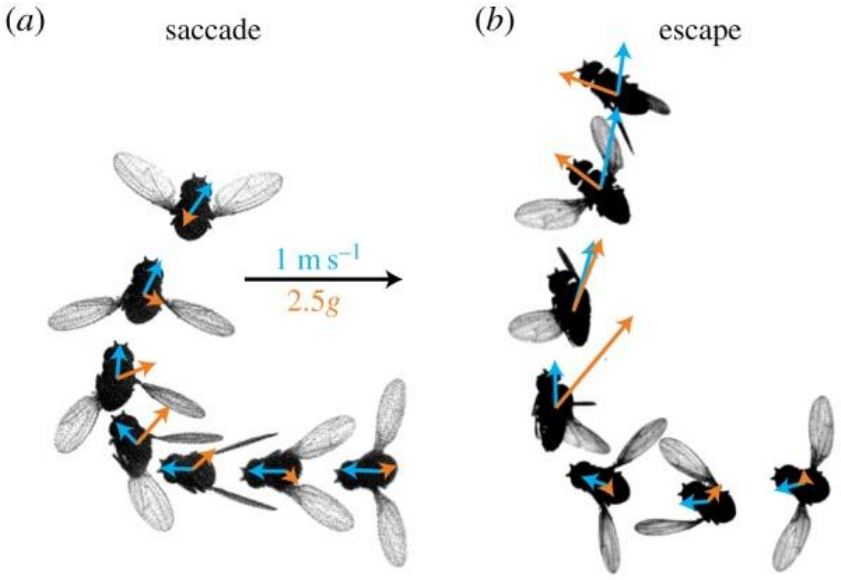

Figure 2. Body saccade and escape maneuvers. Adapted from Dickinson and Muijres (2016).

The precision and stereotypy of these flight behaviors, particularly saccades, make them excellent models for studying sensorimotor integration and motor control. During both straight flight and saccadic maneuvers, flies must continuously integrate multiple sensory modalities, including visual input from the compound eyes and mechanosensory feedback from the wings and halteres. This integration results in precise adjustments of wing kinematics that maintain flight stability while enabling rapid course corrections when necessary. Understanding the neuroanatomical framework that underlies these flight behaviors could be useful in deciphering how sensory information is transformed into the motor commands that drive saccades and other flight-related maneuvers.

1.2. Central Brain

The brain of *Drosophila* exhibits remarkable organizational efficiency within its compact volume, containing approximately 140,000 neurons that form roughly 50 million chemical

synapses (Azevedo et al. 2024). Unlike vertebrate nervous systems, the *Drosophila* brain segregates neuronal cell bodies from synaptic regions, with somata forming an outer cortical rind that surrounds dense synaptic neuropils. Of the 140,000 neurons in the central brain, about 120,000 are intrinsic. The rest can be divided into two groups - afferent (sensory and ascending) neurons, which have their cell bodies outside the brain; and efferent (descending, motor) neurons, whose cell body resides in the central brain but project to the VNC. Most of the non-visual afferent neurons enter the brain via the antennal lobe or the SEZ, which contains the saddle (SAD), gnathal ganglia (GNG), antennal mechanosensory and motor centre (AMMC) and prow (PRW). Visual afferent neurons, on the other hand, enter the brain directly rather than through nerve tracts, projecting from the compound eyes and ocelli (Dorkenwald et al. 2024).

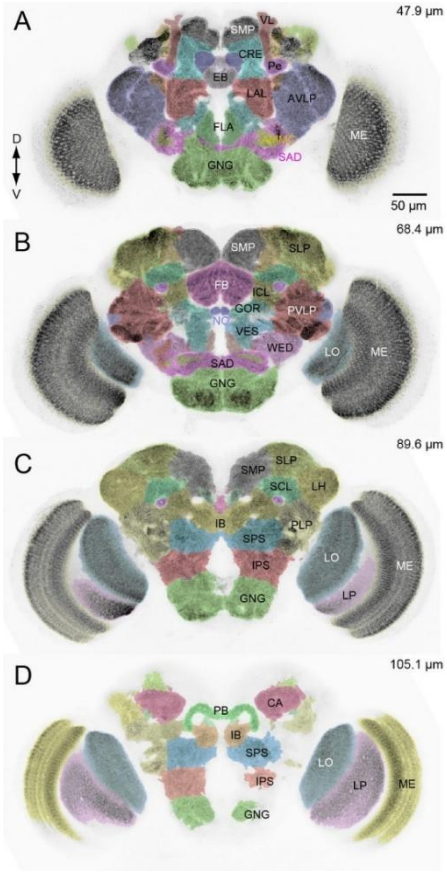

Figure 3. Drosophila central brain neuropils. Adapted from Namiki et al. (2018).

The central brain contains several key processing centers crucial for sensorimotor integration and behavior. The posterior slope serves as a major hub for visual-motor transformation, receiving extensive input from the optic lobes and containing DNs projecting to motor control regions. The LAL functions as a key output region of the navigation system, integrating information from the central complex (Hulse et al. 2021). The gnathal ganglia (GNG) receive diverse sensory inputs including mechanosensory, gustatory, and proprioceptive information (Namiki et al. 2018).

Higher-order processing occurs in specialized regions such as the mushroom bodies, which are essential for associative learning and memory (Li et al. 2020); and the central complex, which comprises the ellipsoid body, fan-shaped body, protocerebral bridge, and noduli, and plays a crucial role in spatial navigation and motor pattern generation (Hulse et al. 2021). The subesophageal zone (SEZ) serves as a major integration center,

processing multiple sensory modalities and housing important motor control circuits (Kendroud et al. 2018).

Within the organized neural architecture of *Drosophila melanogaster*, visual threat detection exemplifies how sensory information is transformed into adaptive motor responses through specialized pathways. The processing of looming stimuli—visual cues signaling approaching predators—showcases the hierarchical organization of sensorimotor circuits in the fly brain, culminating in rapid escape behaviors.

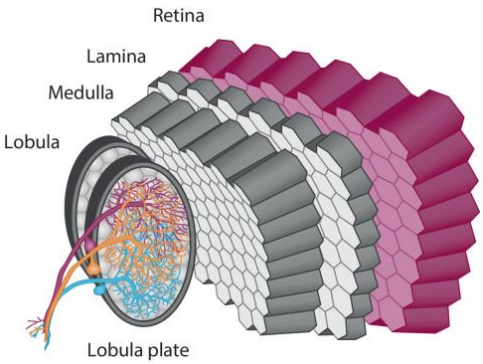

Figure 4. Anatomy of the fly optic lobe. Adapted from Borst and Groschner (2023).

The first stage of visual processing begins with photoreceptors that transduce light into electrical signals. These signals are transmitted to lamina neurons, primarily L1 and L2, which initiate the parallel ON and OFF motion detection pathways, respectively (Joesch et al. 2010; Tuthill et al. 2013). These pathways utilize delay-and-compare computations to extract directional motion information from visual scenes. This early processing converges onto direction-selective T4 and T5 cells in the medulla and lobula. T4 cells process bright edge motion (ON pathway), while T5 cells process dark edge motion (OFF pathway). Each of these cell types comprises four subtypes (T4a-d, T5a-d), each selective for motion in one cardinal direction and projecting to one of four corresponding layers in the lobula plate (Schnell et al. 2012; Maisak et al. 2013). This arrangement creates a retinotopic map of directional motion information essential for downstream processing.

The output from T4/T5 cells provides input to multiple downstream pathways critical for looming detection. One primary pathway involves lobula plate tangential cells (LPTCs), including the horizontal system (HS) and vertical system (VS) cells. These neurons integrate local motion signals across extensive dendritic fields to detect complex motion patterns (Borst and Haag 2002; Schnell et al. 2010). Their response properties functionally resemble the output of correlation-type motion detectors (Reichardt detectors), explaining how non-directional photoreceptor input is transformed into directionally selective signals (Haag, Denk, and Borst 2004).

Parallel to LPTC processing, T4/T5 outputs also feed into specialized looming-detection pathways crucial for escape behavior. Two key neuronal populations have been identified as critical components in this pathway: lobula plate/lobula columnar type 2 (LPLC2) neurons and lobula columnar type 4 (LC4) neurons. LPLC2 neurons possess a unique dendritic architecture that samples from multiple directionally selective T4/T5 cells, conferring selectivity for expanding motion characteristic of approaching objects (Klapoetke et al. 2017). Through systematic silencing experiments and in vivo recordings, LPLC2 neurons have been demonstrated to encode the angular size of looming stimuli (Ache, Polsky, et al. 2019). LC4 neurons, in contrast, primarily encode angular velocity information. These neurons have dendrites spanning multiple retinotopic columns in lobula layers 1, 2, and 4, where they receive input from medulla neurons involved in motion detection (Fischbach and Dittrich 1989; Wu et al. 2016). Functional studies have shown that LC4 silencing specifically reduces giant fiber (GF) responses to high-velocity looming stimuli while preserving responses to slower expansion (Von Reyn et al. 2017). This demonstrates that LC4 functions as a high-pass velocity filter, enhancing detection of rapidly approaching threats when escape speed is most critical for survival.

The giant fiber (GF) neuron serves as the critical integration point for looming information and command neuron for escape behavior. Electron microscopy reconstruction has revealed that the GF receives direct synaptic input from both LPLC2 and LC4 neurons, with these inputs comprising 99.4% of direct visual synapses onto the GF (Ache, Polsky, et al. 2019). The spatial arrangement of these synapses is highly organized, with LPLC2 synapses located more distally on GF dendrites and LC4 synapses more proximally. The complementary nature of these inputs ensures robust looming detection across varying predator approach speeds, with LPLC2 providing consistent size thresholds and LC4 enhancing sensitivity to rapid approaches.

The integration of size and velocity information in the GF determines both the timing and probability of escape takeoffs. A single GF spike is sufficient to trigger a short-mode escape takeoff, characterized by the sacrifice of flight stability for speed (Von Reyn et al. 2014). The precise timing of this spike relative to activation of parallel descending pathways dictates whether a fly will execute a short-mode (GF-mediated) or long-mode (non-GF-mediated) escape.

Genetic manipulation studies have demonstrated the behavioral significance of this dual-feature integration. LPLC2 silencing eliminates nearly all short-duration escapes, indicating its necessity for GF-mediated takeoffs (Ache, Namiki, et al. 2019). LC4 silencing, however, specifically reduces short-mode escapes during fast looming presentations while preserving responses to slower looms. This selective effect highlights LC4's role in enhancing escape probability when rapid evasion is most critical for survival. This sensorimotor pathway also includes inhibitory components that enhance feature selectivity. The GF receives inhibitory input that suppresses responses to large static objects and small expanding objects, ensuring that escape is triggered only by stimuli truly representing approaching threats (Von Reyn et al. 2017; Ache, Polsky, et al. 2019).

The *Drosophila* visual threat detection system exemplifies neural circuit principles found across species: parallel processing of distinct stimulus features, convergence of complementary information, and direct coupling to motor outputs for rapid behavioral responses. The transformation from visual input to motor output involves a progression from local feature detection (direction selectivity in T4/T5), to specialized feature extraction (size in LPLC2, velocity in LC4), to integrative decision-making (in the GF), culminating in adaptive motor programs that enhance survival.

This circuit organization allows the fly to maintain consistent escape timing across varying scenarios while appropriately adapting its escape strategy based on the type of threat. The hierarchical processing from sensory detection to motor command illustrates how the neural circuits controlling saccades can be differentially engaged based on the context, with threat-evoked saccades prioritizing speed over stability compared to their spontaneous counterparts. This demonstrates how neural computations underlying saccadic control can be dynamically optimized for different environmental challenges faced by *Drosophila*.

1.3. Ventral Nerve Cord

The VNC of *Drosophila*, analogous to the vertebrate spinal cord, is organized into distinct neuromeres that process sensory information and coordinate motor behaviors (Court et al. 2020). Located in the ventral thorax, the VNC consists of three thoracic neuromeres and a fused set of abdominal neuromeres. The VNC's architectural organization follows a

clear dorsoventral stratification that reflects its functional specialization. The ventral regions primarily process leg-related sensory and motor information, while the dorsal neuropils are dedicated to wing and flight control (Tuthill and Wilson 2016). This segregation is particularly evident in the thoracic neuromeres, where the leg neuropil contains distinct processing regions, including the ventral association center (VAC) for tactile information and the intermediate neuropil for proprioceptive signals (Mamiya, Gurung, and Tuthill 2018). In contrast to the leg neuropils, the wing neuropil represents a specialized system for flight control. Unlike vertebrate flight appendages, which evolved from modified forelimbs, insect wings arose as novel thoracic appendages (Ross 2017). This distinct evolutionary origin is reflected in the organization of the wing motor system, which consists of only 29 motor neurons controlling both power and steering muscles (Azevedo et al. 2024). The power muscles operate through indirect mechanical coupling with the wings, causing thoracic deformations that drive wing movements, while steering muscles provide fine control through direct attachment to wing sclerites. This unique arrangement allows for remarkable flight maneuverability despite the relatively small number of controlling neurons (Dickinson and Muijres 2016).

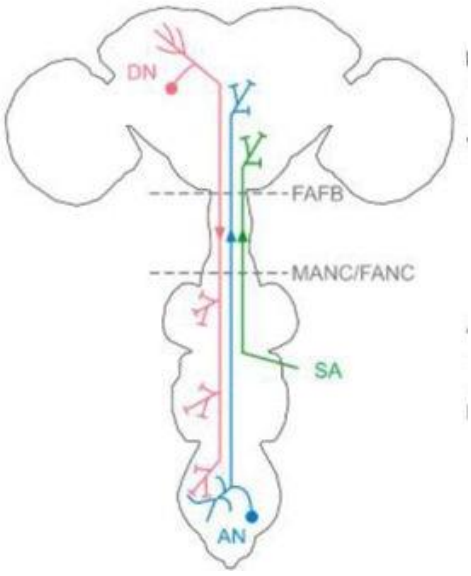

Figure 5. Schematic of the central nervous system with the three neuronal classes that pass through the neck connective. Descending neurons (DNs), ascending neurons (ANs) and sensory ascending neurons (SAs). Adapted from Stürner et al. (2024).

Recent connectomic reconstructions have revealed the intricate organization of pre-motor circuits within the VNC (Azevedo et al. 2024). These studies have highlighted the coordination between leg and wing control systems, particularly during behaviors like takeoff. The integration between these systems occurs in intermediate regions of the neuropil, where interneurons process both leg and wing-related information. This organization allows for precise temporal coordination between leg extension for jumping and wing deployment for flight initiation. For example, the discovery of giant fiber-coupled interneurons that simultaneously activate leg extensor and wing motor neurons

demonstrates how the VNC achieves rapid, coordinated responses during escape behaviors (Von Reyn et al. 2014). These findings highlight how the seemingly simple architecture of the *Drosophila* VNC belies its sophisticated capacity for integrating multiple motor programs into cohesive behavioral outputs. While the VNC provides the motor circuitry for executing flight maneuvers, the control signals that orchestrate these behaviors largely originate from DNs in the brain. Understanding the specific roles of DNs, particularly those involved in generating the rapid saccadic turns characteristic of *Drosophila* flight, is therefore crucial for deciphering the neural basis of this agile behavior.

1.4. Descending Neurons and their roles in behavior

Descending neurons form the crucial link between the *Drosophila* brain and the ventral nerve cord, transmitting signals that ultimately control the fly's motor behaviors, including the intricate flight maneuvers described above. Recent connectomic studies, utilizing comprehensive electron microscopy (EM) datasets such as the female adult fly brain (FAFB), female adult nerve cord (FANC), and male adult nerve cord (MANC), have identified between 1,315 and 1,347 DNs (Stürner et al. 2024). These neurons originate primarily from various regions of the brain, including the superior medial protocerebrum, superior lateral protocerebrum, and the gnathal ganglia (Namiki et al. 2018). DNs are morphologically segregated in the neck connective, occupying more dorsal positions compared to ascending neurons (ANs), and integrate multiple modalities of information before transmitting commands. While only receiving about 2% of their direct input from sensory neurons, DNs show complex patterns of integration through intermediate circuits. Researchers identified 16 distinct clusters of DNs based on their sensory inputs, ranging from those processing specific modalities like gustatory or mechanosensory information to those integrating multiple sensory streams (Stürner et al. 2024). This clustering revealed a spatial segregation, wherein each cluster typically has most of its dendrites in the same brain neuropils.

The connectivity patterns of DNs in the brain reveal surprising complexity. While their principal axonal arbors are in the VNC, DNs make extensive output connections in the brain (413,458 synapses), with 42% of these connections targeting other DNs, and about 45% targeting central brain interneurons. While the extensive connections with central interneurons most likely serve to coordinate DN activity between the two sides of the brain,

the extensive DN-DN interconnectivity suggests coordinated action across these neurons, an idea supported by recent functional studies (Braun et al. 2024). Many of these connections are axo-axonic, raising intriguing questions about their role in gating or modulating DN output (Stürner et al. 2024; Azevedo et al. 2024).

Flight control in *Drosophila* emerges from the coordinated activity of specific DNs originating primarily from several key regions in the central brain: the posterior slope, the gnathal ganglia, and the lateral accessory lobe (Hsu and Bhandawat 2016; Braun et al. 2024). These descending pathways ultimately converge on a sophisticated wing motor system comprising three distinct muscle groups (Dickinson and Tu 1997; Deora, Gundiah, and Sane 2017). The primary flight apparatus consists of thirteen large muscle fibers that generate power through indirect action: six fibers form the dorsal longitudinal muscle (DLM1-6), while seven additional fibers constitute three dorsoventral muscles (DVMs). This arrangement drives wing movements through thoracic resonance and a mechanically sophisticated wing hinge. Complementing these power-generating muscles are twelve steering muscles that directly manipulate wing hinge sclerites, enabling precise flight adjustments, and four tension muscles that modulate thoracic stiffness (Dickinson and Tu 1997).

Many DNs project broadly within the VNC, synapsing onto diverse premotor interneurons and motor neurons in multiple segments. This allows a single DN to potentially influence multiple motor programs and coordinate complex behavioral sequences (Cheong, Boone, et al. 2024). Other DNs show more restricted projection patterns, targeting specific regions of the VNC associated with particular motor outputs, such as leg or wing control. This specificity allows for precise control of individual body parts or movements (Namiki et al. 2018). The axons of many DNs terminate in the dorsal VNC, particularly in the tectulum, a region containing the dendrites of wing and haltere steering motor neurons. This suggests a prominent role for these DNs in flight control (Azevedo et al. 2024; Cheong, Eichler, et al. 2024). To understand how *Drosophila* achieves its remarkable flight agility, it is essential to investigate how DNs contribute to one of the most defining features of *Drosophila* flight: saccades.

1.4.1. Descending Neurons Implicated in Flight Control

Flight control in *Drosophila* emerges from the coordinated activity of specific DNs originating primarily from several key regions in the central brain: the posterior slope, the gnathal ganglia, and the LAL, receiving input from a variety of sources, including other DNs (mainly in the GNG), as well as direct input from the optic glomeruli

The posterior slope serves as a primary visual-motor integration center for flight control, housing DNs that receive organized input through parallel pathways processing specific aspects of visual motion. These DNs predominantly receive direct synaptic connections from lobula plate tangential cells (LPTCs) that encode wide-field optic flow patterns essential for course stabilization during flight (Suver et al. 2016; Dorkenwald et al. 2024). While feature detection circuits involving lobula columnar (LC) and lobula plate-lobula columnar (LPLC) neurons primarily target specialized optic glomeruli rather than the posterior slope. This visual motion processing architecture enables sophisticated flight control, particularly for course corrections and stabilization responses. In addition to processing optic flow, posterior slope DNs integrate information from higher-order motor control centers, particularly the LAL, which functions as an output region of the central complex navigation system (Namiki et al. 2018). These DNs project specifically to the dorsal regions of the VNC, particularly targeting wing and neck motor neuropils in the dorsal tectulum (Cheong, Eichler, et al. 2024).

Complementing this visual-motor pathway, the GNG provides a parallel control channel that integrates diverse sensory inputs including proprioceptive feedback, gustatory information, and mechanosensory signals (Namiki et al. 2018; Dorkenwald et al. 2024). While GNG DNs predominantly project to ventral regions of the VNC associated with leg control, they play crucial roles in coordinating leg and wing movements during complex flight-related behaviors such as takeoff and landing. This organization enables sophisticated coordination between walking and flight behaviors. Recent connectomic analyses have revealed that these DNs form behavior-specific clusters exhibiting mutual inhibition (Braun et al. 2024), providing a mechanism for selecting appropriate motor programs based on current sensory input and behavioral state. This hierarchical organization, from sensory integration through local processing to motor output, enables both rapid reflexive behaviors essential for survival and sophisticated goal-directed flight

maneuvers. Among the many DNs involved in flight control, several have been identified as playing potential roles in saccade generation and execution.

The LAL functions as a pivotal integration hub for DNs that orchestrate complex behavioral outputs in *Drosophila*. Unlike the posterior slope's primarily visual-motor integration role, the LAL serves as a multimodal integration center that processes and combines diverse sensory streams, particularly visual and auditory information, to generate coordinated steering commands (Namiki and Kanzaki 2016; Stürner et al. 2024). Connectomic analyses have revealed that the LAL houses a substantial population of DNs that project via the MTD-II tract to target wing pre-motor circuits in the upper tectulum of the ventral nerve cord, establishing a direct pathway for flight control (Cheong, Boone, et al. 2024). These LAL-originating DNs show extensive interconnectivity with other DNs, forming networks that enable coordinated motor pattern selection (Braun et al. 2024). Notably, the LAL serves as an output region for the central complex navigation system, essentially translating internal compass information and navigational decisions into concrete motor commands (Namiki et al. 2018; Currier and Nagel 2020). This anatomical and functional organization positions the LAL as a critical interface between higher-order decision circuits and the descending motor pathways that implement these decisions, particularly for behaviors requiring sophisticated directional control and navigational responses to complex stimuli (Steinbeck, Adden, and Graham 2020; Yang et al. 2024). Through its dense interconnections with other brain regions and precise targeting of motor circuits, the LAL enables flies to execute contextually appropriate steering maneuvers in response to multisensory environmental cues.

1.4.1.1. DNa15

The DN initially known as DNaX (later renamed to DNa15) was characterized as a cell exhibiting correlation with turning behaviors during flight (Schnell, Ros, and Dickinson 2017). This neuron originates from the posterior slope and shows temporal correlation with increases in left-right wing beat amplitude during turns. DNa15 remains silent in non-flying conditions, confirming its specific role in flight control. Whole-cell patch clamp recordings from DNa15 provide insights into its physiological properties, suggesting it operates through graded potential changes rather than classical action potentials. Changes in DNa15 membrane potential consistently precede behavioral steering

responses by approximately 130 ms, positioning it temporally within flight control circuits (Schnell, Ros, and Dickinson 2017).

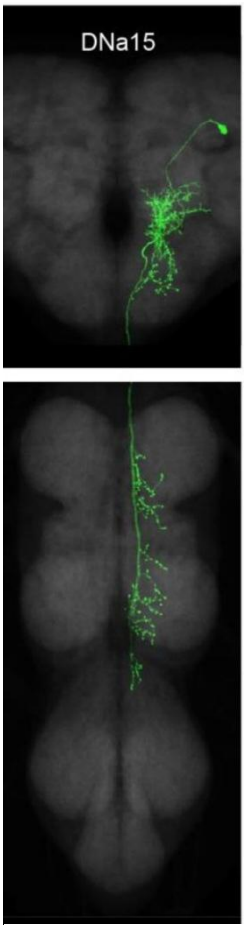

Figure 6. Confocal scan of DNa15 projection in central brain and ventral nerve cord. All following images adapted from Zung et al., 2025.

Regarding its sensory responsiveness, DNa15 shows activity during looming stimuli presented in the contralateral visual field, but importantly, this activity is contingent on the fly executing an evasive turn. When looming stimuli fail to elicit turning responses, DNa15 remains silent, suggesting it functions as a pre-motor rather than a purely sensory neuron. This selective response pattern indicates DNa15 participates in the motor command pathway rather than in primary visual processing. Perhaps more intriguingly, DNa15 shows spontaneous activity that reliably precedes turning maneuvers even in the absence of visual stimulation. The magnitude of these spontaneous bursts correlates with the amplitude of the subsequent turn, suggesting DNa15 may play a direct role in initiating or modulating spontaneous saccades.

To establish a causal link between DNa15 activity and turning behavior, the researchers further employed targeted activation using the ATP-gated P2X2 channel. This manipulation consistently evoked ipsilateral turning responses, demonstrating that activation of DNa15 is sufficient to initiate steering maneuvers. Together, these findings position DNa15 as a key component in the neural circuitry controlling both visually-evoked and spontaneous flight steering in *Drosophila*.

Recent work (Ros, Omoto, and Dickinson 2024) has identified a pair of DNs, DNae014 (which was identified as the same neuron as DNaX/DNa15) and DNb01, that are tightly correlated with saccadic turns in tethered flies. The researchers found that DNa15 activity was very tightly coupled with turning behavior, with nearly every saccade accompanied by a corresponding change in DNa15 activity. This strong correlation between DNa15 activity and turning was observed even in the absence of visual stimuli, further supporting the neuron's role in spontaneous turning behavior.

To test whether DNa15 activity is sufficient to elicit a turn, the researchers used both focal two-photon excitation and the SPARC method to activate DNa15 neurons expressing CsChrimson unilaterally. Both methods yielded similar results: activating the right DNa15 neuron reliably triggered a rightward turn, while activating the left neuron triggered a leftward turn. These results suggest that DNa15 activity alone is sufficient to trigger a saccade (Ros, Omoto, and Dickinson 2024). To assess the necessity of DNa15 activity for saccade generation, the researchers silenced the neuron using both optogenetic silencing and genetic ablation. Optogenetic silencing did reduce the frequency of saccades, but this effect was difficult to interpret due to a simultaneous increase in saccade rate in control flies exposed to the activation light. Genetic ablation of DNa15, however, produced a clearer result, significantly reducing the frequency of saccades compared to control flies. Interestingly, while ablating DNa15 significantly reduced the frequency of saccadic turns, it did not completely abolish them. This suggests that other neural pathways may also contribute to saccade generation.

The DNa15 neuron is part of a network of DNs that control saccades. This network includes another DN, DNb01, whose activity also correlates with saccades. The two neurons appear to form a functional unit, termed "saccade generating unit" (SGU), with one unit for rightward turns and one for leftward turns (Ros, Omoto, and Dickinson 2024). The DNa15 neuron within an SGU makes ipsilateral connections within both the brain and ventral nerve cord, meaning that it connects to neurons on the same side of the body. In contrast, the DNb01 neuron makes contralateral connections to the VNC and has a more complex pattern of connections within the brain. This difference in connectivity, along with other evidence, suggests that the two neurons may drive different elements of the saccade motor program within the VNC.

Additionally, the study found that VES041 neurons - a pair of large inhibitory interneurons - play a crucial role in regulating flight turns, specifically by suppressing spontaneous saccades. Located in the LAL, these neurons achieve this suppression by forming inhibitory connections with the DNa15 and DNb01 neurons. By inhibiting these saccade-generating units, VES041 neurons promote straight flight. This suggests that VES041 neurons are likely involved in regulating transitions between different flight behaviors, such as shifting from local exploration, characterized by frequent turns, to long-distance

dispersal, which necessitates straighter flight paths. VES041 neurons receive input from various brain regions, including those associated with visual and olfactory processing, such as the vest, GNG, LAL, SPS, flange, inferior bridge, and saddle. This diverse input suggests that VES041 neurons integrate information from multiple sensory modalities to modulate turning behavior in response to environmental cues.

1.4.1.2. DNp06

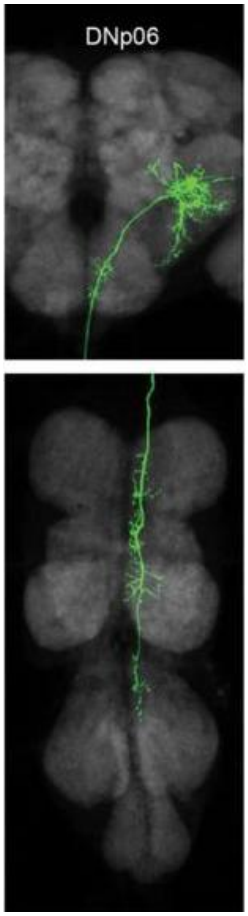

Figure 7. Confocal scan of DNp06 projection in central brain and ventral nerve cord.

Recent work (Kim et al. 2023) has explored the role of DN DNp06 in controlling evasive flight maneuvers in *Drosophila*. Through detailed connectomic analysis, the researchers identified DNp06 as one of three principal DNs receiving direct synaptic input from LPLC2 neurons, a specific type of visual projection neuron (VPN) in the lobula plate. Together with DNp01 and DNp04, these neurons account for approximately 89% of LPLC2's synaptic connections to DNs, establishing a dedicated visuomotor pathway for threat avoidance. This anatomical arrangement suggests that DNp06 plays a key role in transforming visual information about potential threats into rapid motor responses.

Electrophysiological characterization through whole-cell patch clamp recordings demonstrated that DNp06 neurons exhibit sophisticated visual response properties. These neurons show marked sensitivity to both translating spots and looming stimuli, with particularly strong direction selectivity for back-to-front motion. This directional selectivity suggests that DNp06 may be specialized for detecting objects approaching from behind, a crucial capability for avoiding predators or obstacles during flight. A distinctive feature of DNp06 activity is its highly phasic response pattern, especially evident during the presentation of moving bars and laterally translating spots. Notably, these neurons respond robustly to stimuli in the contralateral visual field, suggesting an important role in bilateral visual processing (Kim et al. 2023). The functional significance of DNp06 in flight control was systematically demonstrated through complementary genetic manipulation approaches.

Thermogenetic silencing of the LPLC2 neurons using temperature-sensitive shibire (shi^{ts}) revealed a partial reduction in wing responses to both translating spots and looming discs. In tethered flies, silencing LPLC2 significantly impaired the changes in wingbeat amplitude that normally occur in response to these visual stimuli, indicating that LPLC2 is required for appropriate motor adjustments during visually guided flight. However, the effects of this manipulation were generally small, suggesting that other neurons or pathways may also be involved in these responses. Furthermore, unilateral optogenetic activation of right-hemisphere DNp06 neurons using CsChrimson induced consistent leftward steering responses, demonstrating the sufficiency of DNp06 activation for triggering directional flight responses. The specificity of these effects was confirmed by parallel experiments with DNp04, which showed no significant impact on wing responses under similar manipulations. A particularly intriguing aspect of DNp06 function lies in its transformation of visual information. While inheriting many selectivity properties from its upstream partner LPLC2, DNp06 exhibits more transient activation patterns, suggesting sophisticated processing between these neuronal populations. This temporal transformation may be crucial for converting sustained visual inputs into precisely timed motor commands required for rapid escape maneuvers. The phasic nature of DNp06 responses may help to sharpen the timing of motor output, ensuring that escape maneuvers are executed quickly and efficiently.

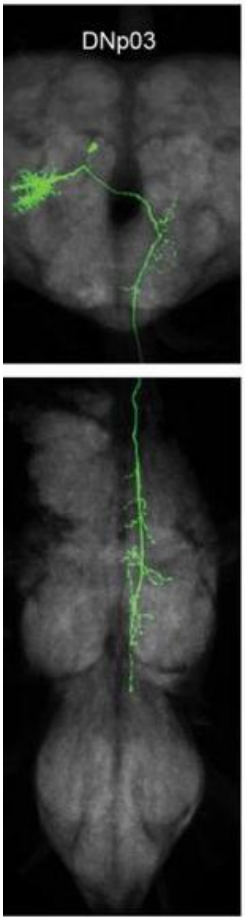

Figure 8. Confocal scan of DNp03 projection in central brain and ventral nerve cord.

1.4.1.3. DNp03

DNp03 represents a key component in *Drosophila*'s visual threat detection system, receiving direct input from looming-sensitive VPNs in the optic glomeruli (Buchsbaum and Schnell 2025). This DN integrates information from multiple VPN types, including LC4, LC22, LPLC1, LPLC2, and LPLC4, suggesting a role in processing complex visual features related to collision avoidance (Dombrovski et al. 2023; Cheong, Boone, et al. 2024). This convergence of multiple VPN inputs suggests that DNp03 may integrate

different aspects of visual information to create a more comprehensive representation of potential threats. DNp03's postsynaptic targets include premotor circuits in both wing and leg control regions of the VNC, suggesting its involvement in coordinating multiple motor systems during escape behaviors. The neuron's complex connectivity pattern and strategic positioning within the descending control system suggest it plays a crucial role in transforming looming-related visual information into appropriate motor outputs.

1.4.1.4. DNg02

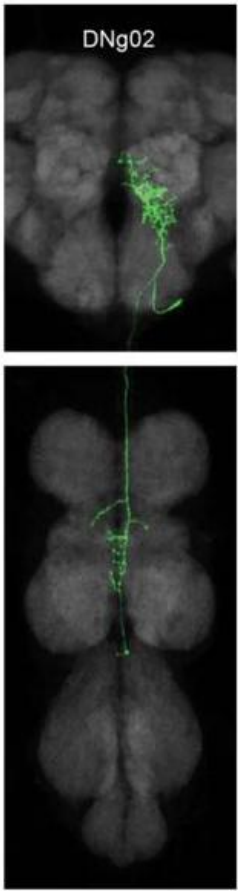

Figure 9. Confocal scan of DNg02 projection in central brain and ventral nerve cord.

The descending neuron class DNg02 is unusual among DNs in that instead of existing as a single bilateral pair, it constitutes a large population of at least 15 pairs of nearly homomorphic cells (Namiki et al. 2022; Palmer, Omoto, and Dickinson 2022). These neurons originate from cell bodies in the gnathal ganglion (GNG) and project to the dorsal regions of the ventral nerve cord associated with the flight motor system. In the brain, they receive inputs primarily from visual processing regions, suggesting their role in visually-guided flight control. Unlike many DNs, the DNg02 population has extensive output terminals in both the wing and haltere neuropils, with projections that cross the midline in the VNC.

Functionally, the DNg02 neurons regulate wing kinematics through a population coding mechanism that provides sensitivity across a large dynamic range. Silencing experiments demonstrate that the magnitude of the optomotor response diminishes proportionally to the number of DNg02 neurons inactivated (Palmer, Omoto, and Dickinson 2022). Conversely, optogenetic activation reveals a robust linear relationship between the number of cells activated and the change in wingbeat amplitude (Namiki et al. 2022). Through two-photon functional imaging, researchers have shown that DNg02 neurons respond strongly to horizontal visual motion during flight, with activity patterns that correlate with contralateral wingbeat amplitude. The neurons can operate both bilaterally and unilaterally depending on visual input – during yaw stimuli, cells on opposite sides of the brain show inverse activity patterns, while during progressive or regressive motion, they exhibit

synchronized activity. This functional organization makes DNg02 neurons particularly well-suited for continuous regulation of flight stability, allowing flies to maintain balanced aerodynamic forces through precise control of wing kinematics. The large number of cells in this population likely provides the high degree of precision required for stable flight, particularly when flies need to compensate for asymmetries in wing condition or changing environmental conditions.

1.5. Genetic Tools for Neural Manipulation

Drosophila melanogaster research has greatly benefited from a powerful suite of genetic tools that enable precise manipulation of gene expression and neuronal activity. These tools have been instrumental in dissecting neural circuits and understanding the genetic underpinnings of behavior.

1.5.1. GAL4-UAS

The cornerstone of *Drosophila* genetics is the GAL4-UAS system, originally adapted from yeast (Brand and Perrimon 1993). This binary expression system relies on the yeast transcription factor GAL4 and its binding site, the Upstream Activating Sequence (UAS). The power of this system lies in its ability to direct gene expression to specific cells or tissues in a spatially and temporally controlled manner. In practice, two separate *Drosophila* lines are created and then crossed to achieve targeted gene expression. One line, known as the "driver" line, expresses the GAL4 protein under the control of a specific promoter or enhancer element. These regulatory elements can be chosen to drive GAL4 expression in a wide variety of patterns, from broad expression in most neurons to highly restricted expression in small subsets of cells. The second line, known as the "responder" or "effector" line, carries a transgene of interest placed downstream of multiple copies of the UAS sequence. This transgene can be anything from a reporter gene like GFP (green fluorescent protein) to a gene encoding a protein that manipulates neuronal activity, such as an ion channel or a toxin. When the driver and responder lines are crossed, their offspring inherit both the GAL4 driver and the UAS-effector construct. In cells where the specific promoter driving GAL4 is active, the GAL4 protein is produced. GAL4 then binds to the UAS sequences in the responder construct, activating the transcription of the downstream transgene. Thus, the transgene is only expressed in cells where the specific promoter driving GAL4 is active, allowing for unprecedented precision in manipulating

gene expression within the complex *Drosophila* nervous system. The combinatorial nature of the system, with numerous driver and responder lines available, allows for a vast number of possible expression patterns to be generated. Furthermore, the system can be adapted for temporal control, for example, by using temperature-sensitive versions of GAL80 or by coupling it with other inducible systems.

1.5.2. Split-GAL4

The split-GAL4 system (Luan et al. 2006; Pfeiffer et al. 2010) represents a further refinement of the GAL4-UAS system, enabling even greater precision in targeting specific cell populations. This system is based on the principle that the GAL4 protein can be divided into two functionally distinct parts: the DNA-binding domain (DBD) and the activation domain (AD). These two domains are expressed separately in transgenic *Drosophila* lines under the control of different promoters or enhancers. Each domain is inactive on its own. However, when both the DBD and AD are present in the same cell, they can interact to reconstitute a functional GAL4 protein. This reconstituted GAL4 can then bind to UAS sequences and drive the expression of a UAS-controlled transgene, similar to the standard GAL4-UAS system.

The key advantage of the split-GAL4 system is its intersectional nature. By carefully selecting the promoters used to drive the DBD and AD, researchers can target transgene expression to cells where both promoters are active. This allows for the targeting of much more specific and restricted cell populations than is possible with a single GAL4 driver. This intersectional strategy has been instrumental in generating driver lines that target highly specific neuronal populations within the *Drosophila* brain, enabling finer dissection of neural circuits (Dionne et al. 2018). The development of large collections of split-GAL4 lines, such as those generated by the FlyLight project at Janelia Research Campus, has significantly advanced the ability of researchers to target and manipulate specific neurons and circuits with unprecedented precision, opening up new avenues for investigating the neural basis of behavior (Namiki et al. 2018). To further refine cell-type targeting or to introduce variability in expression patterns, researchers often turn to techniques based on stochastic expression, such as heat-shock-inducible Flippase (Flp) and the SPARC system.

1.5.3. Stochastic Expression

Further refinement in targeting specific neurons can be achieved by relying on stochastic expression systems. These methods introduce an element of randomness into gene expression, allowing for the labeling or manipulation of a subset of cells within a larger population. This can be particularly useful for studying the heterogeneity of cell types within a seemingly uniform population, or for tracing cell lineages. Two widely used stochastic expression systems in *Drosophila* are the heat-shock-dependent Flippase system and the SPARC system.

1.5.3.1. Heat-shock-dependent Flippase (Flp)

The FLP/FRT system, adapted from yeast, is a powerful tool for achieving both spatial and temporal control over gene expression in *Drosophila* (Golic and Lindquist 1989; Struhl and Basler 1993). This system utilizes the enzyme Flippase (Flp), a site-specific recombinase, and its target DNA sequence, FRT (Flippase Recognition Target). In *Drosophila*, the Flp enzyme is typically placed under the control of a heat-shock promoter, such as hsp70. This means that Flp expression can be induced by exposing flies to a brief period of elevated temperature (e.g., 37° C). The FRT sites are short, specific DNA sequences that are recognized and bound by the Flp enzyme. When two FRT sites are present in the same DNA molecule, Flp can mediate recombination between them. The outcome of this recombination depends on the orientation and location of the FRT sites. If the FRT sites are in the same orientation, the intervening DNA sequence will be excised. If the FRT sites are in opposite orientations, the intervening DNA sequence will be inverted.

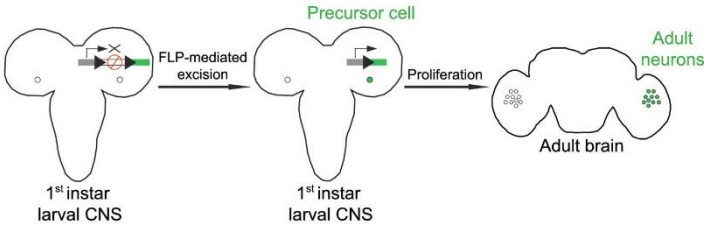

Figure 10. Schematic illustration of a genetic method for stochastic labeling and activation. Adapted from Wu et al., 2016.

To use the Flp-FRT system for stochastic gene expression, researchers create transgenic *Drosophila* lines carrying a gene of interest that is modified to contain FRT sites. Often, a "stop cassette" (a DNA sequence that prevents transcription) is placed between the promoter and the coding sequence of the gene, flanked by FRT sites in the same orientation. In this configuration, the gene of interest is

not expressed because the stop cassette blocks transcription. When these flies are crossed with a line expressing heat shock-inducible Flp, and the offspring are subjected to a heat shock, Flp is transiently expressed in all cells. In a subset of cells, the Flp enzyme will stochastically mediate recombination between the FRT sites, excising the stop cassette and allowing the gene of interest to be expressed. The randomization arises because the recombination event is probabilistic and occurs independently in each cell. The frequency of recombination can be modulated by altering the duration and intensity of the heat shock. This system, also referred to as "Flp-out," allows for the generation of mosaic flies, where a random subset of cells expresses the gene of interest, while neighboring cells do not (Marshall, Wreden, and Heckscher 2024). This is particularly useful for clonal analysis, where the effects of a gene manipulation can be studied in a small group of cells surrounded by a wild-type background. It also allows to achieve a stochastic activation that is, at the same time, sparse enough to identify single neurons, but dense enough to be able to target neurons from small populations.

1.5.3.2. SPARC

The SPARC (Sparse Predictive Activity through Recombinase Competition) is a more recently developed technique for achieving targeted gene expression in predictable proportions of cells (Isaacman-Beck et al. 2020). This method leverages the stochastic nature of the PhiC31 recombinase, an enzyme derived from a bacteriophage, to achieve different levels of gene expression in a predictable manner.

Unlike the Flp-FRT system, which typically relies on a stop cassette that is either present or absent, SPARC utilizes a more nuanced approach based on competing recombination events. In the SPARC system, a genetic construct is created that contains a user-selected effector gene (e.g., a reporter or a gene encoding a protein that modulates neuronal activity) downstream of a stop cassette. This stop cassette is flanked by two different attP recombination sites recognized by PhiC31. One of these attP sites is a canonical (i.e., unmodified) sequence, while

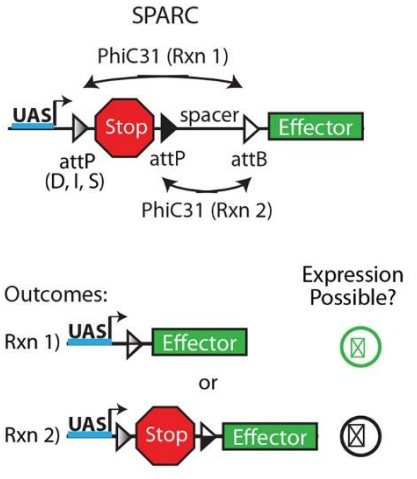

Figure 11. Schematic description of the SPARC method. Adapted from Isaacman-Beck, 2022.

the other is a truncated version. The construct is designed such that PhiC31-mediated recombination between the first attP sequence and a separate attB sequence (present elsewhere in the genome) will excise the stop cassette, enabling effector expression. However, if PhiC31 recombines the second, truncated attP site with the attB site, the stop cassette is retained, and effector expression is prevented. The key to SPARC's predictability lies in the fact that truncated attP sites have a lower recombination efficiency with attB sites compared to the canonical attP site. By changing the length of the truncated attP site, it is possible to control the probability of each recombination event precisely.

Three SPARC variants are available with different attP truncations: D (Dense), I (Intermediate), and S (Sparse). As their names suggest, these variants are expected to produce high, intermediate, and low levels of effector expression, respectively. Importantly, SPARC consistently labeled similar percentages of neurons across a diverse array of cell types. Specifically, the SPARC-D, -I, and -S variants consistently labeled 48-51%, 17-22%, and 3-7% of cells, respectively (Isaacman-Beck et al. 2020). This predictability makes SPARC a powerful tool for generating sparse and consistent labeling of neuronal populations, facilitating the study of individual neurons within a larger circuit.

These stochastic expression techniques are often combined with other genetic tools that allow for precise manipulation of neuronal activity. By expressing proteins that alter neuronal firing rates in a targeted manner, researchers can establish causal links between the activity of specific neurons and circuits and the resulting behavioral output.

1.5.4. Tools for Inhibition of Neurons

One approach for inhibiting neuronal activity involves the overexpression of specific ion channels that can suppress neuronal firing. A widely used tool for this purpose is the inward-rectifying potassium channel Kir2.1, derived from mammals (Hodge 2009). Kir2.1 is a member of a large family of potassium channels that are more permeable to potassium ions flowing into the cell rather than out of it. Over-expression of Kir2.1, which is open at the resting membrane potential, results in increased potassium efflux and membrane hyperpolarization, thus setting the resting membrane potential below the threshold required to fire action potentials. By hyperpolarizing the membrane, Kir2.1 reduces the probability of action potential firing (Baines et al. 2001).

The effectiveness of Kir2.1 in silencing neurons depends on several factors, including the level of expression, where higher densities of Kir2.1 lead to a greater increase in the stimulus threshold required to fire an action potential (Johns et al. 1999). Furthermore, neuronal networks have a tendency to compensate for imposed silencing or hyperexcitability. In mammalian neurons, a homeostatic mechanism can return the firing rate to normal even with continued Kir2.1 expression. However, some studies in *Drosophila* suggest fewer compensatory mechanisms compared to mammalian systems (Hodge 2009). Finally, the specific type of neuron in which Kir2.1 is expressed can also affect the outcome.

Another powerful method for inhibiting neuronal activity relies on the expression of neurotoxins, such as tetanus toxin light chain (TeTxLC) (Sweeney et al. 1995). TeTxLC is a protease derived from the bacterium Clostridium tetani, the causative agent of tetanus. This toxin acts presynaptically to inhibit neurotransmitter release. It achieves this by specifically cleaving neuronal synaptobrevin, also known as N-syb, a key component of the SNARE complex that is essential for synaptic vesicle fusion and neurotransmitter release. When TeTxLC is expressed in a neuron, it cleaves synaptobrevin, preventing the formation of functional SNARE complexes and thus blocking the release of neurotransmitters at the synapse. This effectively silences the neuron's ability to communicate with its downstream targets through chemical synapses. Unlike Kir2.1, which hyperpolarizes the neuron, TeTxLC leaves the neuron's electrical activity largely unaffected but blocks its chemical output. One advantage of TeTxLC is its high specificity for neuronal synapses. The light chain of tetanus toxin is only active when inside the neuron, preventing unintended effects on neighboring cells. It is important to consider that TeTxLC may not be equally effective at blocking the release of all types of neurotransmitters, and that it is chemical-synapse specific, which means it does not inhibit electrical synapses (Martin, Keller, and Sweeney 2002).

Both Kir2.1 and TeTxLC are typically expressed using the GAL4-UAS system, allowing researchers to target their expression to specific neuronal populations. This targeted silencing of neurons enables the investigation of their role in specific behaviors and neural circuits. By comparing the behavioral effects of silencing a particular neuron or circuit with its normal activity, researchers can gain insights into its function.

1.5.5. Optogenetics

Optogenetics has revolutionized neuroscience by enabling light-based control of neuronal activity with high temporal and spatial precision (Boyden et al. 2005). This technique utilizes genetically encoded light-sensitive proteins, called opsins, which are derived from microorganisms such as algae and bacteria. These opsins can be introduced into specific neurons using genetic tools like the GAL4-UAS system, allowing researchers to control the activity of those neurons with light.

One of the most widely used opsins is channelrhodopsin-2 (ChR2), a light-gated cation channel originally discovered in the green alga Chlamydomonas reinhardtii (Nagel et al. 2003). When ChR2 is expressed in a neuron and illuminated with blue light (around 470 nm), the channel opens, allowing an influx of cations (primarily sodium ions) into the cell. This influx depolarizes the neuron, increasing the likelihood of firing action potentials. By controlling the intensity and duration of the light pulse, researchers can control the degree of depolarization and thus the firing rate of the neuron. While ChR2 is a powerful tool for activating neurons, its effectiveness in *Drosophila* can be limited by the poor penetration of blue light through the fly's cuticle. Furthermore, the fly's visual system is also sensitive to blue light, which can introduce unwanted behavioral artifacts.

To overcome these limitations, researchers have developed and adopted red-shifted opsins, such as ReaChR and CsChrimson (Inagaki et al. 2014; Klapoetke et al. 2014). These opsins are activated by longer wavelengths of light (e.g., orange or red light), which penetrate the cuticle more effectively and are less likely to interfere with the fly's visual system. ReaChR, for example, is activated by orange light (around 590-630 nm) and allows for stronger depolarization and faster kinetics compared to ChR2. CsChrimson is activated by even longer wavelengths (red light, around 640 nm) and offers the advantage of being usable in combination with other opsins like ChR2 for independent control of multiple neuronal populations. In addition to activating neurons, optogenetics also provides tools for inhibiting neuronal activity using light. Halorhodopsin (NpHR), derived from the archaeon Natronomonas pharaonis, is a light-driven chloride pump (Zhang et al. 2007). Upon illumination with yellow light (around 580 nm), NpHR pumps chloride ions into the cell, hyperpolarizing the neuron and thus inhibiting its activity. It's important to note that *Drosophila*, unlike mammals, do not naturally produce sufficient amounts of all-trans-

retinal, the chromophore required for opsin function. Therefore, flies to be used in optogenetic experiments typically require dietary supplementation with all-trans-retinal. This is usually achieved by raising flies on food containing all-trans-retinal or by adding it to their food shortly before the experiment (Kim et al. 2015).

When combined with the precise targeting capabilities of the GAL4-UAS system or split-GAL4, optogenetics enables researchers to manipulate the activity of specific neurons or circuits with millisecond precision while simultaneously observing the resulting changes in behavior. This ability to establish causal links between neural activity and behavior has made optogenetics an indispensable tool for studying the neural basis of behavior in *Drosophila* and other model organisms. To fully leverage the power of these genetic manipulations, it is crucial to combine them with methods for precisely observing and quantifying the resulting behavioral changes. In the context of flight control, this requires sophisticated techniques for tracking the rapid and complex movements of freely flying insects in three dimensions.

1.6. Methods for 3D Tracking of Flying Insects

Understanding the intricacies of *Drosophila* flight, particularly rapid maneuvers like saccades, requires precise tracking of their movements in a three-dimensional space. Studies of *Drosophila* flight usually rely on tethered preparations, where flies were fixed in place, allowing for precise measurement of flight forces and wing kinematics (Vogel 1966; Götz 1968). While valuable, tethered preparations constrain natural movement and can alter flight dynamics. For instance, saccades observed in rigidly tethered flies are significantly longer than those in free flight, likely due to the absence of haltere feedback, which is crucial for stabilizing rotations (Frye and Dickinson 2004; Bender and Dickinson 2006b; 2006a).

To overcome the limitations of tethered studies, researchers began developing methods to analyze free-flight behavior. One of the first quantitative studies of free-flight kinematics in *Drosophila* (David 1978) used a wind tunnel and manual observations. While providing important data on body posture and flight speed, this approach lacked the detail needed to capture rapid, three-dimensional movements. Over the past few decades, advancements in camera technology, computer processing power, and computer vision algorithms have led to the development of sophisticated 3D tracking systems capable of

capturing the rapid and complex flight maneuvers of insects like *Drosophila* (Reynolds and Frye 2007; Straw et al. 2010). These modern systems typically employ multiple high-speed cameras strategically positioned around a flight arena. Careful camera calibration, using techniques like bundle adjustment, determines the precise position, orientation, and intrinsic parameters of each camera (Hartley and Zisserman 2018).

During experiments, each camera captures images that are processed in real-time, often using background subtraction to extract the 2D coordinates of the insects (Fry et al. 2008). These 2D coordinates from multiple camera views are then combined through triangulation to estimate the insect's 3D position. This process often involves solving a system of linear equations that relate the 3D point to its 2D projections, considering the calibrated camera parameters (Straw et al. 2010). To further refine the tracking, a Kalman filter is frequently applied to the triangulated 3D positions. This technique uses a motion model of the insect to predict its position and velocity and then corrects this prediction based on the observed 3D positions, effectively handling measurement noise and potential occlusions (Straw et al. 2010).

Many systems are designed to operate in real-time, performing triangulation and updating the Kalman filter estimate multiple times per second. This real-time processing enables closed-loop experiments, where the visual environment or other stimuli can be dynamically updated based on the insect's position. These advancements in tracking technology have opened up new avenues for studying the neural basis of flight control in *Drosophila*. By allowing for the precise measurement of free-flight behavior, these systems, particularly when combined with genetic tools for manipulating neural activity, provide a powerful approach for investigating how specific neurons, such as the DNs involved in saccade control, contribute to natural flight maneuvers.

1.7. Conclusion

The remarkable flight abilities of *Drosophila*, particularly their rapid saccadic maneuvers, provide a powerful model for understanding the neural control of complex behavior. While previous research has identified key DNs involved in various aspects of flight control, including those implicated in saccade initiation and execution, the precise mechanisms by which these neurons contribute to natural flight behavior remain unclear. Specifically, it is unknown whether individual DNs can independently trigger complete saccades in free-

flying flies, or if this behavior requires the coordinated activity of multiple DNs. This knowledge gap highlights the need for experimental systems that combine precise manipulation of neuronal activity with real-time tracking of unrestrained flight behavior. Therefore, the primary aim of this thesis is to investigate the role of specific DNs in controlling saccades during free flight in *Drosophila melanogaster*. To achieve this, I have developed a novel experimental platform that integrates real-time 3D tracking of freely flying flies with optogenetic activation of genetically defined DN populations. This system allows for precise manipulation of neural activity while simultaneously observing the resulting changes in flight behavior with high temporal and spatial resolution. By focusing on DNs implicated in saccade control, including DNa15, DNp06, and DNp03, this research seeks to answer fundamental questions about the neural basis of flight control: Is the activation of a single DN sufficient to elicit a complete saccade in free flight, or does this behavior require the coordinated activity of multiple DNs? Furthermore, do different DNs trigger qualitatively distinct flight maneuvers, suggesting specialized roles within the flight control circuitry? My novel experimental setup, which enables precise spatiotemporal control of DN activation during free flight, provides an unprecedented opportunity to characterize the behavioral repertoire controlled by each DN. By systematically comparing the kinematic signatures produced by activating different DNs individually and in combination, we can map the functional organization of flight control circuits and potentially discover specialized DN subpopulations dedicated to specific aspects of aerial navigation. Addressing these questions will provide crucial insights into the neural mechanisms underlying the generation of rapid flight maneuvers, reveal the functional specialization within descending control circuits, and contribute to our broader understanding of how complex behaviors are encoded, coordinated, and executed by the nervous system.

2. Methods

2.1. Experimental Model and Details

All *Drosophila melanogaster* lines were maintained on standard cornmeal medium at 25° C and 60% relative humidity under a 12-hour light/dark cycle. Experimental flies were aged 3-5 days post-eclosion (*dpe*) before behavioral testing.

To investigate descending neuron's function, I employed the Split-GAL4/UAS binary expression system targeting specific DN populations, including DNa15 (previously annotated as DNaX/DNae014), DNa05, DNp03, DNp06, and DNg02. For optogenetic activation experiments, Split-GAL4 driver lines were crossed with UAS-CsChrimson (BDSC #82181). Neural silencing was achieved by crossing Split-GAL4 lines with UAS-Kir2.1 (BDSC #6595). I implemented two parallel control strategies: first, crossing an Empty Split-GAL4 (BDSC #79603) driver to respective UAS effector lines, and second, crossing UAS effector lines to W[1118] (BDSC #6326) to control for eye color effects. For unilateral activation studies, I utilized either FRT>UAS-CsChrimson (provided by A. Mauss) or SPARC collection stocks (BDSC #84143, #84144, #84145). Controls for these studies were naturally provided due to the stochastic nature of the expression system.

The preparation protocols for bilateral and unilateral optogenetic experiments followed a similar workflow. For bilateral activation experiments, Split-GAL4 x UAS-CsChrimson progeny were raised under standard conditions until reaching 3-5 dpe. They were then moved to a light-shielded vial with ATR-supplemented food (50uL of 100mM ATR). The next day, 10 female flies were randomly selected, and placed in the arena for recording.

For the stochastic activation experiments, I crossed the Split-GAL4 line of choice with the FRT>UAs-CsChrimson driver line. These flies were allowed to lay eggs for about 3 days, and then removed from the vial. I then applied the heat shock to the vial by placing it in a water bath at 37C for 45-60 minutes, following which the vial was removed from the bath and placed back into the incubator. I then selected F1 flies who were 3 days-old eggs at the time of the heatshock, and placed them into a separate vial for 3-5 dpe. A day before the experiment, I moved a single fly to a light-shielded vial supplemented with ATR. The next day I placed the fly into the arena for the experiment duration.

For controls, I used two different methods: first, Canton-S wild-type flies served as behavioral controls, establishing baseline parameters in the free-flight arena and characterizing non-specific responses to optogenetic stimulation. Second, an Empty Split-GAL4 crossed with the driver line of interest were used for genetic controls for both optogenetic and silencing experiments.

2.2. Behavioral Arena

The experimental platform consists of a cylindrical plexiglass arena, measuring 50 cm in diameter with a height of 35 cm, thus providing ample volume for naturalistic flight behavior. For backlighting, the base of the arena was a diffuse plexiglass floor plate. The entire setup was mounted inside a metal frame (Figure 12).

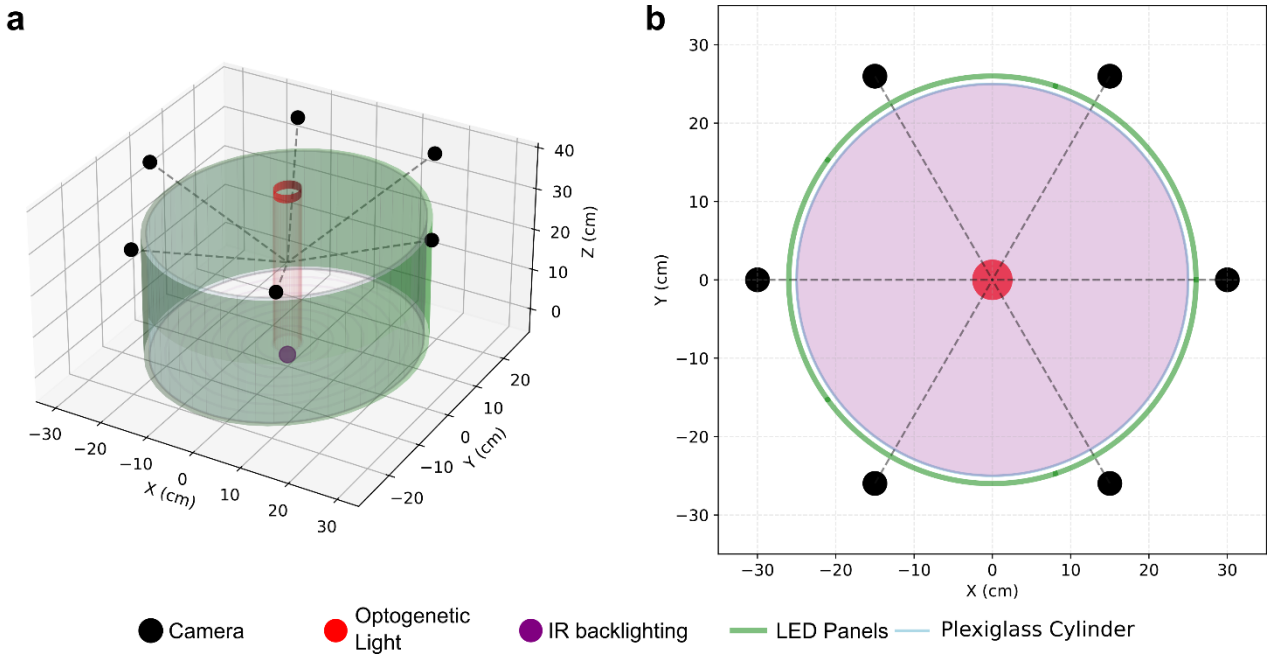

Figure 12. Diagram of the experimental arena. 3D projection of the arena (a) and top view (b) showing the approximate location of the cameras (black circles), optogenetic light column (in red), flexible LED panels (green), and IR backlighting (purple).

Visual stimulation is achieved through an array of programmable flexible LED panels (640x128 pixels total resolution) arranged in a cylindrical configuration around the arena. The LED panels were selected as they provide an easier and more modular solution than projection-based systems. Different types of stimuli can be presented using this setup, including static patterns, open-loop sequences, and closed-loop stimuli triggered by fly

behavior, controlled through custom Python scripts using the PyGame library (McGugan 2007).

The tracking system integrates six high-speed cameras operating at 100 Hz: four Basler ace 2 a2A1920-160umBAS and two Basler ace acA800-510um, mounted in a circle above the arena to ensure complete and overlapping spatial coverage. Each camera is equipped with a 4mm wide-angle lens (Basler Lens C125-0418-5M-P f4mm) and IR-pass filter (IR M46 x 0.75, Edmund Optics) for optimal tracking under infrared illumination. An array of 25 850nm IR LEDs (VSMA1085400X02, Vishay) powered by a lab bench power supply (RS PRO RS3005D, RS Components), provides a uniform illumination for the tracking. Due to the large amount of lighting (from both the camera backlighting and the LED panels), temperature had to be maintained at 25±2° C using multiple PC fans to dissipate heat from the arena, and the humidity was maintained at 55±5% using a humidifier (ReptiZoo Luftbefeuchter) with an integrated humidity-controller.

Three-dimensional tracking is implemented through the open-source Braid software platform (Straw et al. 2010), which allows for calibrated tracking of small objects moving in 3D space using multiple cameras. Camera calibration, including focal length and lens distortion parameters, is performed using a standard 6x9 checkerboard and ROS calibration protocol (Stanford Artificial Intelligence Laboratory et al. 2018).

This design allows for closed-loop optogenetic activation of neurons in free-flight using real-time tracking data, including the position and velocity of flies. While individual identity tracking was not implemented, the system demonstrates robust capabilities for simultaneous tracking of multiple objects within the arena volume.

2.2.1. Optogenetic Stimulus and Experimental Paradigm

The experimental paradigm was developed using custom software in Python. The real-time position of the fly was sent from the Braid software to a Python script, which activated a triggering function when the fly crossed into a pre-defined zone within the arena. This triggering function would either activate a flash of light, or make no light pulse (sham). The optogenetic stimulus was generated by powering a 625 nm LED light source, positioned above the center of the arena. Two light sources were used for optogenetic experiments - first, an array of 3 Red (627nm) LUXEON Rebel LED (Luxeon Star LEDs), and later a

Thorlabs collimated 625 nm LED with a diameter of 5cm. The LED was controlled via an Arduino, which was connected to the main tracking system. The optogenetic stimulus consisted of a 300ms continuous pulse of light. Due to the inhomogeneous nature of the light source, a 3D model of the light intensity of the arena was generated. A photodiode sensor (Thorlabs PM121D) was mounted inside a custom 3D-printed housing which contained four IR LEDs, which can be tracked by Braid. The sensor was moved inside the arena with the optogenetic light activated, and the readings of the sensor were synchronized to the position of the four LEDs, the centroid of which was used as the position of the sensor.

2.2.2. Camera System and Data Acquisition

I implemented a high-speed, high-resolution system to allow for more accurate kinematics tracking of flies using a XIMEA CB160MG-LX-X8G3 machine vision camera (XIMEA GmbH, Münster, Germany) positioned above the center of the experimental arena. Operating at 500 frames per second with 2048 x 2048-pixel resolution, this configuration optimized the trade-off between temporal precision and spatial detail, with a down sampling from the camera's native capabilities (161MPix at 311fps). The substantial data throughput (2GB/s) demanded a specialized acquisition framework developed in Rust, using its robust memory management and parallel processing capabilities to ensure stable and synchronized real-time video capture (Matsakis and Klock, 2014). The acquisition software employed a dual-buffer strategy to record trajectories immediately before and directly after optogenetic manipulation. A circular pre-buffer (250 frames, 0.5 seconds) was continuously recording frames from the camera, while a second buffer (500 frames, 1.0 seconds) remained empty. When a fly was detected within the camera trigger zone, the recording switched from the pre-buffer to the second buffer until it was full, and then both buffers were concatenated and the video was encoded to disk. This enables the recording of event in the past, happening immediately prior to the actual optogenetic or stimulus activation.

Since flies are free to move along all axes in the arena, I incorporated a focus-tunable lens system (EL-16-40-TC, Optotune Switzerland AG). This focusing mechanism operated through a Python-based control interface that processed real-time positional data from the tracking system. Using pre-calibrated response curves, the system

continuously adjusted lens current (which changed the focus of the lens) to maintain the fly within the optimal focal plane, ensuring high-quality behavioral recording throughout the experimental arena.

2.2.3. Markerless Pose Estimation

Flight orientation analysis was performed using the Social LEAP Estimates Animal Poses (SLEAP) toolkit (Pereira et al. 2022), which uses pre-trained convolutional neural networks for pose estimation. The system was trained on manually labeled frames annotating head and abdomen positions, from which I could extract information not available with the standard tracking software, such as actual heading vs the trajectory heading, and possibly also wing and leg position (although this is still ongoing). This markerless approach enabled a more accurate quantification of flight posture.

2.3. Experimental Protocol

2.3.1. Optogenetic Activation Experiments

Following ATR supplementation and food deprivation, flies were briefly cold anesthetized and placed into the arena. The recording session was then started and was stopped after 24 hours had passed. The optogenetic activation occurred whenever a fly was detected in the central zone of the arena (with a 10-second refractory period), within the light activation column. For control purposes, 10% of the trials were sham - meaning, no optogenetic stimulus was used. For bilateral experiments, the flies were removed from the arena and disposed of; for unilateral experiments, an inverted food vial supplemented with apple vinegar and yeast extract was placed on a hole on the top of the arena until the fly was captured. The flies were then allowed to remain in the food vial for 1-3 days until dissection and immunohistochemistry.

2.3.2. Looming Stimuli Experiments

To investigate how flies process and respond to approaching threats during flight, I wrote a closed-loop display system, which used the real-time tracking data incoming from Braid to calculate the exact timing and position of a looming stimulus. The system was designed to present looming stimuli when flies were detected in the arena's center, with a minimum inter-stimulus interval of 10 seconds to prevent habituation.

Flight trajectory analysis employed a sliding window approach, calculating the fly's average heading direction by analyzing velocity vectors from the preceding 10 frames of tracking data. The system converted these measurements from the tracking system's frame-of-reference to the display screen's coordinates using pre-calculated calibration tables, ensuring precise stimulus presentation relative to the fly's position and heading.

The visual stimulus consisted of a black circle expanding exponentially against a white background, with the angular size (α) increasing from 5° to approximately 75° over 300ms. Classically, in tethered setups, a natural-looking looming stimulus is presented using a specific formula (Gabbiani, Krapp, and Laurent 1999); however, this type of expansion does not work well during free-flight, due to the much faster velocities and heading changes. I instead opted to use an exponentially expanding stimulus, since it generally has a faster timescale, and was used previously in other free-flying setups (Muijres et al. 2014). The final stimulus size was calculated using the following equation:

$$\alpha = 2 \times \arcsin\left(\frac{r}{d}\right)$$

Where α = visual angle in degrees, r = final radius of the stimulus in centimeters, and d = distance from the fly's eye to the stimulus (assumed constant at 25 cm for center-triggered stimuli). Based on empirical optimization and previous studies, I selected a final α value of 75°, corresponding to an approximate diameter of 78 pixels or 30 cm on the display.

2.4. Immunohistochemistry Protocol

Adult *Drosophila* were cold-anesthetized on ice, surface-sterilized with 70% ethanol, and dissected in phosphate-buffered saline (PBS, pH 7.4). The dissected central nervous systems were fixed in 4% paraformaldehyde in PBS for 30 minutes at room temperature. Following fixation, samples were washed three times for 15-minute in PBS containing 0.44% Triton X-100 (PBS-Tx) for tissue permeabilization, followed by blocking (to prevent on-specific binding) using 4% normal goat serum (NGS) in PBS-Tx for 20 minutes at room temperature.

Primary antibody incubation was performed overnight at 4°C with gentle agitation in PBS-Tx containing 4% NGS. After primary incubation, samples were washed three times for 15 minutes in PBS-Tx, followed by a second overnight incubation at 4°C with fluorophore-

conjugated secondary antibodies diluted in PBS-Tx with 4% NGS. Samples were finally washed three more times for 15-minutes in PBS-Tx, and then mounted in Vectashield antifade mounting medium (Vector Laboratories) on glass slides. For experiments requiring hemispheric identification, the mounting orientation was documented. Slides were air-dried overnight in a chemical fume hood before storage at 4°C.

2.5. Confocal Microscopy and Image Acquisition

High-resolution imaging was performed using Leica SP8 or Leica Stellaris laser scanning confocal microscopes equipped with a tunable white light laser system. Image acquisition parameters were controlled through Leica LAS-X software. Detector gain and laser power settings were optimized for each sample to maximize signal-to-noise ratio while preventing photobleaching and signal saturation. For whole-brain imaging, 20x objectives were used with 2048 x 2048-pixel resolution. Higher magnification imaging (40x and 63x objectives) was employed for detailed analyses requiring tile scanning. Z-stacks were collected with optimal step size as determined by the Leica LAS-X software, and were processed using FIJI/ImageJ software (Schindelin et al. 2012) for maximum intensity projections and analysis.

Analysis of confocal z-stacks was limited to qualitative assessment of neuronal labeling patterns. Specifically, image data were examined to identify which descending neurons (if any) expressed the fluorescent reporters of interest, with particular attention to discriminating between DNa15, DNa05, and other labeled neurons. This qualitative approach enabled verification of genetic targeting specificity and determination of expression patterns (bilateral vs. unilateral) in stochastic labeling experiments, providing essential context for interpreting optogenetic behavioral results. No quantitative measurements of fluorescence intensity or volumetric analysis were performed on these image stacks.

2.6. Quantification and Analysis of Free-flight Behavior

The analysis of flight behavior required robust quantification of three-dimensional trajectories and precise characterization of rapid maneuvers. I developed a pipeline implemented in Python to process and analyze the positional data obtained from our multi-camera tracking system.

Initially, data was filtered based on the duration of recording (at least 300 frames or 3 seconds), as well as the median position of the trajectory (had to be within the center volume of the arena) and the distance covered by the trajectory (at least 30 cm). This was used to filter out both sporadic/erroneous tracking, as well as walking bouts.

For each extracted trajectory, I then extracted angular kinematics, by first computing the instantaneous heading direction from the horizontal velocity components using the two-argument arctangent function:

$$\theta = atan2(v_y, v_x)$$

This computation yielded the heading angle in the range $[-\pi, +\pi]$. However, this raw angular measurement introduces discontinuities at the $\pm\pi$ boundary. I addressed this limitation by implementing an angle unwrapping algorithm that detects and corrects these discontinuities, producing a continuous representation of angular position:

$$\theta_{unwrapped} = unwrap(\theta)$$

The unwrapped angular trajectory was then processed through a Savitzky-Golay filter (window size = 21 frames, polynomial order = 3) to remove high-frequency noise while preserving the rapid movements characteristic of saccadic maneuvers. Angular velocity was computed through central difference differentiation of the filtered angular trajectory, with appropriate scaling to convert to degrees per second (van Breugel, Kutz, and Brunton 2020).

Identification of saccades used a simple peak finding algorithm (*scipy.find_peaks*) on the angular velocity traces. Saccades were defined as rapid rotational movements exceeding an angular velocity threshold of 300 degrees per second, a threshold established in previous research (Tammero and Dickinson 2002b; Mronz and Lehmann 2008).

Results are generally presented using two methods – either stimulus-centered, or saccade-centered. For stimulus-centered, all traces are extracted and averaged around the stimulus index (either optogenetic or looming stimulus). For saccade-centered, all the traces are extracted and averaged around the peak of the response, regardless of its timing in relation to the stimulus.

2.7. Statistical Analysis

All statistical analyses were performed using custom Python scripts utilizing the SciPy statistics module (Virtanen et al. 2020), NumPy (Harris et al. 2020), and the PyCircStat package for circular statistics. Initial distribution analyses using Shapiro-Wilk tests confirmed the non-normality of most behavioral parameters across experimental conditions ($p < 0.001$ for angular velocity, linear velocity, and saccade interval distributions), necessitating predominantly non-parametric statistical approaches throughout the analyses.

For comparing behavioral parameters between experimental and control groups (e.g., DNa15>csChrimson vs. Empty-Split>csChrimson), Mann-Whitney U tests were employed due to their robustness with non-normal distributions and uneven sample sizes. Effect sizes for these comparisons were quantified using Cliff's delta, which provides a robust measure of effect magnitude for non-parametric data, with values of approximately 0.11, 0.28, and 0.43 corresponding to small, medium, and large effects, respectively (Meissel and Yao 2024). For multi-group comparisons, such as analyzing responses across different optogenetic stimulation intensities or durations, Kruskal-Wallis tests were used and post-hoc analyzes using Dunn's test with Bonferroni correction for multiple comparisons were applied to identify specific between-group differences when significant effects were detected.

Circular statistics were essential for analyzing directional data, particularly heading angles during spontaneous and evoked saccades. Angular measurements were analyzed using the PyCircStat implementation of circular statistics, with circular means (μ) and concentration parameters (r) calculated to characterize directional preferences and response consistency, when applicable. The concentration parameter r ranges from 0 (uniform distribution) to 1 (perfect concentration in one direction), providing a standardized measure of angular dispersion.

Relationships between continuous variables (e.g., pre-saccade characteristics and optogenetically-evoked responses) were assessed using both Pearson's correlation coefficient for linear relationships and Spearman's rank correlation coefficient for non-linear associations

For evaluating the combined effects of multiple predictors (e.g., time in trigger zone, stimulus intensity) on behavioral outcomes, multiple linear regression analysis was utilized. In cases where parametric assumptions were violated, permutation-based approaches were implemented, with significance assessed through 10,000 random reassignments of response variables (Anderson 2001).

For spatial analyses of tracking uncertainty, both descriptive statistics (mean ± SD) and inferential tests comparing central versus peripheral regions were employed. Position and velocity uncertainties were analyzed across the behavioral volume, with data binned into 50×50 grids for visualization and statistical comparison. When comparing specific spatial regions, Mann-Whitney U tests were used to assess differences, with outliers above the 99th percentile excluded to improve clarity of spatial patterns.

Results are presented consistently as mean ± standard deviation for all parameters, regardless of distribution properties, to maintain consistency. For key comparisons where median values might better represent central tendency in highly skewed distributions, these are additionally provided alongside interquartile ranges (IQR).

For all statistical tests, significance was established at $p < 0.05$, with specific p-values reported for key comparisons according to the standardized format. In figures, error bars/shaded areas represent ±1 standard deviation unless otherwise noted. In cases where substantial outliers would distort visualization, data above the 99th percentile were clipped for display purposes only, while statistical analyses were performed on complete, unclipped datasets.

2.8. Materials and Resources

2.8.1. Fly Stocks

Resource	Source	Identifier	Notes
D. melanogaster: Canton-S	Bloomington *Drosophila* stock center	BDSC: #64349	
D. melanogaster: split-GAL4[VT025718.AD; R56G08.DBD]	Michael Dickinson	None	DNaX (DNa15+DNa05)
D. melanogaster: UAS-FRT-stop-FRT-CsChrimson-Venus	Alex Mauss	None	Heatshock-FlpOut with csChrimson
D. melanogaster: UAS-Hsap\KCNJ2.EGFP	Michael Dickinson	None	
D. melanogaster: UAS-CsChrimson.mCherry	Bloomington *Drosophila* stock center	BDSC: #82181	
D. melanogaster: UAS-SPARC2-D-Syn21-CsChrimson::tdTomato	Bloomington Drosophila stock center	BDSC: #84142	
D. melanogaster: P{y[+t7.7] w[+mC]=nSyb-IVS-phiC31}attP18; S[1]/CyO; Pri[1]/TM6B, Tb[1]	Bloomington Drosophila stock center	BDSC: #84151	
D. melanogaster: w[1118]; P{y[+t7.7] w[+mC]=VT048835-p65.AD}attP40; P{y[+t7.7] w[+mC]=VT017682-GAL4.DBD}attP2	Bloomington Drosophila stock center	BDSC: #75896	DNa05+DNp11
D. melanogaster: w[1118]; P{y[+t7.7] w[+mC]=VT023750-p65.AD}attP40; P{y[+t7.7] w[+mC]=VT039465-GAL4.DBD}attP2	Bloomington Drosophila stock center	BDSC: #75972	DNg02
D. melanogaster: w[1118]; P{y[+t7.7] w[+mC]=R91C05-p65.AD}attP40; P{y[+t7.7] w[+mC]=R31B08-GAL4.DBD}attP2/TM6B, Tb[1]	Bloomington Drosophila stock center	BDSC: #75817	DNp03
D. melanogaster: w[1118]; P{y[+t7.7] w[+mC]=VT019018-p65.AD}attP40; P{y[+t7.7] w[+mC]=VT017411-GAL4.DBD}attP2	Bloomington Drosophila stock center	BDSC: #75885	DNp06
D. melanogaster: w[1118]; P{y[+t7.7] w[+mC]=p65.AD.Uw}attP40; P{y[+t7.7] w[+mC]=GAL4.DBD.Uw}attP2	Bloomington Drosophila stock center	BDSC: #79603	Empty Split-GAL4

2.8.2. Software and Algorithms

Resource	Source	Notes
Fiji (ImageJ)	None	v2.16.0
Braid	Prof. Dr. Andrew Straw	v0.11.1
Triggerbox	Prof. Dr. Andrew Straw	v0.4.1
Python	Python Software Foundation	v3.8-3.12
Rust	Rust Foundation	v1.77.0
braid-opto-arena	This study	

ximea_camera	This study	
Pylon Viewer	Basler AG	
Arduino IDE	Arduino S.r.l.	
Leica Application Suite X	Leica Microsystems GmbH	
Robot Operating System	Open Robotics	Ros Noetic

2.8.3. Hardware

Resource	**Source**	**Notes**
P2.5mm Flexible Soft LED Display Module	Linsn LED	https://www.linsnled.com/p2-5mm-flexible-soft-led-display-module.html
Linsn RV908M32 Receiving Card	Linsn LED	https://www.linsnled.com/linsn-rv908m.html
Linsn TS921 Sending Card	Linsn LED	https://www.linsnled.com/linsn-ts921-sending-card.html
MeanWell LRS-350-5	MeanWell	https://www.meanwell.com/productPdf.aspx?i=459
Arena enclosure	This study	N/A
Orson Black PowerStar IR-LED	RS-Online	Cat# 796-1772
RS PRO RS3005P Power supply	RS-Online	Cat# 175-7367
PLEXIGLAS XT Farblos 0A070 GT	KUS Kunststofftechnik	https://www.kus-kunststofftechnik.de/
PLEXIGLAS LED Weiss WH72 GT	Plexiglas-shop	Cat# Weiss WH72 GT
Thorlabs 625nm Collimated LED	Thorlabs	Cat# M625L4-C1
Thorlabs T-Cube™ LED Driver	Thorlabs	Cat# LEDD1B
Thorlabs Digital Console with Photodiode Sensor	Thorlabs	Cat# PM120D
Arduino	RS-Online	Cat# 769-7409
Arduino Nano	RS-Online	Cat# 696-1667
Arena enclosure	This study	N/A
RS PRO RS3005P Power supply	RS-Online	Cat# 175-7367
PLEXIGLAS XT Farblos 0A070 GT	KUS Kunststofftechnik	https://www.kus-kunststofftechnik.de/
PLEXIGLAS LED Weiss WH72 GT	Plexiglas-shop	Cat# Weiss WH72 GT
Basler ace acA800-510um	Rauscher GmbH	Cat# acA800-510um
Basler ace2 a2A1920-160umBAs	Rauscher GmbH	Cat# a2A1920-160umBAs
Ximea CB160MG-LX-X8G3	Ximea GmbH	Cat# CB160MG-LX-X8G3
SP8 LIGHTNING Confocal Microscope	Leica Microsystems	
Stellaris Confocal Microscope	Leica Microsystems	

3. Results

3.1. Development and Validation of Flight Tracking System

To investigate the neural basis of flight control in *Drosophila melanogaster*, I developed a novel behavioral arena enabling simultaneous 3D tracking and closed-loop optogenetic manipulation during free flight. This experimental platform integrates precise behavioral quantification with targeted neuronal activation to dissect the functional role of descending neurons in flight maneuvers.

3.1.1. Flight Tracking System

The experimental system comprises a cylindrical plexiglass arena (50 cm diameter × 30 cm height) designed to optimize natural flight behavior (Figure 13). These dimensions represent a balanced compromise between larger setups (100 cm diameter; Straw et al., 2017) and more constrained environments (30 cm diameter; (Muijres et al. 2014; Whitehead et al. 2022), promoting flight patterns that favor central arena occupancy rather than wall-proximal trajectories. The tracking system initially employed four cameras (800x600 resolution, 100 Hz sampling rate) mounted above the arena in a circular configuration, pointed in an angle towards the center area of the arena, with an overlap in area coverage. This was subsequently upgraded to a six-camera array with enhanced resolution (1920×1200), significantly improving positional measurement precision.

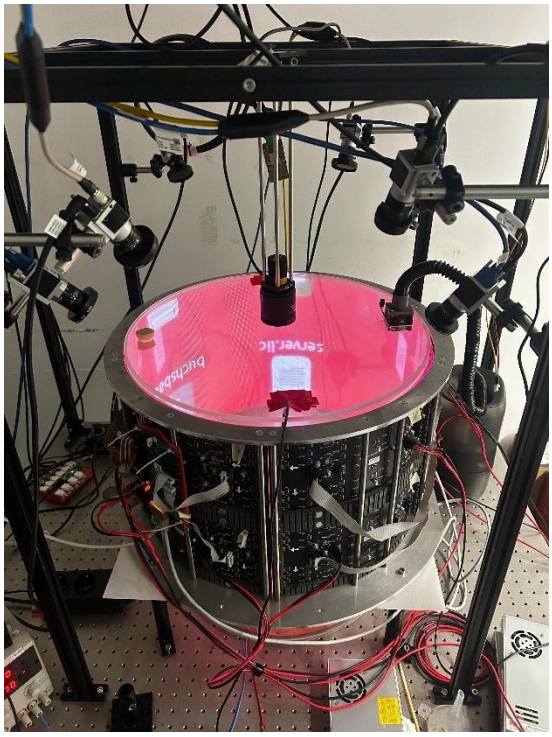

Figure 13. Photo of the behavioral arena.

Visual stimulation is delivered via ten flexible LED panels arranged in a 5×2 configuration surrounding the arena. This modular display system enables the presentation of diverse visual stimuli, including random dot patterns, looming stimuli, and gratings. For targeted optogenetic intervention, a collimated 625 nm light source (5 cm diameter) is positioned

directly above the arena center. This stimulation system operates in a closed-loop configuration with the tracking apparatus, automatically triggering 300 ms illumination periods when flies enter a predefined "trigger zone" beneath the light source.

3.1.2. Quantification of spatial and temporal resolution

Before starting with the genetic/optogenetic manipulation experiments, I first wanted to quantify the accuracy of the system, both the spatial and temporal aspects. Tracking accuracy was quantified through analysis of the system's covariance (P) matrices, computed for each tracked position (x, y, z). The P matrix represents the covariance matrix of the Kalman filter state estimate, encoding the system's uncertainty in three-dimensional position prediction. Each element P_{ij} quantifies the covariance between spatial dimensions, with diagonal elements (P_{ii}) representing positional variance in each dimension. The trace of P provides a scalar metric of overall tracking uncertainty (Bar-Shalom, Li, and Kirubarajan 2004).

3.1.3. System calibration and error analysis

Spatial distribution analysis of measurement uncertainty revealed systematic positional variations across the arena volume. Both position and velocity uncertainty parameters exhibited location-dependent patterns within the experimental space. For subsequent analyses, I extracted 687 flight trajectories from three independent experiments comprising 60 individual 3–10 days old female Canton-S wild-type flies, presenting a simple random static pattern on the LED screens. I then applied basic filtering on the data, to make sure I use only valid behavioral information: first, all detections occurring outside the physical arena boundaries were removed to clean spurious tracking events; second, a duration-based filter excluded all trajectories shorter than 300 frames (equivalent to 3 second at the 100 Hz acquisition rate), ensuring sufficient temporal continuity for meaningful behavioral analysis. Based on this data, overall uncertainty was 0.001 ± 0.001 m for position and 0.061 ± 0.011 m/s for velocity data. Analysis of the more central region of the arena (radius ≤ 20 cm, 5 cm ≤ z ≤ 30 cm) showed modest improvements in tracking precision, with average uncertainties of 0.001 ± 0.001 m and 0.058 ± 0.011 m/s for position and velocity, respectively (Figure 14). These uncertainty values are particularly notable given the small size of *Drosophila melanogaster*, which has a body length of only 2.5-3 mm. The position uncertainty of 1 mm thus represents only approximately one-third of the

fly's body length, demonstrating the high precision of the tracking system even when tracking such small objects in a relatively large behavioral volume. The consistent performance across the arena volume, as indicated by the small effect sizes in uncertainty differences between central and peripheral regions, suggests robust tracking capability throughout the experimental space.

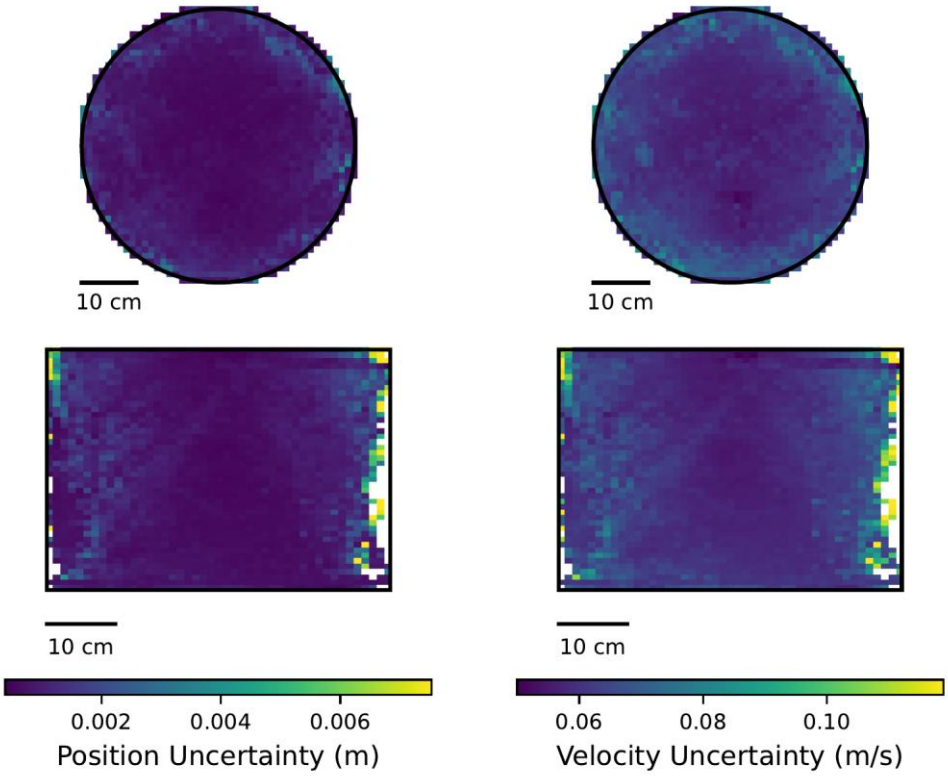

Figure 14. Spatial Distribution of position and velocity uncertainty in the behavioral tracking setup. Top: top-down view (XY plane); bottom: side view (XZ plane) error distribution heatmap of the behavioral arena. Left column displays position uncertainty while right column shows velocity uncertainty. The circular boundary (top) represents the horizontal extent of the arena (50 cm diameter), while the rectangular boundary (bottom) shows the vertical extent (35 cm height). Color intensity indicates the magnitude of uncertainty, with darker purple representing lower uncertainty values. Scale bars: 10 cm. Data was binned into a 50x50 grid and outliers above the 99th percentile were clipped to improve visualization of the spatial patterns.

3.1.4. Integration of Closed-loop Optogenetic Stimulation

I next wanted to measure the delay between the object detection to the optogenetic activation. This is a vital component of the setup, since the light stimulus has to become active while the fly is still within the activation area, and so it requires a very low latency between detection and activation.

The temporal precision of my closed-loop system was quantified by measuring the delay between fly detection and stimulus activation. The total system latency comprises several components: image acquisition, object detection and localization, network communication, and stimulus/light triggering. After characterizing these individual components, I measured a mean system response time of 7.4±1.2 ms (Figure 15). This latency is particularly noteworthy given the complexity of the processing pipeline, which includes real-time 3D position estimation and triggering. Given the tracking system's frame acquisition period of 10 ms (100 Hz), this activation latency represents less than one frame duration. The sub-frame response time ensures that behavioral responses to stimuli can be accurately attributed to the detected fly positions, making the temporal delay negligible for subsequent behavioral analysis. The consistent sub-10 ms performance demonstrates the efficiency of our implementation and its suitability for real-time closed-loop experiments with freely moving flies.

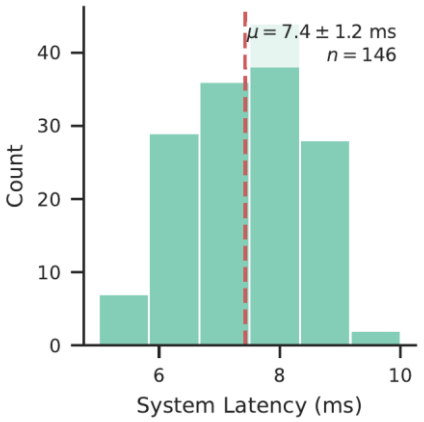

Figure 15. Distribution of system response latency measured from object detection to stimulus activation.
Histogram showing the temporal delay between fly detection and the triggering of optogenetic or visual stimuli (n = 146 trials). The mean latency of 7.4±1.2 ms (dashed line) is less than the frame acquisition period of 10 ms, ensuring robust closed-loop performance.

3.1.5. Spatial Light Distribution Analysis

Next, I wanted to verify that the light intensity generated by the optogenetic collimated light source is strong enough to elicit a consistent optogenetic activation. The light intensity was measured using a Thorlabs power meter, mounted inside a frame containing four IR LEDs equidistant from the sensor' center. These IR LEDs were then tracked using the Braid tracking system (Straw et al. 2010) along with concurrent recording of the power intensity from the light meter, and thus the position of the power meter sensor was the average of all four LEDs. The spatial analysis revealed highly uniform illumination across the designated activation zone (Figure 16). Mean intensity levels of 226±58.63 $\mu W/mm^2$ were measured within the activation column. This uniformity ensures that flies receive

consistent optogenetic stimulation regardless of their position within the activation volume, which is essential for reliable behavioral experiments.

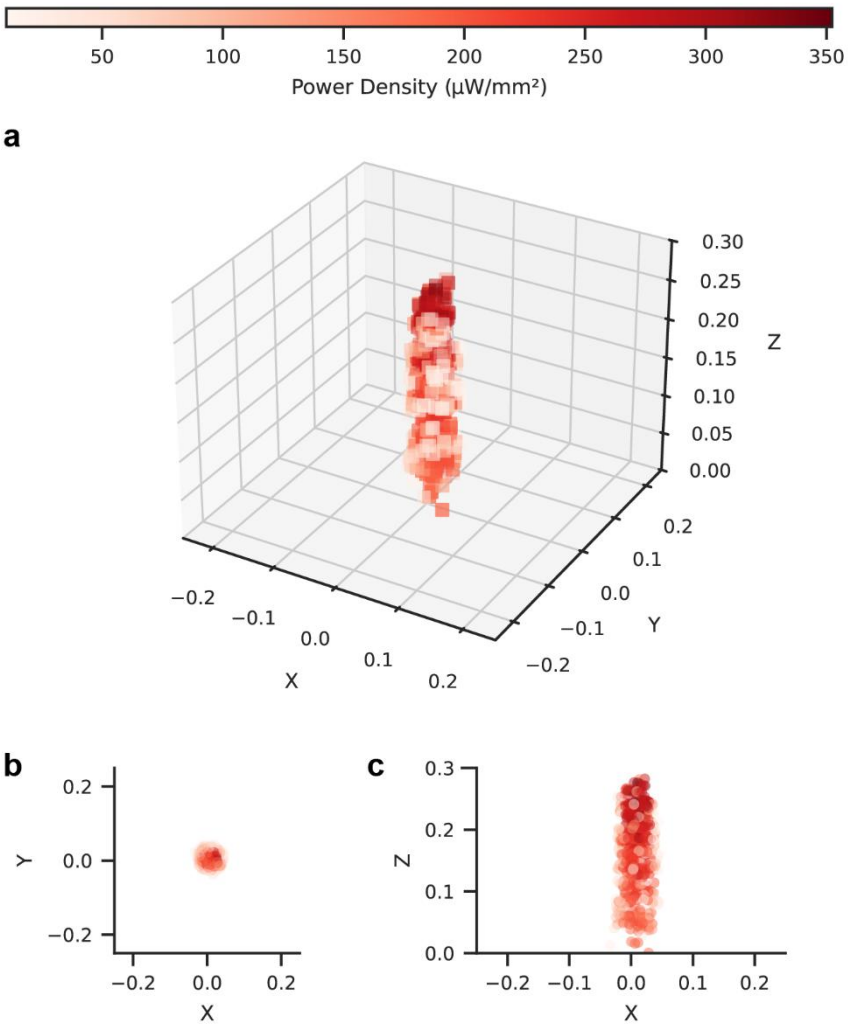

Figure 16. Spatial distribution of light intensity across the trigger volume.

(a) Three-dimensional heatmap showing illumination levels throughout the activation zone. (b) Horizontal (XY) and (c) vertical (XZ) cross-sections through the center of the volume demonstrate uniform light delivery across the activation region. Measurements were taken using a calibrated photodiode power sensor mounted on a tracked positioning frame, enabling precise spatial mapping of illumination patterns. All distance units are in meters. Color intensity represents measured power density in $\mu W/mm^2$.

3.2. Characterization of Natural Flight Behavior

3.2.1. Basic Flight Parameters in Free Flight

After validation of the tracking setup accuracy, I characterized the general flight behavior of *Drosophila*. The angular velocity component of flight is specifically important, as it is very highly correlated with saccadic movements. For this analysis, the same flight data was used as for the spatial accuracy validation. During flight, flies maintained relatively slow forward velocities (0.13±0.12 m/s), with the distribution showing considerable positive skew, reflecting occasional rapid forward movements (Figure 17a). Angular velocity measurements (Figure 17b) demonstrated highly structured turning behavior. The distribution exhibited a Laplacian-like shape, characterized by a sharp central peak at zero and extended tails, indicating that flies typically maintain straight flight trajectories punctuated by rapid turning maneuvers (3.1±450 °/s). The symmetry of this distribution (skewness = 0.0003) suggests no directional bias in turning behavior. Individual flight bouts showed a heavily right-skewed distribution (skewness = 10.15), with most flights lasting under 5 seconds (median = 4.975 ± 20.8 s; Figure 5c).

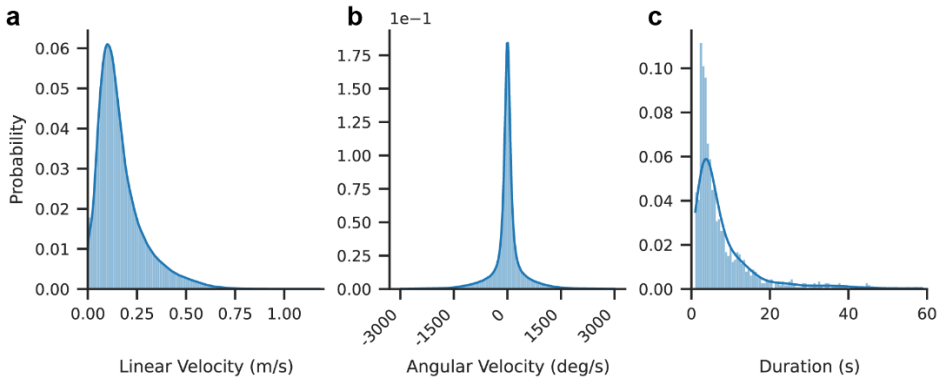

Figure 17. Quantitative analysis of flight behavior in freely flying *Drosophila melanogaster*. Distribution histograms show key kinematic parameters of flight behavior tracked in 3D. (a) Linear velocity reveals a right-tailed distribution, with flies predominantly executing forward flight at moderate speeds, characteristic of their typical exploratory behavior. (b) Angular velocity follows a Laplacian distribution centered at zero, reflecting the flies' tendency to maintain straight flight paths punctuated by rapid turns. (c) Flight duration exhibits an exponential decay, demonstrating that flies typically engage in brief flight bouts, with extended flights becoming progressively rarer (n = 1228 flight trajectories)

3.2.2. Analysis of Spontaneous Saccadic Maneuvers

3.2.2.1. Saccade detection and characterization

To investigate the fine temporal structure of *Drosophila* flight behavior, I utilized a simple detection algorithm for rapid turns (saccades) based on the flies' angular velocity. The saccade detection algorithm first used a peak-detection algorithm to find any peaks (both positive and negative) in the raw angular velocity trace, with a threshold of 300 °/s. Then, the detected peaks were filtered based on their position in the arena, to remove tracking errors and walking bouts. Example analysis of a representative trajectory (Figure 18) demonstrates the stereotyped nature of these maneuvers. Over a flight duration of 46.3 seconds, 72 distinct saccadic events were detected, accounting for a saccade rate of 1.5 saccades/s, and an average absolute angular velocity of 1271 ± 203 °/s peak amplitude. Furthermore, each saccade event was coupled with a sharp decrease in the linear velocity, characteristic of saccades during free flight (Mronz and Lehmann 2008).

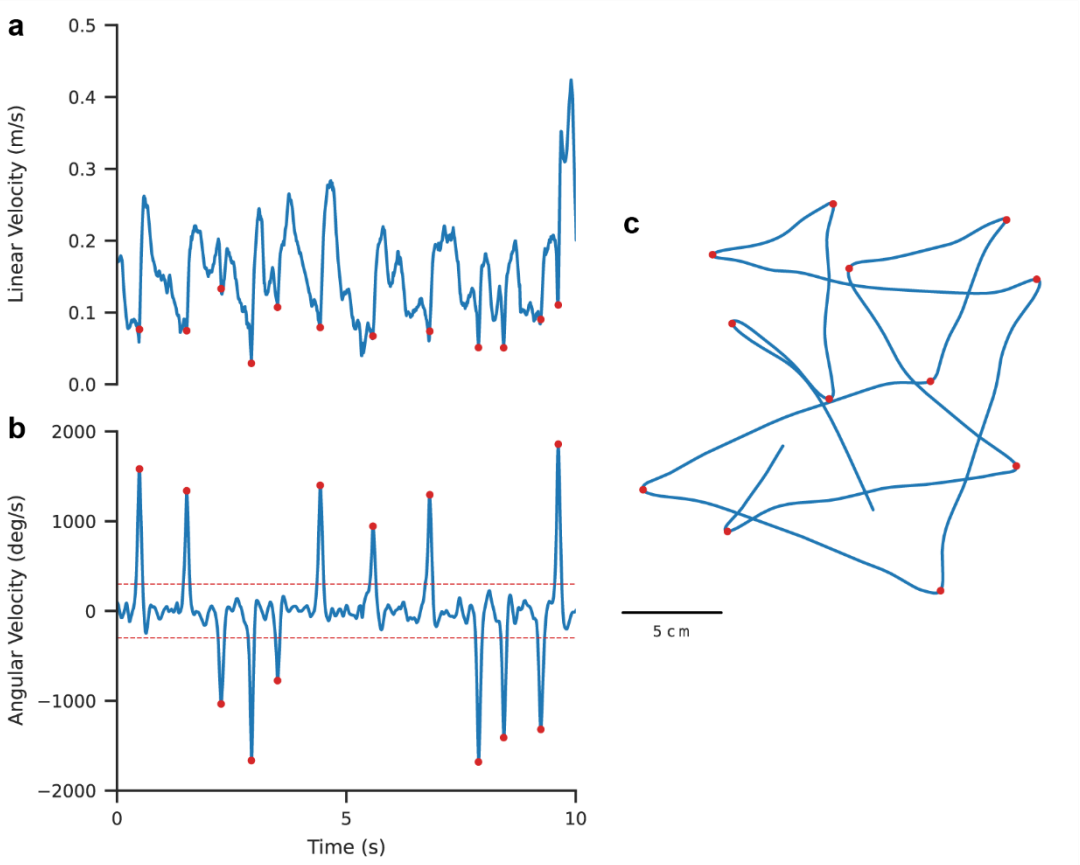

Figure 18. Automated detection of saccadic flight maneuvers in *Drosophila*. Representative flight trajectory showing detected saccades (red dots) during free flight

behavior. (b) Linear velocity profile corresponding to the trajectory in (a), demonstrating characteristic modulation of forward speed during saccades. (c) Angular velocity profile revealing sharp angular accelerations (>300 °/s) that define saccadic turns, with automated detection (red dots) capturing both clockwise and counterclockwise turning events. Scale bar: 5 cm.

3.2.2.2. Analysis of saccade kinematics

The saccadic turns performed by *Drosophila* during free-flight are highly stereotyped maneuvers, with very well-characterized modulations of both angular and linear velocity. I wanted to use the abundance of data collected using my tracking setup to perform a simple population-level kinematic analysis of saccades.

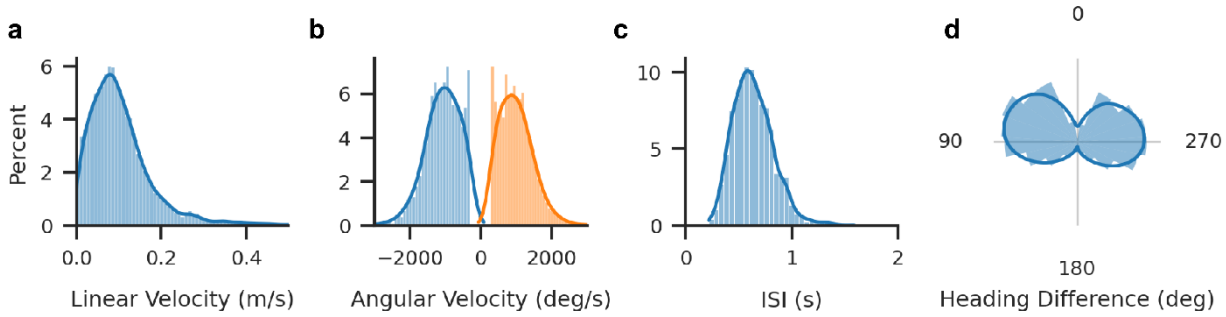

Figure 19. Kinematics of Spontaneous saccades during free-flight. (a) Distribution of linear velocities during saccade execution shows a right-skewed distribution with a clear peak, indicating stereotyped modulation of forward speed during turning maneuvers. (b) Peak angular velocities during saccades for both rightward (orange) and leftward (blue) saccades. (c) Distribution of inter-saccade intervals. (d) Polar histogram of heading changes induced by saccades reveals a characteristic bimodal distribution centered around ± 90 °, suggesting a preferred magnitude of heading changes in spontaneous flight behavior. Lines indicate the kernel density estimate (KDE) of the distribution.

Saccadic turns were characterized by sharp changes in angular velocity, with a mean peak angular velocity of 1027.4 ± 572.6 °/s (Figure 19b) and a mean linear velocity of 0.12 m/s (Figure 19a). The broad distribution of peak angular velocities indicates some variability in turn execution. The inter-saccade interval showed a slightly low median value of 0.8 saccades/s - however, this may be due to the usage of more strict saccade filtering, to make sure no walking bouts are included in this analysis. For each saccade detected, the heading difference was calculated by measuring the difference between the mean heading before and after the saccade. Analysis of these heading changes revealed a clear organization, with a bimodal distribution of turn angles centered around at ± 85 degrees, with no clear directional preference (50.5% of the turns were to the right). These results

are in line with previous studies, which also indicated that spontaneous (body) saccades have a highly characteristic kinematic profile, with similar angular velocity and changes in heading (Fry, Sayaman, and Dickinson 2005; Dickinson and Muijres 2016).

3.2.2.3. Spatial organization of saccades

It is known the avoidance/escape saccades have different kinematics parameters and execution than spontaneous saccades (Dickinson and Muijres 2016). I was interested in comparing the different flight parameters recorded in my setup, to try and identify whether saccades that occur in the central area of the arena (which are more likely to be spontaneous rather than escape) have different kinematics than saccades occurring close to the walls of the arena (which are more likely to be visually-evoked). The analysis encompassed 11,453 rapid turns from the same dataset described before, revealing a clear spatial organization in the execution of these maneuvers (Figure 20). The majority of turns (65.7%, 7529) were initiated within the central region ($r \leq 15$ cm), suggesting a strong bias toward the center of the behavioral arena (Figure 20a-b). However, an analysis of the saccade rate as the function of distance from the center (Figure 20c) revealed a more complex profile, where the flies increased their saccade rate the closer they were to the walls of the arena.

When flies did approach the arena periphery, their saccadic response was not significantly different from spontaneous saccades occurring within the center - both had a similar amplitude (987 ± 441 °/s for center saccades, 901 ± 436 °s for periphery), and similar distribution of heading changes (75 ± 36 deg for center, 65 ± 35 deg for periphery).

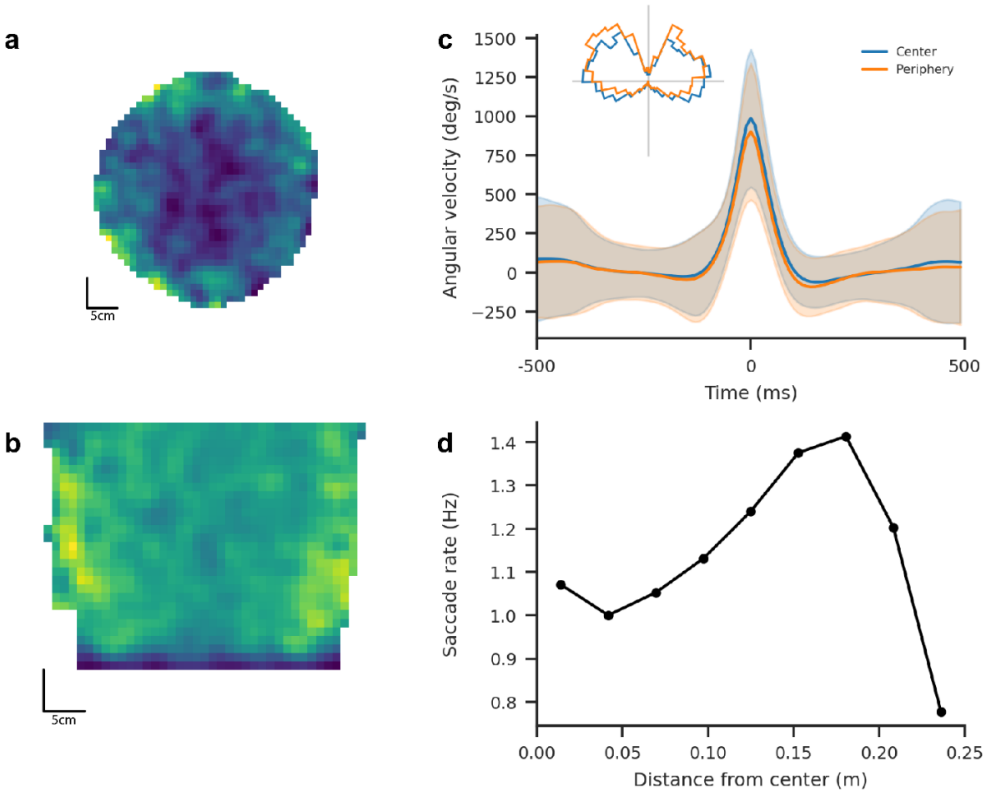

Figure 20. Spatial distribution and kinematic characteristics of rapid turns during flight. (a,c) Probability heatmaps showing the spatial distribution of rapid turns in the horizontal (xy) and vertical (xz) planes, revealing a non-uniform distribution of turn initiation locations. Color intensity indicates the probability of turn initiation, normalized by occupancy time. Scale bars: 10 cm. (b) Angular velocity for saccades in the center (n=7529) vs in the periphery (n=3924) of the arena. In the inset, the distribution of changes in heading for the two groups. Shown are the mean ± SD across saccades. (d) Saccade rate as a function of distance from the center of the arena.

Together, these findings suggest that flies tend to avoid the periphery of the arena, most likely by performing sharp saccades on approach to avoid collision. This is further strengthened by the findings that saccade rate increases as the flies approach the walls of the arena. The lack of difference in the angular velocity profile of center vs. peripheral saccades suggests that, unlike in escape saccades, expected collision-avoidance saccades may be more tightly controlled, and have similar characteristics to spontaneous saccades.

3.2.3. Behavioral Responses to Looming Stimuli

My initial analysis indicated that saccades occurring close to the walls have similar kinematic parameters to saccades in the center of the arena. This was surprising, as I

initially hypothesized that wall-avoidance saccades will have a different signature than those executed spontaneously as part of exploration. However, it is possible that there is also a difference between different types of collision-avoidance saccades. A wall collision response may be more tightly controlled, as the fly has more control over the approach. However, when a surprising incoming stimulus appears - for example, a predator or another unexpected collision - the fly must more quickly and sharply change its direction, and therefore it may have less control over the execution of the maneuver.

To characterize the precise kinematic parameters that distinguish spontaneous from "surprising" collision/escape saccades, I performed a series of experiments using an aversive looming stimulus. The stimulus was designed to expand from 5° to 75° visual angle over a 300 ms period and was presented in closed-loop at a position directly aligned with the fly's heading direction. To ensure consistent stimulus presentation conditions across trials, the looming stimulus was triggered only when flies entered a designated central region of the arena, thereby maintaining a constant distance between the fly and the display screen. This experimental design allowed for systematic comparison of kinematic parameters between baseline spontaneous turns and those elicited by a visual threat stimulus.

From 211 stimulus presentations in 20 flies over 2 experiments, I observed an escape response rate of 85.3% (180 responses), measured as the number of times out of the total where flies performed a saccade following the looming presentation. Furthermore, the response latency of the flies – measured as the time difference between the stimulus onset and the response saccade peak - had a clear peak at 360 ms. These escape saccades show similar kinematics to spontaneous saccades, with a sharp increase in angular velocity (1420.37 ± 665.28 °/s), along with a decrease in linear velocity. This was also reflected in the saccadic heading changes, which had a mean heading change of ± 135° and an angular dispersion of 44° (Figure 21).

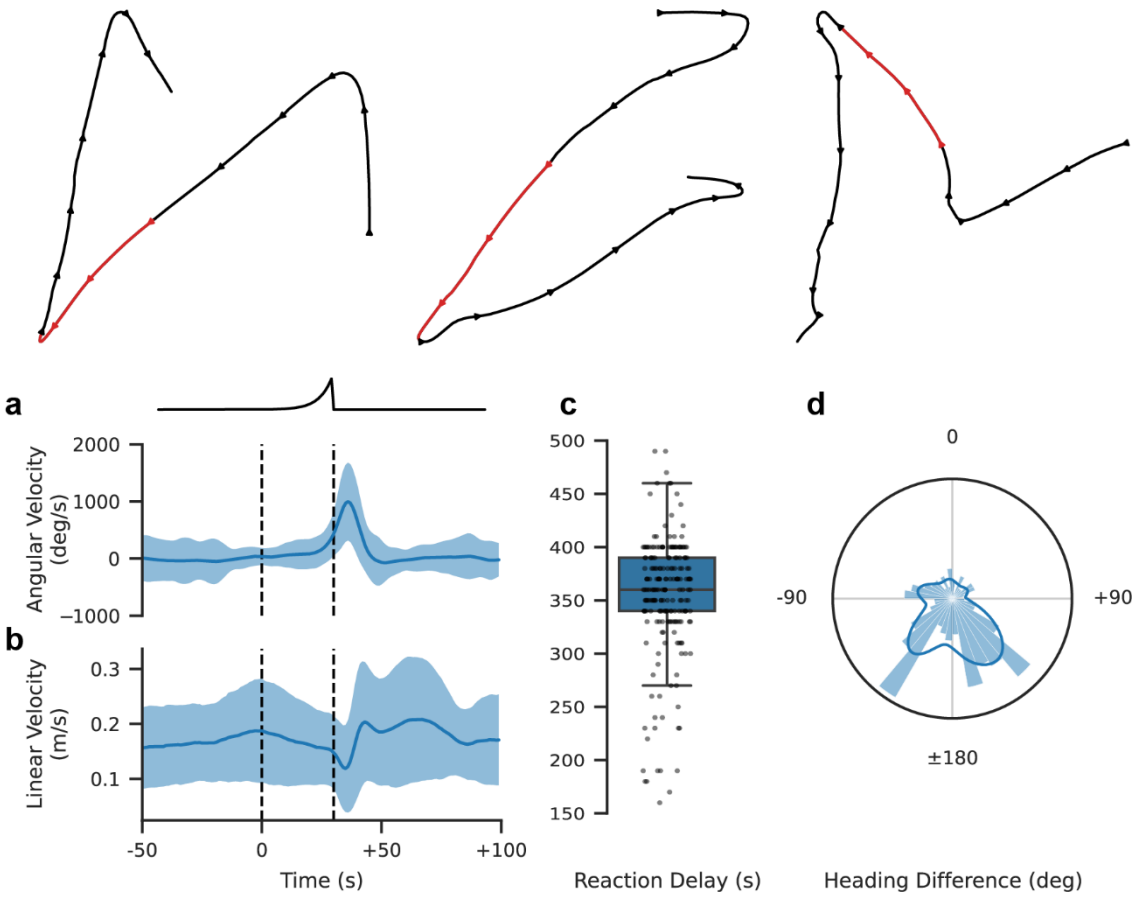

Figure 21. Analysis of escape responses to looming stimuli during free flight. Top: Representative flight trajectories showing characteristic escape maneuvers (red segments indicate stimulus presentation). Bottom: (a) Average angular velocity and (b) linear velocity responses during the presentation of a looming stimulus. (c) reaction delay from the onset of the stimulus to the peak turning response. (d) polar histogram showing the distribution of heading changes occurring due to the presentation of the looming stimulus. Dashed lines represent the onset and maximum span of the looming stimulus.

3.2.3.1. Comparison with Spontaneous Saccades

To further validate the system's sensitivity and confirm previous findings in *Drosophila*, I quantified the distinct kinematic parameters between spontaneous and visually evoked saccades. This analysis utilized the same dataset from the looming-saccade experiments, where I systematically extracted and categorized all saccadic events into either looming-evoked (n = 210) or spontaneous (n = 2425) saccades.

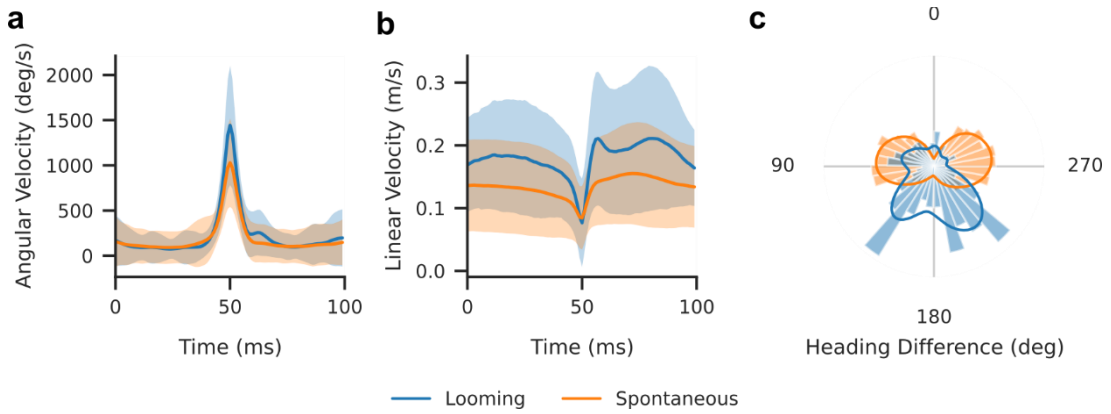

Figure 22. Comparative analysis of looming-evoked and spontaneous rapid turns reveals distinct kinematic signatures. (a) Population-averaged angular velocity profiles showing higher peak velocities during looming-evoked turns (blue) compared to spontaneous turns (orange). (b) Linear velocity profiles demonstrating characteristic modulation patterns for both types of turns. (c) Polar distribution of heading changes showing broader directional tuning in looming-evoked responses compared to spontaneous turns, suggesting distinct neural control strategies. Lines represent kernel density estimates.

Looming-evoked saccades showed clear kinematic differences in comparison to spontaneous/body saccades (Figure 22). Looming-evoked turns exhibited significantly higher peak angular velocities compared to spontaneous turns (1618.0 ± 570.04 °/s vs. 991.99 ± 464.8 °/s; Mann-Whitney U test, $U = 139316$, $p < 0.001$; Figure 22a). Furthermore, while both groups showed a reduction in linear velocity at the peak of the saccade (Figure 22b), looming-elicited saccades were accompanied by sharper decreases from baseline (-0.167 ± 0.074 m/s) in comparison to spontaneous saccades (-0.126 ± 0.063 m/s). This could indicate the lack of fine control during surprising looming events, in comparison to the more organized spontaneous turns. Finally, the distributions of heading changes showed a clear difference in the turning angles - while spontaneous saccades usually cause a change in direction of about ± 90° characterized by two clear peaks (Figure 22c), looming-elicited saccades showed a more distributed response, with peaks at ± 135° but higher variability in the response. This, again, indicates the variable nature of escape saccades, which are less controlled than body saccades (Muijres et al. 2014; 2015).

Taken together, these results both validate the ability of the tracking system to perform tightly coupled closed-loop experiments with a low latency; and show that the saccadic

response of the fly to an unexpected looming stimulus is different than either a spontaneous or wall collision-avoidance responses.

3.3. Circuit Analysis of DNa15 in Flight Control

To investigate the neural basis of saccade control, I initially focused on the descending neuron DNa15, which has been previously implicated in directional saccade control (Schnell, Ros, and Dickinson 2017; Ros, Omoto, and Dickinson 2024). First, I conducted silencing experiments using the inward-rectifying potassium channel Kir2.1 to assess DNa15's contribution to both spontaneous and looming-evoked saccades. Next, I performed bilateral optogenetic activation experiments using csChrimson expressed under DNa15 Split-GAL4 control during free flight. Finally, I investigated the specificity of DNa15's function through unilateral csChrimson expression, examining the relationship between the hemisphere of expression and the directionality of evoked turning behaviors.

3.3.1. DNa15 Silencing Experiments

3.3.1.1. Effects on Spontaneous Saccades

Silencing DNa15 neurons revealed their distinctive role in modulating spontaneous flight maneuvers (Figure 23). Analysis showed a significant but negligible difference in peak amplitude of the angular velocity between the DNa15>Kir2.1 and Empty-split>Kir2.1 groups (Figure 23a; 1139.55 ± 670.51 °/s vs 1223.35 ± 693.64 °/s, Mann-Whitney U = 4577762.0, n_1 = 1665, n_2 = 5943, $p<0.001$, Cliff's Delta = -0.07), with no significant differences in inter-saccade intervals (0.60 ± 0.36 vs 0.62 ± 0.49 saccades per second; Mann-Whitney U = 3873799.0, n_1= 1382, n_2 = 5719, $p>=0.05$, Figure 23c). However, the linear velocity profile exhibited a notable alteration in pattern (Figure 23b). While control flies displayed the characteristic sharp dip and return to baseline typical of saccades, experimental flies demonstrated a distinct kinematic difference - a mild dip followed by a rebound increase exceeding baseline levels before eventually returning to baseline. The most striking difference emerged in the heading change distribution (Figure 23d). Control flies exhibited the expected bi-modal distribution with peaks at ±87°, whereas experimental flies showed a multi-modal pattern with distinct peaks at ±45° and ± 130°.

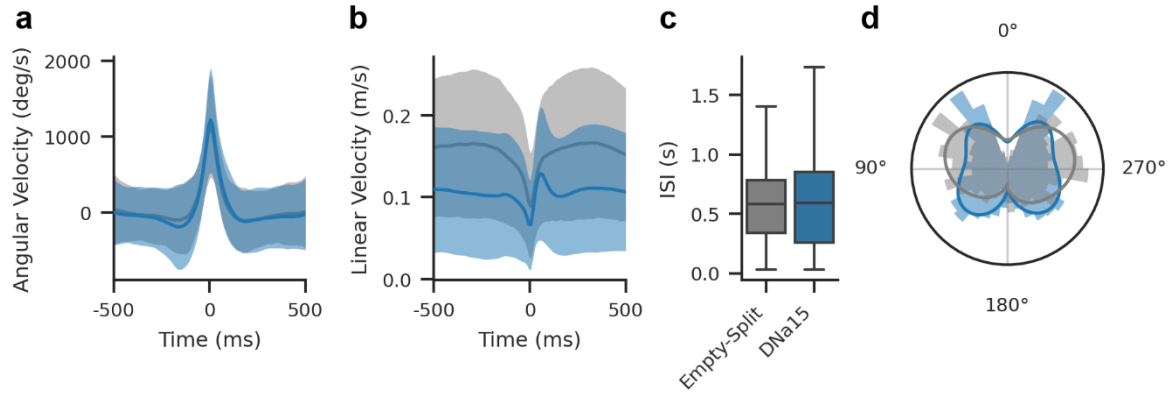

Figure 23. DNa15 silencing reveals a role in shaping spontaneous flight maneuvers. (a) Average angular velocity profiles comparing Empty-split controls (gray) and DNa15>Kir2.1 flies (blue). (b) Linear velocity dynamics during spontaneous turns show distinct modulation patterns between genotypes. (c) Boxplots showing the difference in the distribution of the inter-saccadic interval between the groups. (d) Polar distribution of heading changes demonstrates a disruption of the canonical ± 90° turn preference in DNa15>Kir2.1 flies (blue) compared to the stereotyped bimodal distribution in wild-type controls (gray).

It should be noted that these results warrant careful revalidation using more refined silencing techniques, as the current Kir2.1-mediated genetic silencing may induce developmental remodeling and compensatory mechanisms that potentially affects other saccade-related neural circuits.

3.3.1.2. Effects on Looming-elicited Saccades

While spontaneous saccades didn't exhibit large differences between experimental and control flies, it is still possible that DNa15 has a larger role in the initiation and control of visually elicited saccades than in spontaneous ones. To test this hypothesis, I used the same experimental and control flies as before, but instead focused only on saccades that were elicited by an incoming looming stimulus.

Analysis of looming-evoked saccade revealed significant differences in the behavioral profiles of DNa15-silenced flies compared to empty-split controls. The experimental group (n = 36 trials, 20 flies, 2 sessions) exhibited an enhanced escape response with significantly higher peak angular velocity relative to controls (n = 371 trials, 20 flies, 2 sessions) (Figure 24a; 1712.80 ± 608.55 °/s vs 1414.11 ± 834.93 °/s; Mann-Whitney U = 4692.0, n_1 = 371, n_2 = 36, p\<0.05, Cliff's Delta = -0.30). The linear velocity profile showed no significant differences in the response between the two groups, although the

experimental flies showed a slightly higher baseline velocity in comparison to controls (Figure 24b). Analysis of the reaction time (the delay between stimulus onset and behavioral response) showed that both control (349.19 ± 61.50 ms) and experimental flies (343.89 ± 59.41 ms) initiated escape responses with comparable latencies, suggesting that DNa15 silencing does not affect threat detection or response initiation (Figure 24c; Mann-Whitney U = 7153.0, n_1 = 371, n_2 = 36, p >= 0.05). Finally, while control flies showed an escape heading-change response similar to the one seemed before, with a peak at 107.9 ± 42°, experimental flies showed a less organized response, with a mean direction change of -150.52 ± 59.94° (Figure 24d). This slight directional bias may result from the closed-loop nature of the stimulus display, as it is possible that due to slight errors in calibration, the looming stimulus appeared slightly to the left or right of the incoming fly. Additionally, the low number of traces recorded in the experimental group may also cause an imbalance, and therefore makes direct assessment of the true effect difficult.

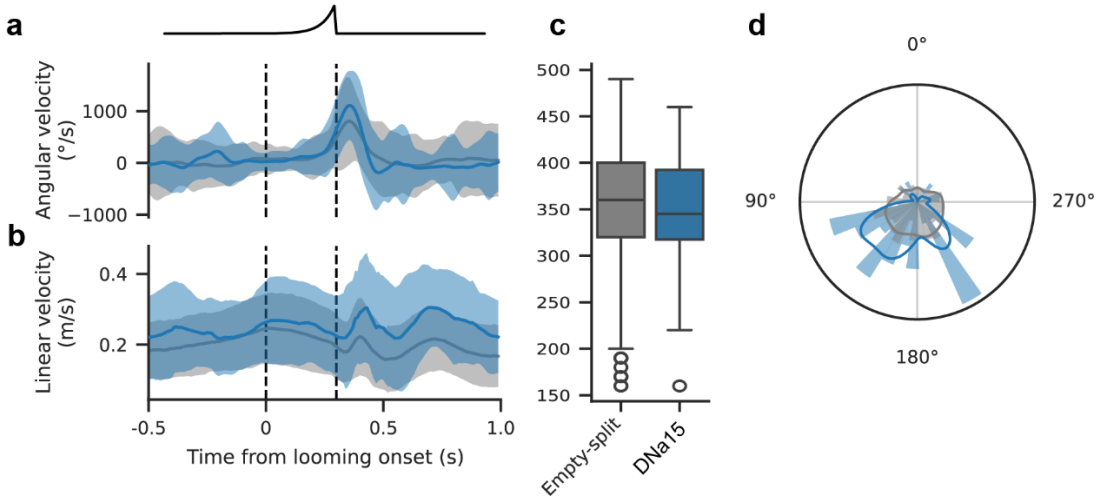

Figure 24. DNa15 silencing has little effect on looming-evoked saccade generation and control. Population-averaged angular velocity (a) and linear velocity (b) profiles during escape responses for EmptySplit-GAL4>Kir2.1 controls (gray, n = 371 trials) and DNa15>Kir2.1 (blue, n = 36 trials) flies. Dashed lines indicate stimulus presentation duration. Vertical dashed lines indicate stimulus period. (c) Quantification of reaction delays shows comparable response initiation times between genotypes. Box plots show median, quartiles, and outliers. (d) Polar distribution of escape trajectories reveals distinct organizational patterns between control (gray) and DNa15>Kir2.1 (blue) flies, with overlaid kernel density estimates.

3.3.2. Bilateral DNa15 Activation Effects

After testing the role of DNa15 using genetic silencing tools, I sought to use optogenetic tools (csChrimson) to test how direct activation of these neurons affects their flight behavior.

3.3.2.1. Power Threshold and Duration Determination

To establish optimal parameters for optogenetic manipulation, I first characterized the behavioral response of DNa15>csChrimson flies to varying light intensities. I initially attempted these experiments with a different descending neuron line, which is known to trigger backward walking upon activation. However, the behavioral responses proved inconsistent and challenging to quantify reliably, leading me to use the DNa15>csChrimson line for subsequent experiments. Flies expressing CsChrimson in DNa15 neurons were released into the behavioral arena and tracked in real-time. Optogenetic stimulation (625 nm, 200 uW/mm^2, 300 ms duration) was automatically triggered when flies entered a predefined cylindrical volume (5 cm diameter, 20 cm height) in the center of the cylindrical arena.

When exposed to red light stimulation, these flies exhibited rapid increases in angular velocity, indicating a strong turning response (Figure 25). The behavioral response scaled with stimulus intensity, showing mean peak angular velocities ranging from 451 °/s at baseline to 920 °/s at pulse-width modulation (PWM) 128 (a value of 128 on a scale of 0-255, representing approximately 50% of maximum LED intensity through pulse-width modulation), though with considerable trial-to-trial variability (Figure 25). While the highest mean response was observed at PWM 128, the differences between intensity levels were not statistically significant (Kruskal-Wallis test, H = 6.555272, df = 4, p = 0.16), an effect that is better explained by the duration flies spent within the light column, which is investigated in depth in the following section.

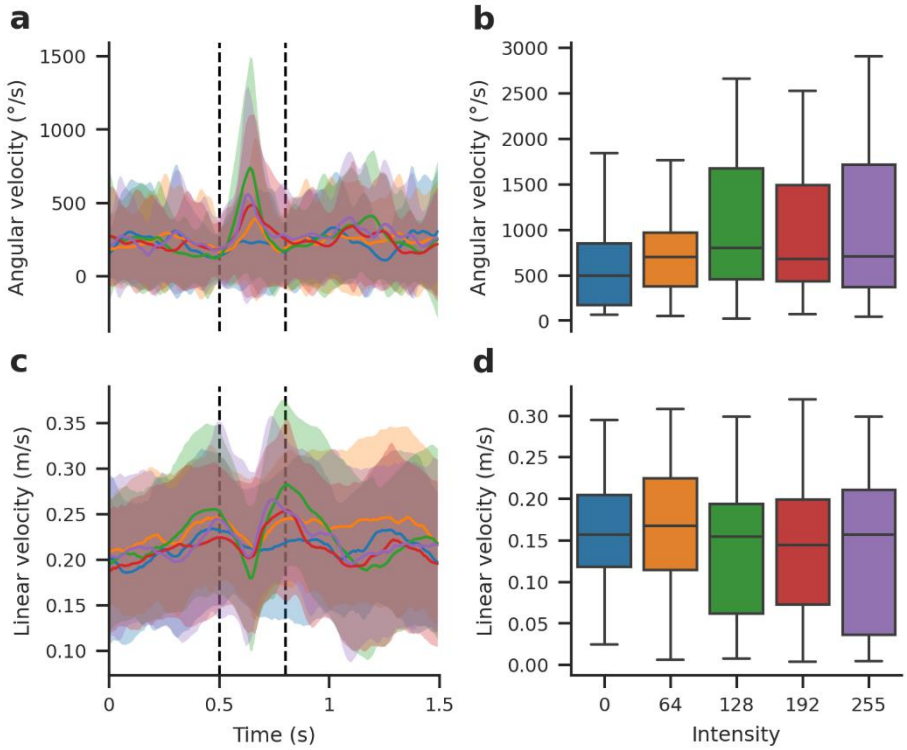

Figure 25. Characterization of optogenetic activation parameters in DNa15>csChrimson flies. Behavioral responses to red light stimulation across different intensities (left columm). Traces show mean angular velocity (a) and linear velocity (b) before, during, and after light stimulation. Response magnitude analysis at different light intensities (PWM values 0-255, right). Box plots show the distribution of peak angular velocities (a) and linear velocities (b) during stimulation. Individual data points represent single trials. Lines across boxes indicate median values, boxes show interquartile ranges, and whiskers extend to the most extreme non-outlier values.

Based on these characterization results, I selected the maximum intensity (PWM 255) for further experiments. This decision was motivated by two key factors: the anticipated variation in csChrimson expression levels across different experimental contexts, particularly in stochastic labeling experiments, and the absence of light-induced behavioral artifacts in control flies across all tested intensities (see following section).

Given that the intensity analysis suggested a more complex relationship between stimulation and behavioral output, I next investigated how the duration flies spent within the optogenetic light stimulus column influences their response magnitude. Using the high-intensity stimulation data (PWM ≥ 128), I categorized trials based on the number of frames each fly spent within the activation column (1 frame = 0.01 second). Analysis revealed a strong relationship between stimulus duration and response magnitude (Figure

26). Specifically, flies that remained in the light column for more than 20 frames (0.2 seconds) showed substantially higher peak angular velocities (median ≈ 900-1400 °/s) compared to those that stayed for shorter durations (median ≈ 200-400 °/s for 10-15 frames). Statistical analysis confirmed significant differences between duration groups (Kruskal-Wallis test, H = 51.358329, df = 5, $p < 0.001$), with post-hoc analysis revealing particularly strong differences between flies staying 10-15 frames versus those staying longer than 20 frames (Dunn's test with Bonferroni correction, $p < 0.001$). The temporal dynamics of the response also differed across duration groups, with longer-duration flies showing more pronounced peaks in angular velocity at stimulus onset (Figure 26). These findings indicate that the behavioral output is determined both by the duration of exposure to the optogenetic stimulus and its intensity.

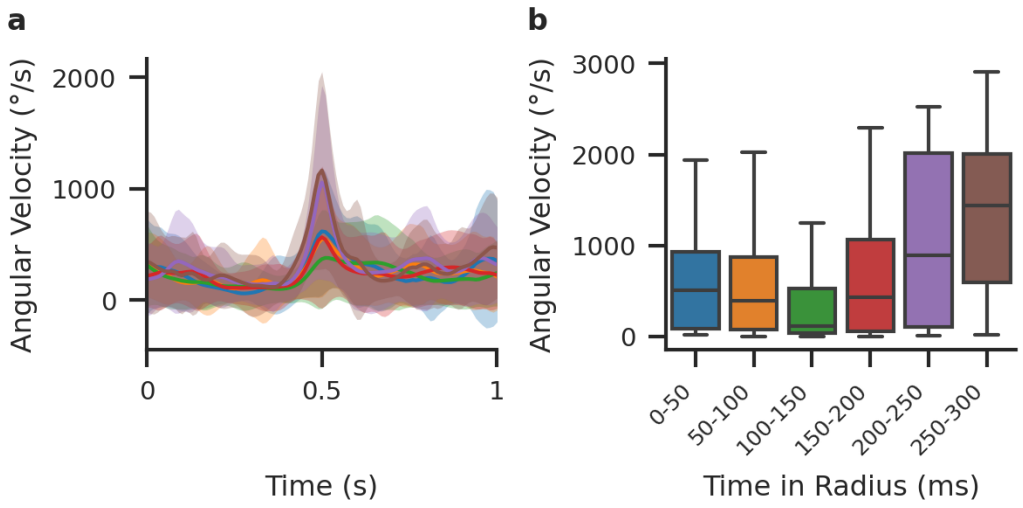

Figure 26. Response magnitude scales with duration of light exposure. (a) Time-resolved angular velocity traces for flies grouped by the number of frames spent in the activation column. Lines show mean values and shaded areas represent standard deviation. (b) Peak angular velocities across different duration bins. Box plots show median, quartiles, and range, excluding outliers. Data includes only high-intensity stimulations (PWM ≥ 128).

To more rigorously assess the relationship between stimulus intensity and duration, I performed a permutation-based two-way ANOVA (Anderson 2001). This approach was chosen over traditional parametric ANOVA due to violations of normality and uniform variance across groups in the data, as well as the lack of a robust non-parametric alternative. The analysis revealed significant main effects of both intensity ($F(4,608) = 3.50$, $p = 0.007$) and duration ($F(5,608) = 20.72$, $p < 0.001$), as well as a significant

interaction between these factors (F(20,608) = 2.00, p = 0.008). The permutation approach, based on 10,000 random reassignments of the response variables, provides robust statistical inference without relying on parametric assumptions. These results confirm that while both factors influence the behavioral output, the duration of exposure has a substantially stronger effect (as indicated by the larger F-statistic), suggesting it is the primary determinant of response magnitude. However, the significant interaction term indicates that the relationship between duration and response is not uniform across different intensity levels, highlighting the complex nature of optogenetic circuit manipulation.

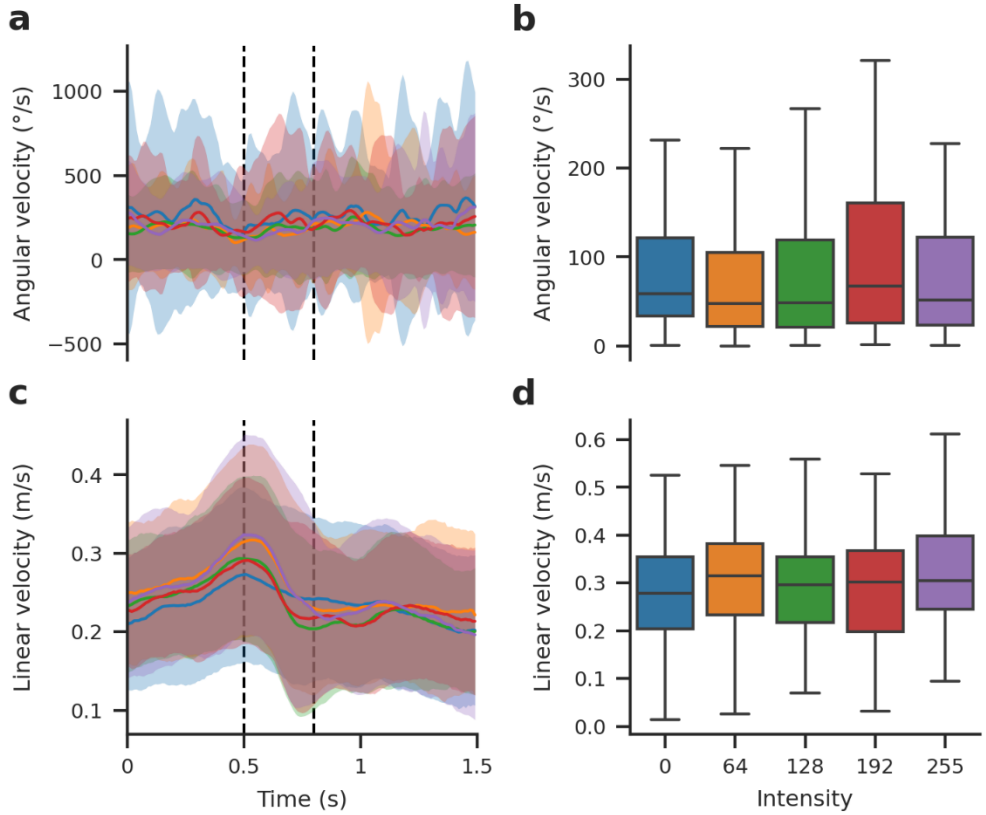

Figure 27. Control flies show no systematic response to red light stimulation. Behavioral responses of empty-split control flies exposed to different light intensities. Left panels show mean angular velocity (top) and linear velocity (bottom) across time, with shaded areas representing standard deviation. Right panels show peak velocities for different light intensities. Box plots indicate median, quartiles, and range; circles represent outliers. Control flies exhibit no systematic changes in either angular or linear velocity regardless of light intensity, confirming the specificity of the optogenetic manipulation in experimental flies.

To validate that the observed effects were specific to DNa15>csChrimson flies, I performed identical analyses on the empty-split control (Figure 27). These control flies showed no systematic changes in angular or linear velocity in response to red light stimulation, either across different light intensities (Kruskal-Wallis test, $H = 6.60$, $df = 4$, $p > 0.05$) or exposure durations (Kruskal-Wallis test, $H = 1.15$, $df = 5$, $p > 0.05$). The absence of intensity- or duration-dependent effects in control flies confirms that the behavioral responses observed in DNa15>csChrimson flies were indeed due to optogenetic activation rather than unspecific effects of the light stimulus.

3.3.2.2. Optogenetic activation leads to a sharp and fast turning response

Optogenetic activation of DNa15 neurons revealed their sufficiency to trigger rapid flight maneuvers (Figure 28). In response to the light stimulus, DNa15>csChrimson flies showed a strong increase in peak angular velocity in comparison to Empty-Split>csChrimson controls (2063.73 ± 301.35 °/s vs. 788.01 ± 646.08 °/s, Mann-Whitney $U = 4569.0$, $n_1 = 129$, $n_2 = 704$, $p<0.001$, Cliff's Delta = -0.90; Figure 28a), demonstrating that DNa15 activation is sufficient to drive strong and sharp turns (Figure 28d). Interestingly, these turns were usually accompanied by a secondary "latent" turn with a lower amplitude, which will be explored more in-depth in the next section. These increases were accompanied by a mirrored decrease in linear velocity, with a very sharp decrease for the primary, optogenetically induced turn, and a slower, more transient decrease for the secondary turn.

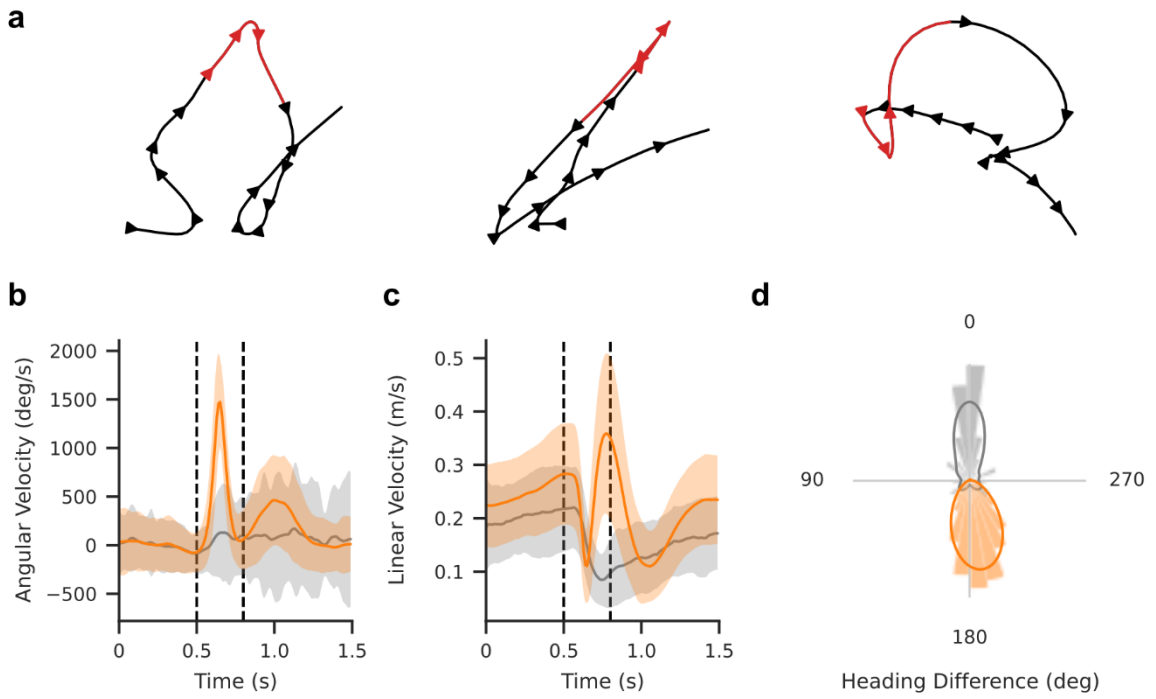

Figure 28. Optogenetic activation of DNa15 neurons evokes rapid turning maneuvers. (a) Representative flight trajectories showing induced turns in empty-split controls (gray) and DNa15>CsChrimson flies (orange). Red segments indicate light stimulation period. (b) average angular and (c) linear velocity traces for the two groups. (c) polar histogram of heading differences distribution as a result of the optogenetic light. Dashed lines represent duration of optogenetic stimulus.

Most strikingly, DNa15 activation produced strong changes in heading. While control flies in general showed a low reaction to the light activation, as evident by the mean heading difference of 1.89 ± 68.9° (indicating a continued straight flight), experimental flies showed a much stronger turning reaction to the light, with a mean heading change of -171 ± 31° - which is indicative of a complete change of direction in flight heading on average. Furthermore, analysis of the turn direction showed them to be completely stochastic, with about 50% of the turns heading to the left vs right (Figure 29).

These results demonstrate that DNa15 neurons are sufficient to trigger a turning response when activated, although with a higher amplitude and change in heading in comparison to spontaneous saccades (see later section for more in-depth analysis). This suggests these neurons may have a command-like role in a saccade generation circuit. However, it is possible the nature of these opto-elicited turns (strong and sharp) is an artifact of the artificially long and strong activation paradigm. Furthermore, bilateral activation most likely

does not reflect their normal activity pattern, which makes drawing exact conclusions difficult. Nevertheless, it is clear from both the silencing and activation experiments that DNa15 plays a role in the generation and modulation of saccades.

3.3.2.3. Relationship between Primary and Secondary Turns

As seen in Figure 28, the main optogenetically-elicited turns were usually followed by a second weaker and slower turning response. To test whether there was any relationship between the primary and secondary turns, I performed a transition probability analysis, focusing on the direction and amplitude of the turns. The transition probabilities between successive turns demonstrated a balanced distribution of directional changes, with approximately equal probabilities (~0.5) for maintaining or switching turn direction regardless of the initial turning state (Figure 29a; χ^2 test, $\chi^2(1) = 1.16$, $p = 0.28$). Furthermore, no correlation was found between the amplitude of the primary and secondary turns, whether the fly maintained its direction or changed it (Figure 29b).

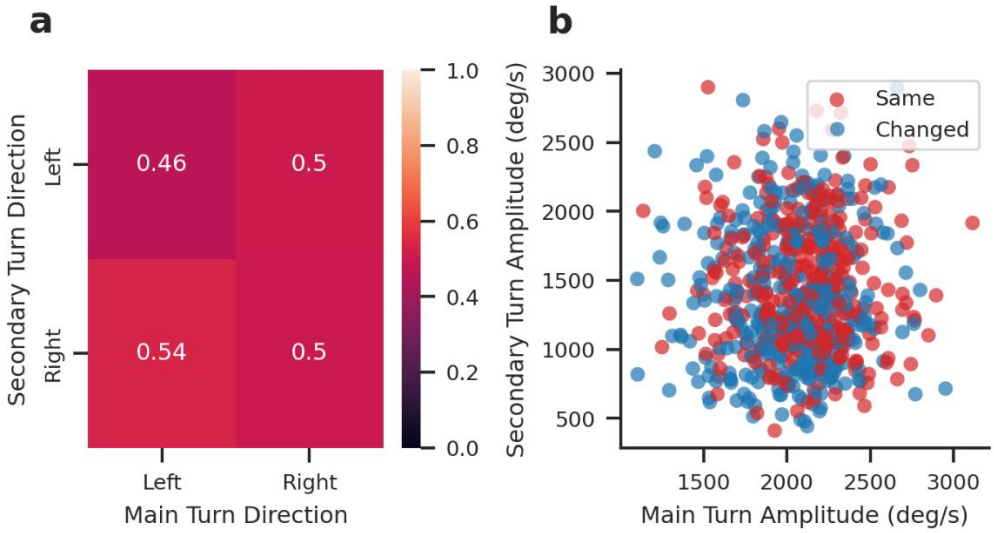

Figure 29. DNa15 activation leads to a secondary turn which is uncorrelated with the primary. (a) Transition probability matrix showing the relationship between initial (main) and subsequent (secondary) turn directions during optogenetic stimulation. Values indicate the probability of transitioning between directional states. (b) Relationship between main and secondary turn amplitudes, colored by directional consistency (red: same direction maintained, blue: direction changed).

The fact that the secondary turning direction appears to be completely random and uncorrelated with the primary response suggests this may not be a rebound effect, but rather an artifact of the artificially strong optogenetic activation. Alternatively, the

secondary turn may be some compensatory response to return to the initial flight direction - although then it would be expected that the secondary turn will more likely be in the opposite direction to the primary turn.

3.3.2.4. Effect of previous spontaneous saccade on optogenetic saccade direction

To investigate potential interactions within the saccade-generation circuit, I chose to examine whether recently executed spontaneous turns influenced the amplitude or direction of the opto-elicited saccade.

Analysis of the interaction between spontaneous and optogenetically-evoked behaviors revealed systematic dependencies in the control of flight maneuvers (Figure 30). The directional relationship between spontaneous and evoked turns demonstrated structured variability, with transition probabilities showing a slight bias toward maintaining turn direction for leftward pre-saccades (0.53) and switching direction for rightward pre-saccades (0.60). Chi-squared analysis confirmed that these transition probabilities deviated significantly from chance-level expectations (χ^2 test, $\chi^2(1)$ = 4.68, p = 0.030, Cramer's V = 0.071), though with a negligible effect size (Figure 30a).

The amplitude relationship between spontaneous and optogenetically-elicited turns also showed not correlation (1026.36 ± 477.51 °/s vs. 1913.45 ± 537.09 °/s, Pearson's r = -0.05, p > 0.05), with optogenetically-triggered responses spanning a broad range (500-3500 °/s) regardless of pre-saccade amplitude (Figure 30b). This amplitude independence persisted whether the fly maintained its original turn direction or executed a directional reversal.

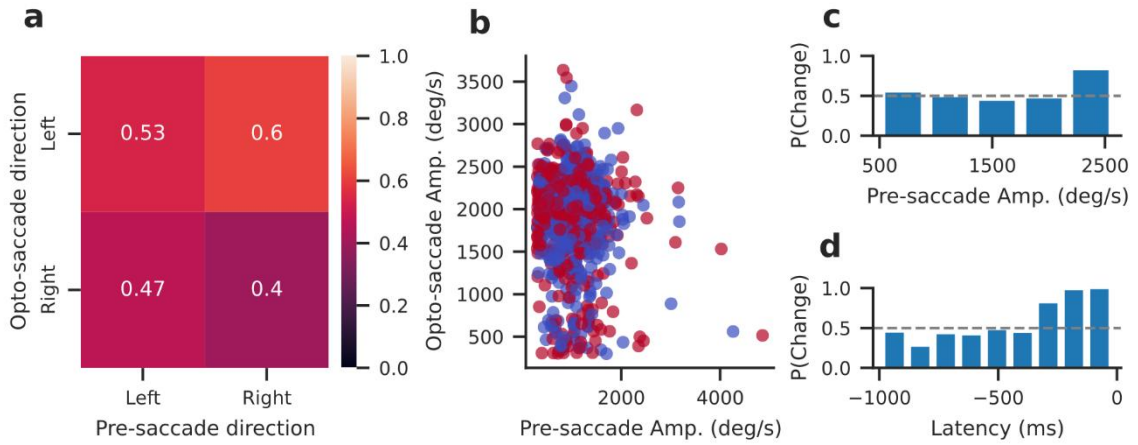

Figure 30. DNa15 activation is influenced by recent behavioral history. (a) Transition probability matrix showing the relationship between spontaneous pre-saccade and optogenetically-evoked turn directions. Values indicate transition probabilities between directional states. (b) Relationship between pre-saccade and optogenetically-evoked turn amplitudes, with points colored by directional consistency (blue: maintained direction, red: direction changed). (c-d) Probability of direction changes as a function of pre-saccade amplitude (c) and temporal latency between spontaneous and evoked turns (d). Dashed lines indicate chance level (0.5).

However, while population level analysis revealed no clear dependence of opto-saccade on previous spontaneous saccades, further analysis revealed that the probability of direction changes was partially dependent on the pre-saccade amplitude (Figure 30c) and latency (Figure 30d), as defined by the time difference between the previous spontaneous saccade and opto-saccade. The probability of direction change remained on chance level for all pre-saccade amplitude bins, except for the highest amplitude bin, which showed an increase to a 75% chance of direction change. Additionally, the temporal relationship between spontaneous and evoked turns showed a marked effect, with shorter latencies (<500 ms) associated with lower probabilities of direction changes, while longer intervals (>500 ms) exhibited increased probabilities of directional reversals (Figure 30d).

These findings suggest that the activity of DNa15 may be influenced by recurrent inhibitory connections, so that when a fly turns to a certain direction, a neuron within the saccade initiation or generation network on that side undergoes hypoerpolarization, thus reducing the probability of it immediatly eliciting a saccade to the same direction. Such a network was recently suggested by Ros, Omoto, and Dickinson 2024, who demonstrated that DNa15 and DNb01 form functional saccade-generating units with recurrent inhibitory

connections. Their connectome analysis revealed that DNb01 forms inhibitory connections to contralateral DNa15 cells, creating a reciprocal inhibitory network motif. This circuit organization could explain why recent activity in one turning direction temporarily reduces the probability of subsequent turns in that same direction, particularly at short latencies.

3.3.2.5. Comparison of optogenetic-elicited with spontaneous saccades

Optogenetically elicited saccades show a unique kinematic signature in comparison to spontaneous saccades. To better study the exact differences, I performed a comparative analysis of both saccade types by time-aligning them and measuring the different kinematic parameters (Figure 31). The optogenetically-induced saccades showed a significantly higher average peak in comparison to spontaneous saccades (1607.35 ± 800.61 °/s vs. 1179.12 ± 678.91 °/s; Mann-Whitney U test, U = 12872924.5, $p < 0.001$, Cliff's delta = -0.366; Figure 31a). This was also reflected in the sharp decrease in linear velocity seen in experimental flies; however, this is confounded by their baseline flight velocity being higher than wild-type or control flies, which will require further investigation. Most importantly, while spontaneous saccades exhibited the classic ±90° turning preference (Figure 31c), experimental flies - as seen before - showed a strong and sharp turning response, changing their heading by 180° on average.

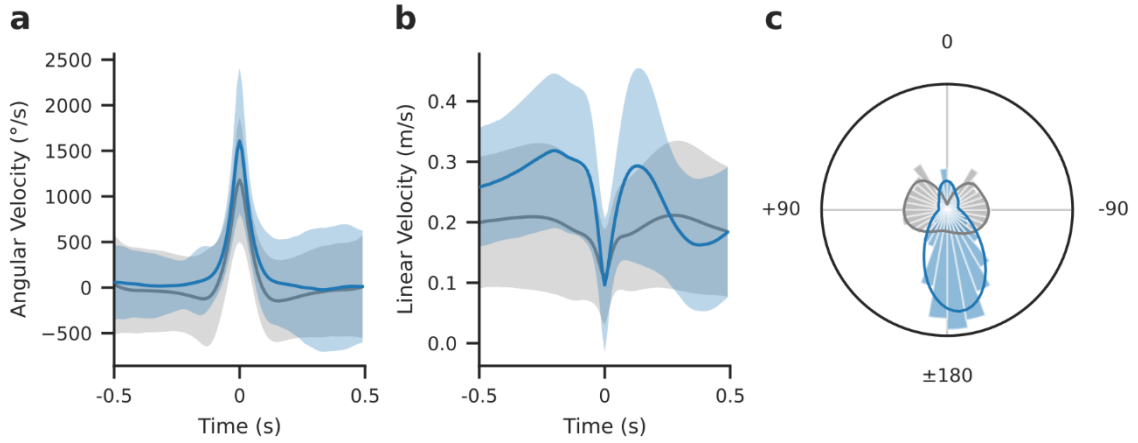

Figure 31. Optogenetic activation of DNa15 neurons evokes high-amplitude turning behavior with distinct kinematic features. (a) Population-averaged angular velocity profiles showing enhanced rotational responses during DNa15 activation (blue) compared to spontaneous turns (gray). (b) Linear velocity profiles revealing distinct modulation

patterns between evoked and spontaneous turns. (c) Polar distribution of heading changes demonstrates increased directional stereotypy in optogenetically-evoked turns.

As mentioned before, however, the artificiality and strength of this type of optogenetic activation, along with the bilateral expression pattern - as reflected in the much stronger turning behavior compared to spontaneous turns - makes it difficult to explore whether activation of DNa15 is enough to elicit a “proper” saccade or a different type of turning behavior.

3.3.3. Unilateral Activation Experiments

The previous bilateral activation experiments indicated that DNa15 has a role in the generation or control of saccades, and that activation of these neurons leads to a turning behavior which is much stronger in both amplitude and heading change in comparison to wild-type and empty-split control flies. However, the artificial nature of the optogenetic activation, along with the bilateral nature, precludes exact analysis. To overcome this limitation, I have chosen to use stochastic labelling tools. These tools could enable expression of our effector of interest (csChrimson) in a subset of cells within the population defined by the Split-GAL4 line, with the direct purpose of expressing the effector only on one side of the brain. Following the behavioral experiment, the fly can be retrieved from the arena, and the exact expression pattern validated using immunohistochemistry.

3.3.3.1. FlpOut System Implementation

My initial approach to achieve unilateral manipulation of DNa15 neurons employed the heat-shock-inducible FlpOut system (Figure 31). Through optimization experiments, I settled on a protocol using a 1-hour heat shock at 37°C, applied to the progeny at 3-days post egg-laying.

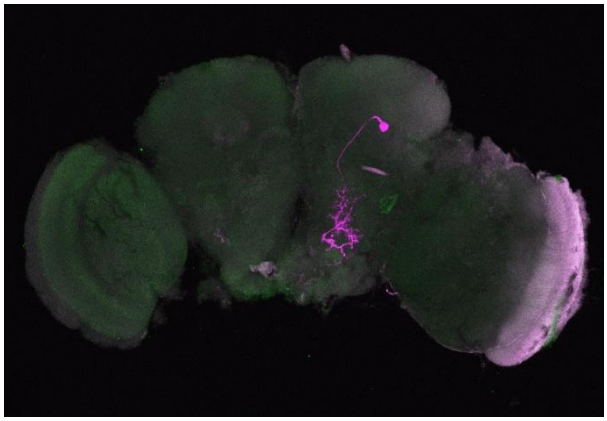

Figure 32. Example of unilateral labelling in a DNa15>FlpOut fly.

Analysis of 28 heat-shocked brains demonstrated moderate success rates, with approximately 3 flies (~10%) showing bilateral expression, 14 flies (50%) showing unilateral expression, and the rest (11, ~40%) showing no expression. However, I discovered our DNa15 split-GAL4 line leads to

expression in two types of descending neurons - DNa15 and DNa05. This made the analysis more difficult, as both neurons have a very similar morphology, and exact identification proved difficult.

Perhaps most concerning was the frequent disconnect between anatomical expression patterns and behavioral responses to optogenetic stimulation. I encountered numerous cases where flies showing clear anatomical expression of csChrimson failed to exhibit any behavioral response to light activation. Conversely, and equally problematic, I observed robust behavioral responses in flies where careful confocal analysis revealed no detectable csChrimson expression. This fundamental inconsistency between anatomical and functional readouts raised serious concerns about the reliability of the FlpOut system for precise circuit manipulation studies in our system.

Nevertheless, several heat shock-dependent flippase experiments showed interesting results. Analysis of three individual flies demonstrated how unilateral expression can influence directional control during optogenetically-triggered behaviors (Figure 33). The first fly, showing no detectable csChrimson expression, showed a negligible response to the optogenetic light (622.83 ± 603.09 °/s, n = trials) with relatively straight trajectories (-0.33 ± 48.83°). In contrast, a second fly with left-hemisphere expression showed stronger turning responses (1126.19 ± 533.33 °/s, n = trials) with a clear leftward turning bias (-87.50 ± 44.39°). Finally, a third fly with right-hemisphere expression displayed elevated turning responses (994.48 ± 512.60 °/s, n = trials) coupled with consistent rightward turns (74.54 ± 46.97°). However, none of the flies showed a turning response as strong as seen in the bilaterally-expressing DNa15 group, either in the angular velocity peak or the heading difference changes.

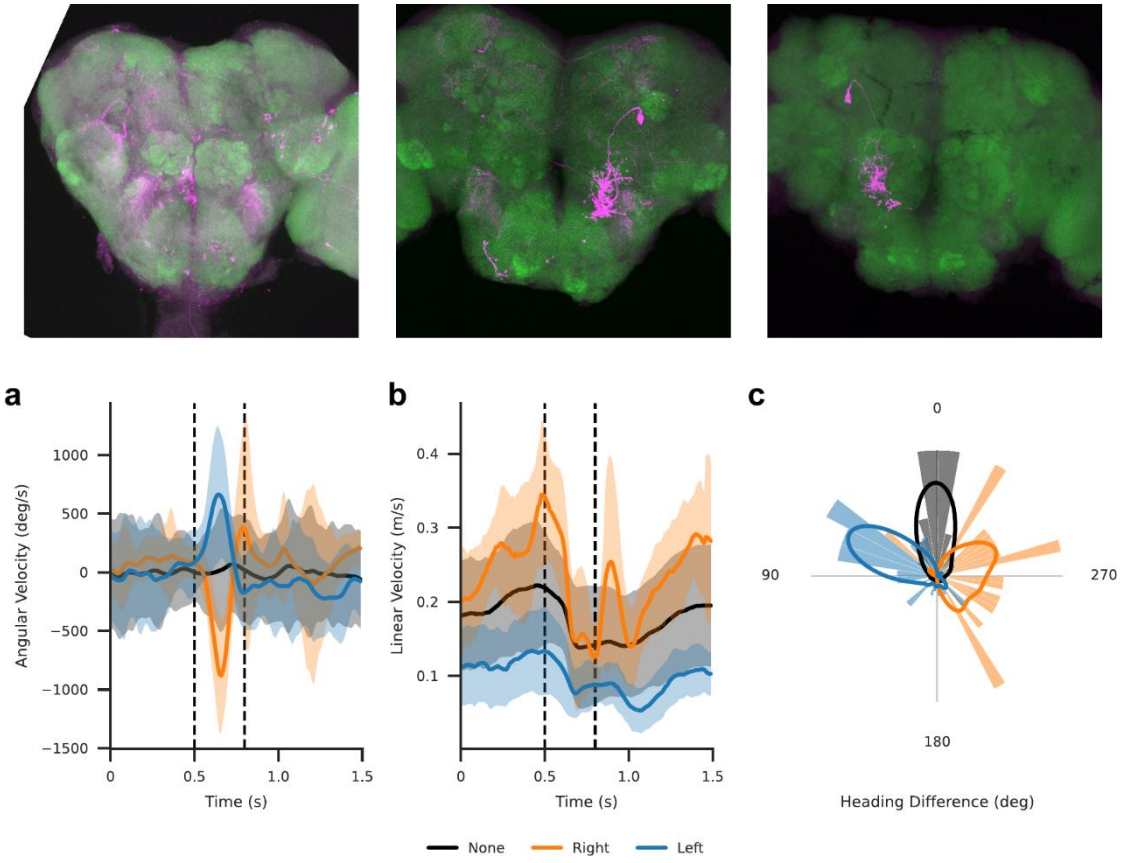

Figure 33. Unilateral DNa15 activation can drive directional turning behavior. Top: Example of three *Drosophila* brains, showing different csChrimson expression patterns (from left to right: no expression, unilaterally left, and unilaterally right). Bottom: (a) Angular velocity response of each fly to the optogenetic stimulus (black - no labeling, blue - unilateral left, orange - unilateral right). (b) Linear velocity response of each group. (c) Distribution of heading differences for each group, showing no preference for flies without csChrimson expression, and an ipsilateral turning preference for the other two flies.

When analyzing the aggregate data across all DNa15>FlpOut flies (excluding flies with fewer than 5 activation trials), no significant qualitative differences emerged between the expression pattern groups (none, bilateral, and unilateral). The peak angular velocities remained comparable across conditions (none: 843 ± 279 °/s, bilateral: 742 ± 184 °/s, unilateral: 824 ± 635 °/s), with similar patterns observed in linear velocity measurements. Notably, these values were markedly lower than those observed in flies expressing csChrimson bilateral in DNa15, who exhibited peak angular velocities approaching 2000 °/s (Figure 34a). The linear velocity profile (Figure 34b) similarly showed no clear differences, and the average heading difference distributions (Figure 34c) for all groups were centered around 0°.

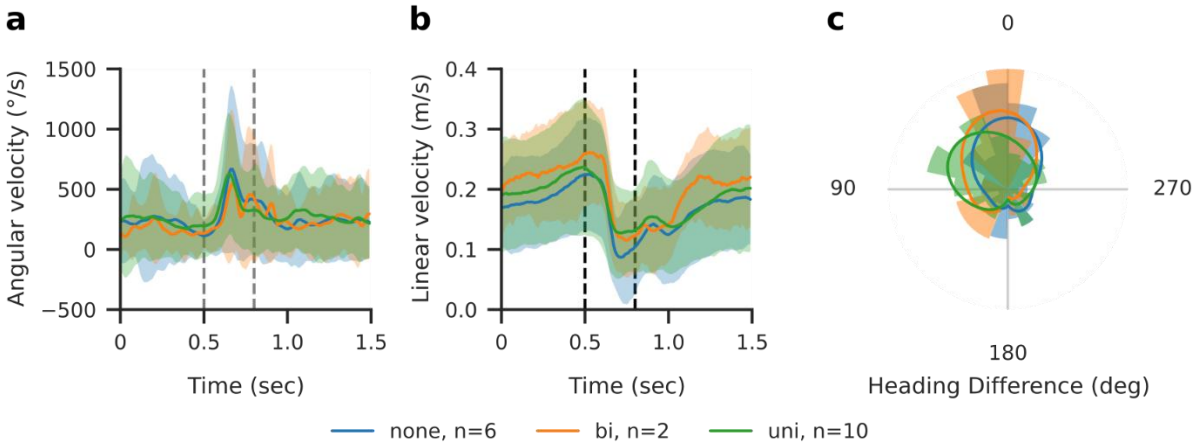

Figure 34. Average behavioral responses to optogenetic activation in FlpOut experimental flies. (a) Angular velocity profile showing distinct patterns in response to stimulation, with varying magnitudes and directions of turns. (b) Linear velocity measurements demonstrating different forward movement patterns during and after stimulation periods. (c) Distribution of heading differences. Data represents three groups of stochastic labelling: flies with no csChrimson expression (blue, n = 6 flies), bilateral expression (orange, n = 2 flies), and unilateral expression (green, n = 10 flies).

While individual cases suggested a potential command-like response, where activation of a single neuron on one side may elicit a saccadic behavior, the population level analysis complicates this conclusion. Perhaps more intriguing was the behavioral responses observed in flies showing no detectable expression through immunohistochemistry. Although the genetic background of the driver or effector line may cause a non-specific light induced response, the lack of similar behavior in control lines (Empty-Split>csChrimson or FlpOut:csChrimson>DNa15 without heat shock) rules out this explanation. Alternatively, the immunohistochemistry procedure may have been unsuccessful, due to an issue with the antibodies or other reagents.

3.3.3.2. SPARC System Approach

Due to the inconsistent results and technical challenges of heat-shock dependent stochastic expression methods, I implemented the more reliable SPARC (*Sparse Predictive Activity through Recombinase Competition*) system (Isaacman-Beck et al. 2020). This approach offers significant advantages over traditional FlpOut methods: it eliminates the need for carefully timed heat shocks by utilizing PhiC31 integrase and competing recombination sites with different efficiencies. The SPARC system enables precise targeting of predictable proportions of cells within a population through variants

with different truncated attP sites. The most restrictive version (SPARC-S) consistently labels approximately 5% of cells in a population, while the intermediate (SPARC-I) and permissive (SPARC-D) variants label about 20% and 50% of cells, respectively, enabling reliable sparse labeling for single-cell analysis.

Usage of the SPARC system provided more reliable results. Out of 25 experimental flies, 9 showed bilateral expression pattern, 11 no expression, and 5 unilateral expressions. However, similarly to the FlpOut lines, there were cases where a fly with no expression showed a behavioral response, although those were less common. Alternatively, there were cases where a bilateral expression was seen, with a mixture of neurons - a single DN on one wide and two on the other. Furthermore, even among the flies showing unilateral csChrimson expression (n = 5), none showed a neuron-specific expression pattern; instead, different expression patterns were seen, such as expression in DNa15 in one side concurrent with DNa05 on the other side (see later), or labeling of both DNa15 and DNa05 on the same side. Thus, it was difficult to attribute the optogenetically-elicited behavior to one specific DNs. Additionally, some flies showed non-specific labeling - meaning, neurons other than DNa15 and DNa05 showed strong expression following immunostaining, which may indicate a leakage of csChrimson expression as a result of the SPARC system.

However, several individual flies did show a strong unidirectional turning response, which correlated with the appropriate expression pattern. Three such examples are in Figure 35 (gray, n = 15, 388.42 ± 280.34 °/s), one with expression only on the left (blue, n = 14, 1079.27 ± 417.65 °/s), and one with expression only on the right (orange, n = 13, 1061.77 ± 309.10 °/s). Both flies exhibiting a unilateral expression pattern showed a clear increase in angular velocity compared to the control flies (Figure 35a), which was accompanied by a decrease in linear velocity (Figure 35b), and the corresponding changes in heading differences as a result of the saccade. The flies with no expression of csChrimson showed a continued straight flight as a response to the light (heading difference 8.75 ± 31.13°), while the fly with unilateral left expression showed a tendency to turn to the left (99.15 ± 38.73°) and vice versa for the unilateral right (-80.82 ± 55.88°) (Figure 35c).

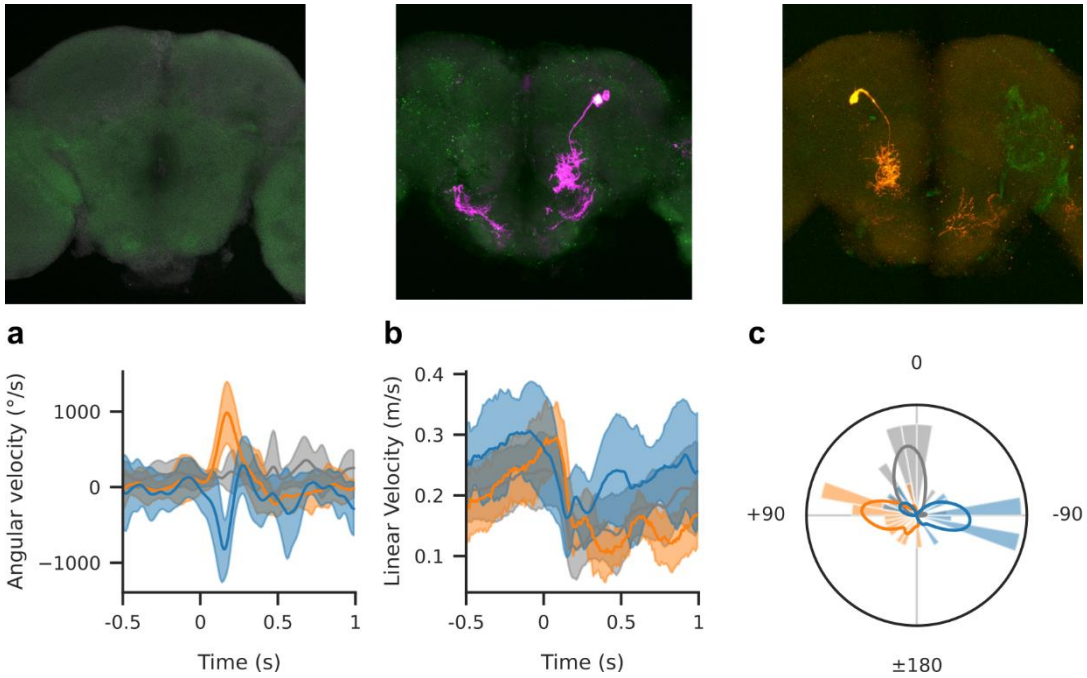

Figure 35. Example of SPARC-driven unilateral expression patterns and behaviors. Top: Example of three *Drosophila* brains, showing different csChrimson expression patterns (from left to right: no expression, unilaterally left, and unilaterally right). Bottom: (a) Angular velocity response of each fly to the optogenetic stimulus. (b) Linear velocity response of each group. (c) Heading change distribution. Data represents three flies, where: gray - no labelling; blue - labelling on the left; orange - labelling on the right).

Furthermore, and unlike the FlpOut>DNa15 flies, SPARC flies showed a more stable (although less pronounced) population response (Figure 36). When performing a population average, both bi- and uni-laterally expressing flies showed a clear (but diminished in comparison to csChrimson>DNa15 flies) peak angular velocity response, while the flies with no expression (none) showed no turning response. However, similarly to FlpOut>DNa15, the average turning response of SPARC flies was weaker than of the non-stochastic bilateral csChrimson>DNa15 flies.

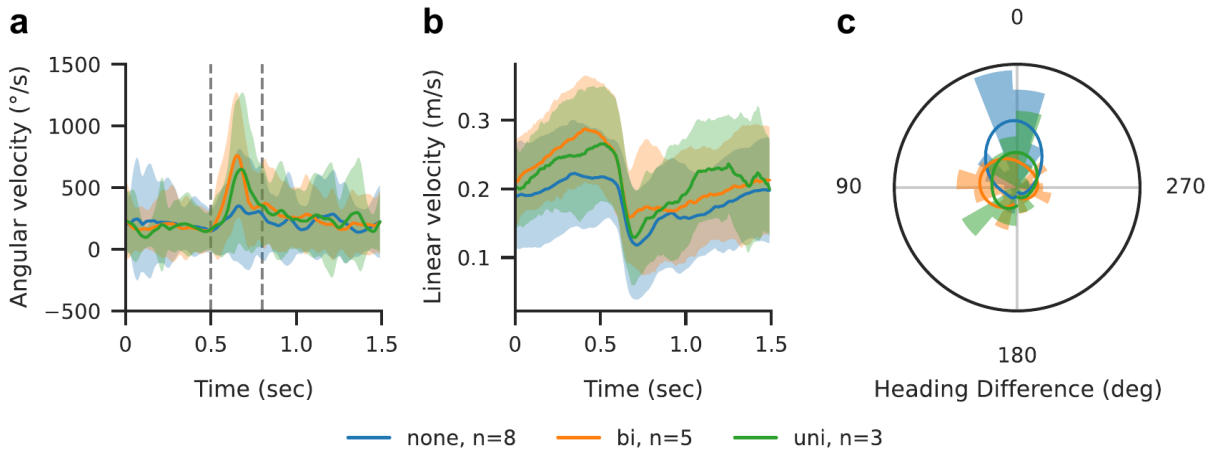

Figure 36. Averages of all identifiable SPARC-labelled flies. Angular (a) and linear (b) velocity traces for each of the different groups. (c) heading differences distribution for each of the labelling groups. Data represents three groups of flies, where blue are flies that showed no expression of csChrimson (n = 8), orange are flies who showed bilateral expression (n = 5), and green showed unilateral expression (n=3).

3.4. DNa05

When analyzing the immunohistochemistry from the csChrimson-expressing flies, I noticed that very often another neuron within our DNa15 line was labelled. This neuron was identified as DNa05, which shares many input and output partners, as well as a very similar morphology with DNa15. I therefore chose to test how optogenetic activation of DNa05 affects the behavior of flies in flight. It is important to notice, however, that even the DNa05 line used has co-expression with DNp11; it will therefore be imperative to perform more accurate experiments using either a split-GAL4 line which is unique to DNa05 or testing several different lines which label DNa05 along with other neurons, to try and isolate its influence on flight behavior.

3.4.1. Optogenetic activation of DNa05

Optogenetic activation of DNa05 led to several unique findings (Figure 37). First, DNa05>csChrimson flies (n = 34) showed significantly higher mean peak angular velocity compared to controls (n = 124) (2417.93 ± 574.89 °/s vs. 788.01 ± 646.09 °/s; Mann-Whitney U test, U = 177.0, $p < 0.001$, Cliff's delta = 0.645, Figure 37a). This effect was similar to what I observed with DNa15 activation. However, unlike DNa15, activation of DNa05 showed a very different kinematic profile - rather than having a single sharp peak, the angular velocity increased significantly and then slowly returns to the baseline. When

inspecting the actual flight trajectory, a distinct pattern emerged (Figure 37, top) - following the optogenetic activation, the flies continued to loop for about a second on the x and y axes. This is also reflected in the linear velocity traces, where experimental flies showed the standard sharp dip at the peak of the turn, followed by a quick return to baseline (Figure 37b). This behavior also makes analysis of turning direction difficult, as there is not a clear cutoff for the "end" of the turn - this is reflected in the heading difference analysis (Figure 37c), which shows the controls generally do not respond to the optogenetic activation (1.90 ± 68.93 °/s), while the experimental flies show a generally broader distribution of heading changes (-153.36 ± 62.76 °/s), with a slight bias to the left.

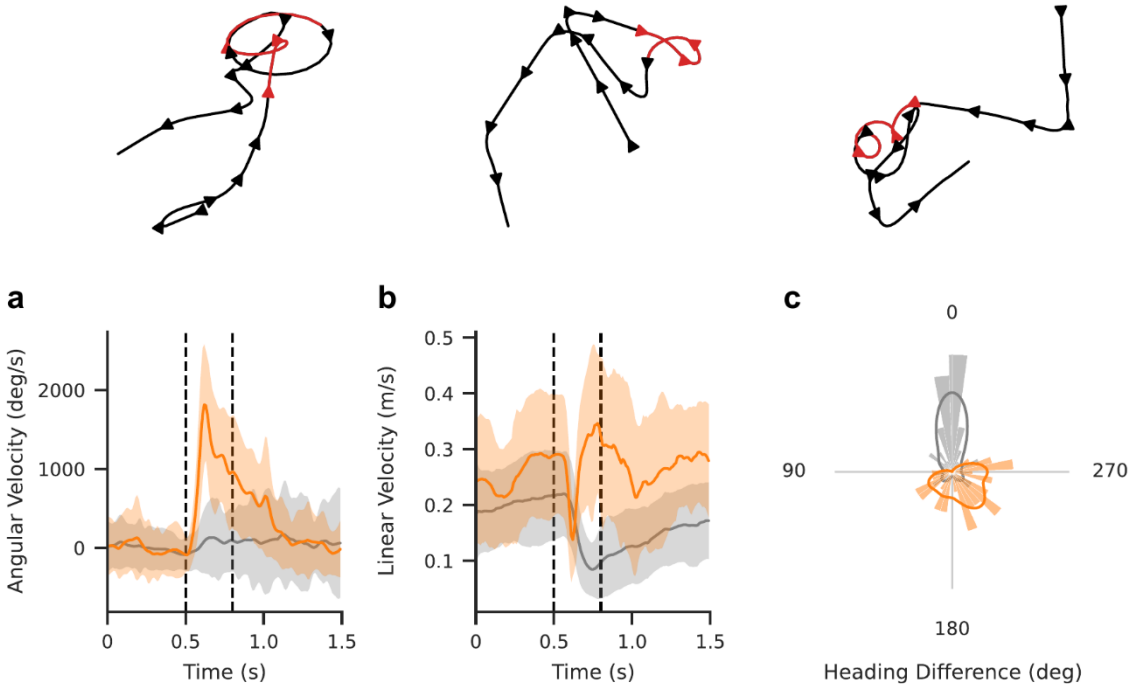

Figure 37. Optogenetic activation of DNa05 leads to an increase in angular velocity with less organized directionality. Top: Representative flight trajectories showing rapid turns in DNa05>CsChrimson flies (orange) compared to empty-split controls (gray). Red segments indicate light stimulation period. Bottom: (a) Average angular velocity and (b) linear velocity responses to the optogenetic light stimulus. (c) Polar distribution of heading changes. Dashed lines indicate the duration of optogenetic activation.

Taken together, these results could indicate that activation of DNa05 leads to some recurrent activity within the turning circuit. Alternatively, DNa05 activity may have a long decay time, but it may be inhibited by other neurons in the system. Furthermore, the long

off-kinetics of csChrimson and prolonged activation may elicit a stronger response in these subsets of DNs specifically.

3.4.2. Silencing of DNa05

I next wanted to further examine the role of DNa05 in saccade generation and control using silencing tools, similar to DNa15. Silencing DNa05 neurons did not reveal significant changes in saccade generation for either spontaneous (Figure 38) or looming evoked (Figure 39) saccades. The same set of experiments were used for both the analysis of spontaneous saccades as well as looming-evoked saccades. These experiments used a total of 20 flies over 2 recording sessions, yielding a total of 284 trajectories with 1465 saccades for the Empty-split control group, and 18 trajectories with 192 saccades for the DNa05>Kir2.1 group. For the looming evoked experiments, the control group flies were presented with an oncoming loom 426 times, while the experimental group had only 37 trials.

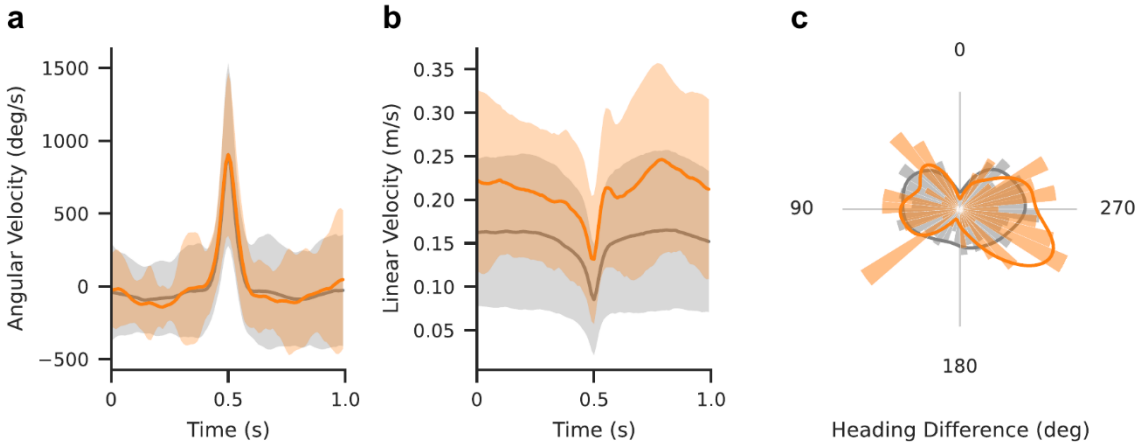

Figure 38. DNa05 silencing reveals no specific contributions to spontaneous flight maneuvers. (a) Population-averaged angular velocity profiles comparing spontaneous turns between DNa05>Kir2.1 (orange) and control flies (gray). (b) Linear velocity profiles demonstrating elevated baseline flight speeds in DNa05>Kir2.1 flies while maintaining characteristic modulation patterns. (c) Polar distribution of heading changes showing preserved directional preferences despite DNa05 silencing.

Spontaneous saccades showed as similar angular (Figure 38a) and linear (Figure 38b) velocity profiles, as well a similar distribution of heading changes (Figure 38c). Similarly, silencing of DNa05 showed no difference in the flies' response to an aversive looming stimulus (Figure 39). The peak angular velocity (Figure 39a) values for both the control

and experimental groups were statistically significantly different, but with a negligeble effect size (1142 ± 579 °/s vs. 1054 ± 491 °/s; Mann-Whitney U = 8238, p < 0.05, Cliff's delta = 0.09) .Additionally, no clear differences were found in the reaction delay to the onset of the looming stimulus (Figure 39b; 33 ± 9 ms vs 30 ± 10 ms; Mann-Whitney U = 7131.5, p > 0.05). While the heading difference plot (Figure 39c) shows a slightly more noisy circular distribution for the experimental flies, this is most likely a result of the low number of trials.

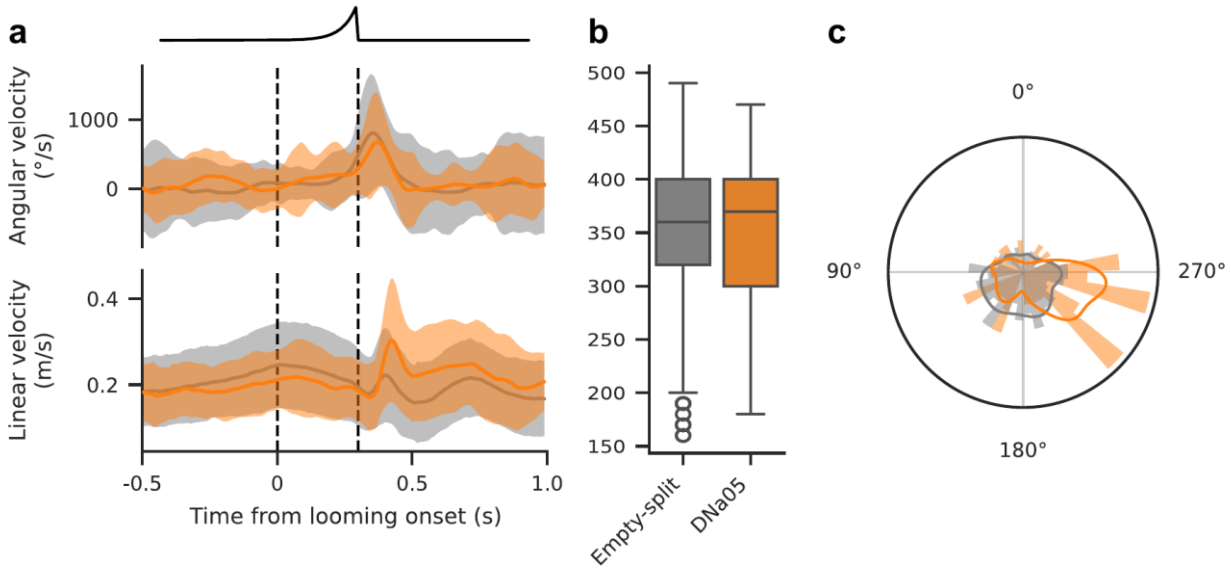

Figure 39. DNa05 Neuronal Silencing Does Not Significantly Affect Looming-Evoked Escapes. Average angular velocity (a) and linear velocity (b) traces for DNa05>Kir2.1 (orange) vs empty-split>Kir2.1 (gray) flies. (c) Reaction time distributions showing comparable response latencies between genotypes. (d) Polar distribution of heading changes reveals maintained directional organization despite DNa05 silencing. Vertical dashed lines in A, B indicate the stimulus presentation period.

These results suggest that DNa05 plays a smaller role in the generation and control of saccades in comparison to DNa15. Optogenetic activation does not lead to a clear sharp turn, and inhibition does not lead to highly noticeable effects on behavior. The same caveats from the DNa15 experiments apply here - strong bilateral optogenetic activation will most likely lead to artifacts and unnatural behaviors, and so a more complex analysis is required. Moreover, the Kir2.1 seemed to have had a general detrimental effect on the DNa05 split-GAL4 line, as those flies flew much less than empty split controls (18 vs 284 flight bouts over a recording of 24 hours), which led to a strong imbalance in the

comparison of both spontaneous and looming-evoked saccades. Therefore, a more precise approach to silencing may be needed to clearly elucidate the role of DNa05 in the control of flight.

3.5. Neural manipulation of other DNs

The tracking system provides an opportunity to investigate other descending neurons of interest, particularly ones with a suspected role in the control of flight. Accordingly, I selected neurons which may be involved in flight control and saccadic behavior: DNp06, which was hypothesized to contribute to evasive saccade maneuvers (Kim et al., 2023); DNp03, which receives direct looming-sensitive visual input and projects to wing-related motor centers in the VNC (Buchsbaum and Schnell 2025); and DNg02, which modulates linear flight velocity rather than turning behavior (Namiki et al. 2022; Palmer, Omoto, and Dickinson 2022) While these neurons have been previously studied in tethered flight preparations, our system enables their functional characterization under more naturalistic flight conditions, providing valuable comparative insights into their behavioral roles.

3.5.1. Optogenetic activation

I first chose to test how each of these neurons moderate the flight behavior of flies using the optogenetic paradigm as described before. Figure 40 shows the analysis for all three lines, along with a neuron diagram illustrating their physiology and projection patterns.

Optogenetic activation of DNp06 (Figure 40, top, green, n = 274 trials) showed a moderate increase in angular velocity (Figure 40a; 1249.64 ± 688.44 °/s mean peak amplitude). The timing of this turn was also variable, with a response latency of 163.2 ± 78.6 ms from the stimulus onset. The heading differences distribution similarly showed very broad tuning (113.40 ± 80.10°, r = 0.02), indicating no preferred turning direction following optogenetic activation.

Conversely, activation of DNp03 (Figure 40, middle, red, n = 92 trials) led to a consistent and accurately timed turning response, as evident by the high peak in the angular velocity trace (1905.99 ± 485.44 °/s), along with a more consistent response latency distribution (148 ± 46 ms). This was also reflected in the distribution of heading changes, which showed a clear peak towards 180° with a high concentration parameter (174.39 ± 46.83°, r = 0.67), indicating a very sharp turn.

Finally, DNg02 activation showed a very different response, including a moderate increase in angular velocity (1323.79 ± 814.30 °/s) and a relatively slow and broad latency (189.9 ± 73.9 ms). However, unlike DNp06 and DNp03, activation of DNg02 led to a long latent increase in angular velocity, which maintained for several seconds following the end of the optogenetic stimulus. These effects were also reflected in the heading direction distribution, which showed no clear tuning preference (16.11 ± 77.44°, r = 0.09).

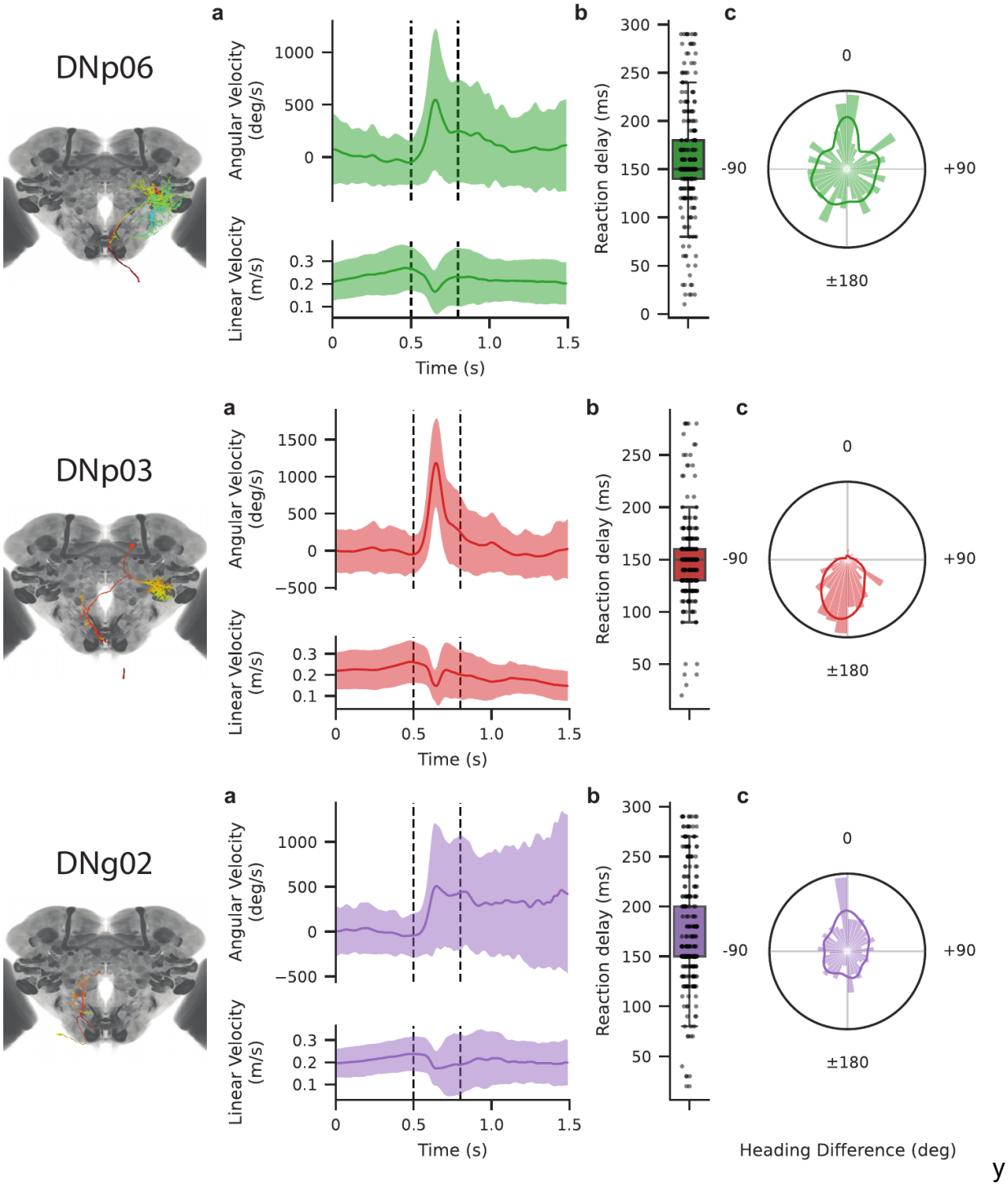

Figure 40. Optogenetic activation of other flight-related DNs. Top: DNp06, Middle: DNp03, Bottom: DNg02. For each figure: (a) top, angular velocity response to optogenetic stimulus (duration in between dashed lines); bottom, linear velocity response. (b) reaction time delay from onset of optogenetic stimulus to turning response (ms). (c) heading difference of turning response (deg).

3.5.2. Silencing Experiments

To elaborate on the optogenetic activation experiments, I similarly performed silencing experiments in the selected lines to test the effect of silencing on their ability to generate either spontaneous saccades or looming-evoked escape saccades. This proved more difficult than expected, as flies expressing Kir2.1 seem to fly less than other genetically modified flies - both in terms of total flight trajectories, as well as the total duration of each trajectory. Thus, the total number of flies and trajectories recorded is relatively low for DNp06 (n = 20 flies over 2 sessions, with a total of 265 trajectories and 2914 spontaneous saccades, and 206 looming-evoked saccades) and DNp03 (n = 20 flies over 2 sessions, with a total of 36 trajectories and 685 saccades, and 99 looming-evoked saccades), while DNg02 flies did not generate any usable data. The control group consisted of empty-split GAL4 crossed with the Kir2.1 line, yielding a total of 20 flies recorded over 2 sessions, yielding a total of 1665 spontaneous saccades and 331 looming-evoked saccades.

3.5.2.1. Spontaneous Saccades

Analysis of spontaneous saccades revealed no clear effect of silencing on the behavior of genetically silenced flies. Both groups showed a slight but statistically significant increase in the saccade peak angular velocity (DNp06: 1334 ± 1111 °/s; DNp03: 1516 ± 1178 °/s) in comparison to empty-split controls (1139 ± 670 °/s), although with only a small effect size (Figure 41a; DNp06: Mann-Whitney U = 45059, $p < 0.001$, Cliff's delta = 0.27; DNp03: Mann-Whitney U = 470055, $p < 0.001$, Cliff's delta = 0.14). This could indicate the loss of some fine-tuning capabilities during saccade initiation. While both groups showed an elevated baseline linear velocity in comparison to controls, both also showed the characteristic dip in linear velocity accompanying a saccade (Figure 41b). Neither of the groups showed a specific modulation of heading difference for the spontaneous saccades, with a mean heading difference of ±90 degrees (Figure 41c)

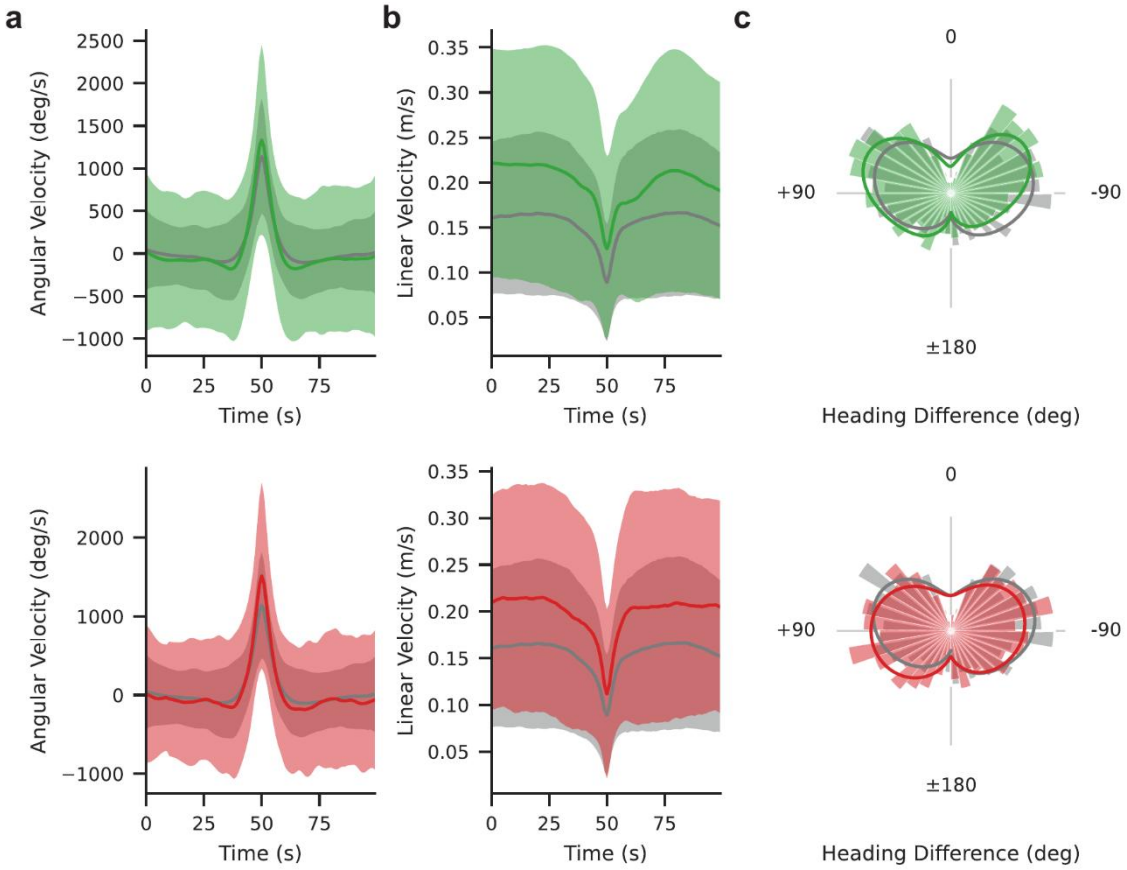

Figure 41. Kinematics of spontaneous saccades in Kir2.1-silenced DNs. Top, green: DNp06; Bottom, red: DNp03. Angular (a) and linear (b) velocity of spontaneous saccades in DNp06-silenced (experimental, green) vs Empty split-silenced (control, gray) flies. (c) Distribution of heading changes for experimental vs control flies.

Therefore, it appears that genetically silencing either DNp03 or DNp06 does not cause strong effects on the spontaneous saccadic behavior of flies, suggesting that neither one plays a significant role in those maneuvers.

3.5.2.2. Looming-evoked saccades

While genetic silencing showed only a small effect on spontaneous saccades, looming-evoked saccades showed a stronger effect on saccade generation. Specifically, genetic silencing of the neurons showed a reduction in peak response (Figure 42a) for both DNp06 (964.61 ± 577.10 °/s; Mann-Whitney U test, U = 58592.00, $p < 0.001$, Cliff's delta = 0.3) and DNp03 (942.91 ± 580.21 °/s; Mann-Whitney U test, U = 26401.00, $p < 0.001$, Cliff's delta = 0.26) compared to empty-split controls (1414.11 ± 834.93 °/s). Furthermore, DNp06 shows a significant (but with a small effect size) reduction in the reaction delay from the onset of the looming stimulus (Figure 42b) in comparison to controls (322.43 ±

65.36 ms vs 332.90 ± 59.26 ms for empty controls; Mann-Whitney U = 27946, p < 0.05, Cliff's delta = 0.09), DNp03 shows no such reduction (321.86 ± 66.03 ms; Mann-Whitney U = 17910, p > 0.05). This is most likely due to the larger sample size of DNp06 (n = 206 looming presentations) in comparison to DNp03 (n = 97 looming presentation). Finally, both groups showed a change in the distribution of heading differences - while the control group showed a general tendency to turn away from the stimulus (circular mean = 168 ± 99°, r = 0.23), both DNp06 (mean = 26 ± 114°, r = 0.13) and DNp03 (mean = 13 ± 94°, r = 0.26) show an inversion in their turning angle, such that their turns lead to a weaker change in heading in comparison to controls (Figure 42c).

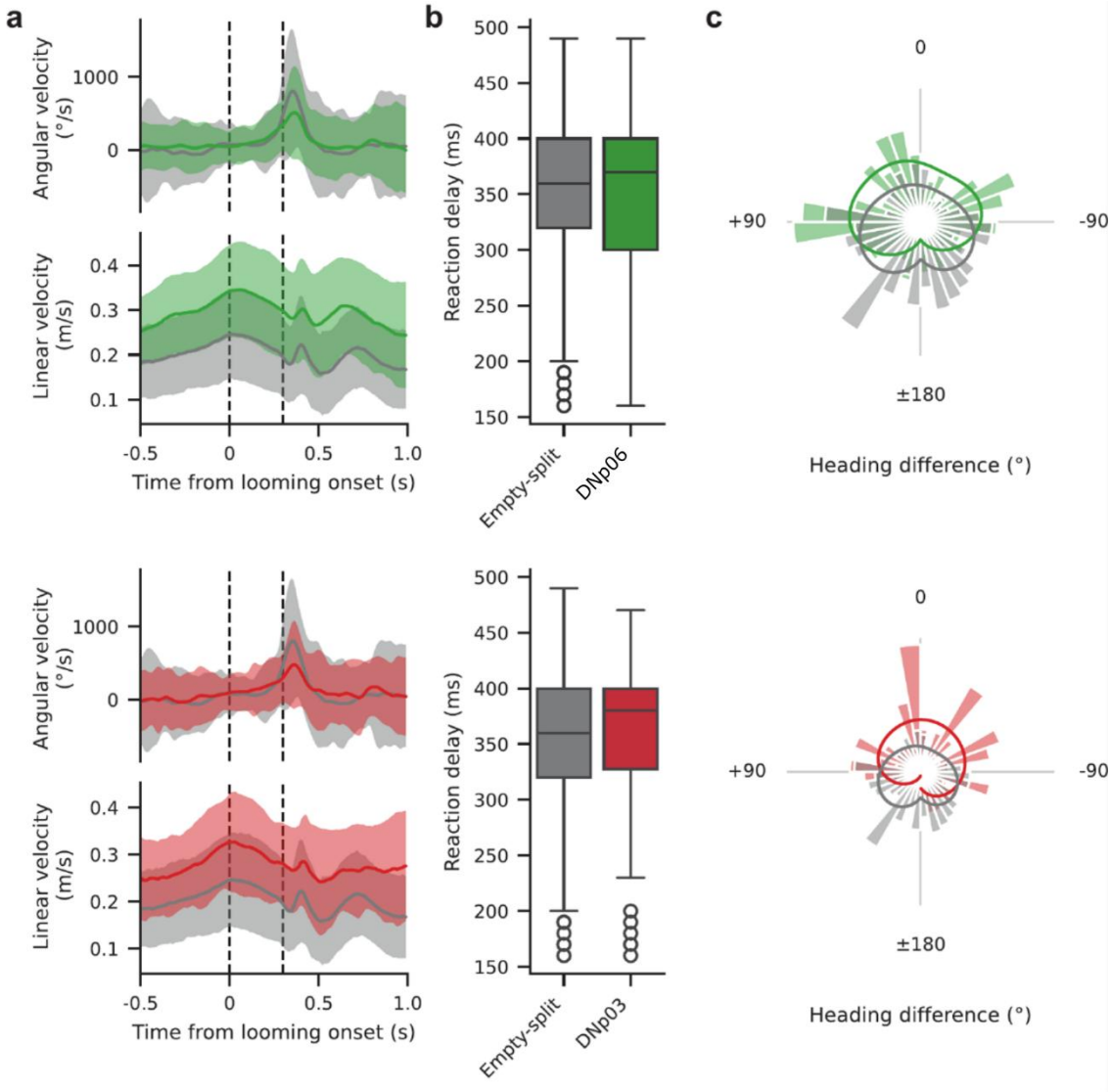

Figure 42. Response of KIR2.1-silenced DNs to a looming stimulus. Top, green: DNp06. Bottom, red: DNp03. Angular (a, top) and linear (a, bottom) velocities. (b)

comparison of reaction delay from the onset of the looming stimulus until peak angular velocity response (ms). (c) distribution of heading changes for experimental vs control groups. Dashed lines represent the onset and end of the looming stimulus.

In summary, these results suggest a role for both DNp03 and DNp06 in the generation and control of saccades. More specifically, DNp03 seems to drive strong and sharp turns during optogenetic activation, and its inhibition lowers the peak angular velocity amplitude in response to looming stimulus but not during spontaneous saccades. Similar results were seen in DNp06, except for the effects of optogenetic activation, which leads to only a small increase in angular velocity and a largely uniform distribution of heading changes. DNg02, on the other hand, shows a wholly unique behavioral profile, characterized by an increase in angular velocity, which is maintained for several seconds following the optogenetic activation window. Taken together, these results suggest DNp03 has a more low-level control of saccade generation, while DNp06 is situated more high-level in the saccade generation circuits, and both neurons seem to contribute to different aspects of saccade generation, with a focus on visually evoked responses. However, these experiments require more comprehensive follow-ups, focusing on using a more natural optogenetic stimuli focusing on one neuron at a time, as well as more time-dependent silencing of these neurons - either using genetic tools such as a heat shock-dependent GAL80, or optogenetic silencing tools.

3.6. High-Resolution Analysis of Flight Maneuvers

The optogenetic experiments revealed substantial variability in flight responses, particularly during unilateral stimulation. To more rigorously characterize these dynamic behaviors, I implemented high-speed video recording to capture flight kinematics during optogenetic activation with precise temporal resolution. Subsequent analysis using computer vision algorithms (OpenCV) enabled extraction of both positional coordinates and heading orientation of individual flies (Figure 43).

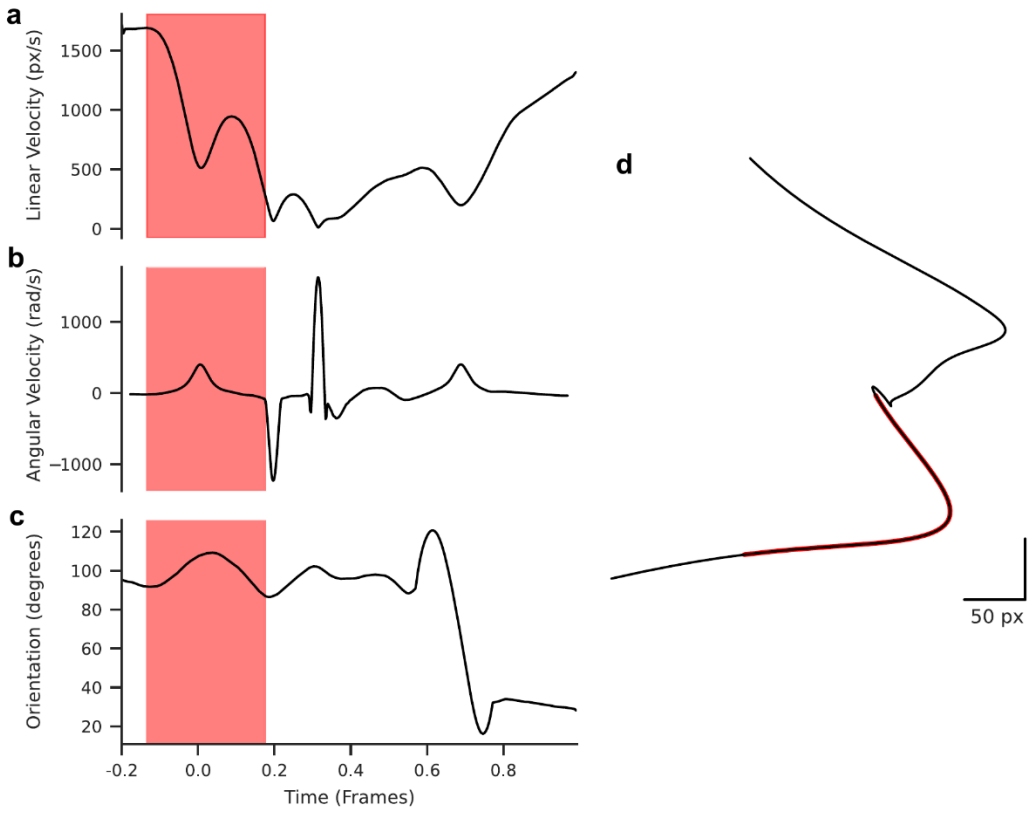

Figure 43. Example analysis from a high-speed, low-resolution camera. (a) linear velocity (px/s); (b) angular velocity (deg/s); and (c) orientation (deg) of the tracked fly.

Initial analyses uncovered an unexpected behavioral response pattern. Rather than executing conventional saccadic turns, a subset of flies exhibited distinctive aversive reactions to optogenetic stimulation—characterized by a sudden reduction in linear velocity and a reverse in the movement (backwards flight/hovering), followed by resumption of normal flight. As illustrated in Figure 43d, these responses manifest as apparent hairpin turns in the trajectory immediately following optogenetic activation. While traditional analysis methods would categorize these movements as saccades based on angular velocity and linear velocity profiles (Figure 43a-b, showing characteristic sharp increases in angular velocity and decrease in linear velocity, which is also characteristic of saccades), examination of body orientation metrics revealed that fly heading remained remarkably constant during these maneuvers (Figure 43c). Direct video analysis confirmed that flies responded to optogenetic stimulation by decelerating, flying backwards, and then resuming forward movement — a complex behavioral sequence that

would be misclassified by conventional tracking systems that capture position without orientation data.

The initial high-speed cameras available for this study presented limitations in spatial resolution that precluded comprehensive analysis across all experimental videos. To address this constraint, I implemented a camera system with enhanced spatial resolution while preserving high frame rate capabilities. This imaging setup was further improved with a liquid-lens mechanism, enabling continuous focus maintenance as the fly navigated through different z-positions during flight.

A significant technical challenge emerged with this advanced camera configuration. The combined improvements in frame rate and resolution increased data throughput substantially - from approximately 229 MB/s to 2982 MB/s, representing a tenfold increase. This data volume exceeded the processing capabilities of standard Python implementations, which typically demonstrate lower performance compared to compiled languages for computationally intensive operations.

To overcome this bottleneck, I developed the necessary algorithmic framework in Rust, a modern systems programming language designed specifically for performance optimization and memory safety. The selection of Rust had another advantage, as it aligned with the architecture of the Braid tracking system employed in this research. This technical convergence provided dual benefits: enhanced processing capabilities for high-volume imaging data and more in-depth insights into the underlying mechanics of the tracking system

With this optimized system, I captured high-resolution recordings of flies during visual stimulus presentation for in-depth behavioral analysis. The post-acquisition analytical pipeline incorporated a convolutional neural network (CNN) specialized for animal pose estimation (SLEAP, Pereira et al. 2022), which I trained to track two anatomical landmarks—the head and abdomen. These reference points provided sufficient information to derive precise heading vectors and orientation dynamics.

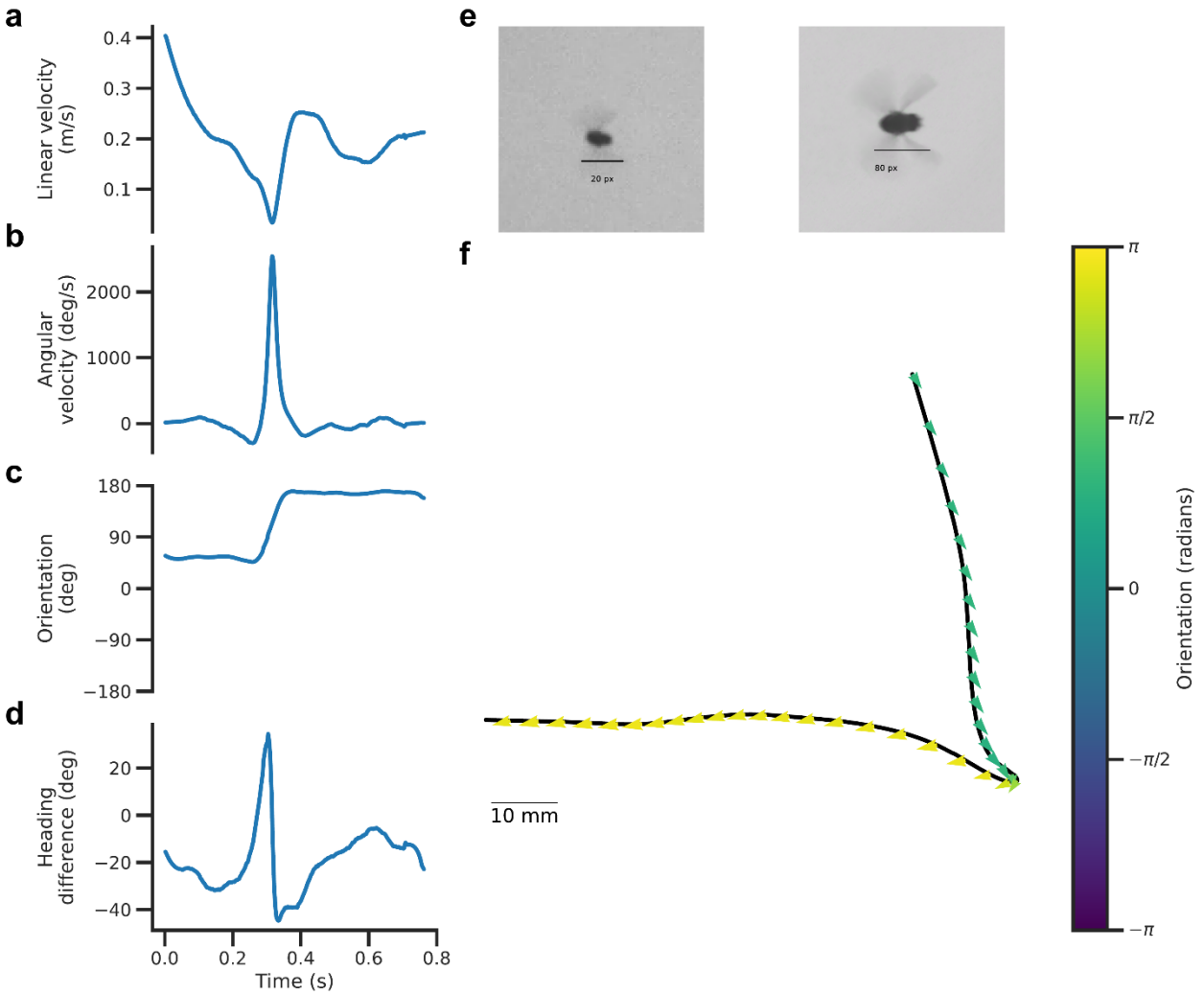

Figure 44. An example of analysis from a high-speed, high-resolution camera recording. (a) Linear velocity, (b) angular velocity, (c) orientation, and (d) heading difference. (e) example of the fly's view from the old camera (left) and new high-resolution camera (right). (f) trajectory reconstruction overlaid with the actual heading of the fly (colored arrow).

While these results remain preliminary, Figure 44 demonstrates the capabilities of this approach. The example shows a fly executing a sharp saccadic turn, evident in both the angular velocity profile (Figure 44 b) and corresponding orientation dynamics (Figure 44c-d). Importantly, the system now enables extraction of precise flight vectors by calculating the orientation between the abdomen and head, providing critical insights into the relationship between gaze direction and body trajectory (Figure 44e).

This methodological advancement opens promising research avenues for investigating the aerodynamic principles governing *Drosophila* flight responses to both visual and

optogenetic stimuli, enabling deeper characterization of sensorimotor integration in this model system.

4. Discussion

4.1. Introduction and Key Findings

Uncovering the neural mechanisms that transform sensory input into coordinated motor output during complex behaviors remains a fundamental challenge in neuroscience. This thesis investigated the specific roles of DNs in the generation and control of flight maneuvers in *Drosophila melanogaster*, with particular focus on saccadic turns. By combining genetic manipulation techniques with free-flight behavioral analysis, I sought to determine whether individual DNs function as command neurons capable of triggering complete saccades or if saccade generation emerges from distributed activity across multiple neurons

First, I successfully established a novel free-flight experimental paradigm that integrates real-time three-dimensional tracking with closed-loop optogenetic manipulation. This system enables precise activation of genetically defined neuronal populations during natural flight behavior, with a minimal system response latency and high spatial tracking precision. This technical advance provides a robust platform for investigating the causal relationship between neural activity and naturalistic flight behaviors.

Second, quantitative analysis revealed distinct kinematic differences between spontaneous and looming-evoked saccades. Looming-evoked escape saccades exhibited significantly higher peak angular velocities and broader distributions of heading changes in comparison to spontaneous saccades. These differences suggest potentially distinct neural mechanisms underlying these two categories of turning behaviors.

Third, optogenetic activation of specific DNs demonstrated that different neurons elicit distinct behavioral effects when activated during free flight. Bilateral activation of DNa15 triggered sharp, rapid turns with high angular velocities and consistently steep heading changes. DNa05 activation produced a notably different response pattern, characterized by persistent circling behavior that continued well beyond the stimulation period. DNp03 activation generated strong turning responses with angular velocity profiles similar to DNa15 but with more variable directional control, while DNp06 evoked more modest turning behaviors without clear directional preferences. In contrast, DNg02 activation

resulted in prolonged turning behavior that developed gradually and persisted for extended periods.

Finally, silencing experiments revealed a potential separation of neural pathways for different types of saccades. DNa15 silencing primarily affected spontaneous saccade kinematics while minimally impacting looming-evoked escapes, whereas DNp03 silencing specifically reduced the amplitude of escape responses to looming stimuli without affecting spontaneous saccades. This double dissociation suggests functional specialization within the descending control system for different behavioral contexts.

Collectively, these findings provide new insights into the neural basis of flight control in *Drosophila* and offer a framework for understanding how relatively small populations of DNs orchestrate complex behavioral sequences through specialized yet interconnected functional circuits.

4.2. Spontaneous vs. Escape Saccades

My tracking setup enabled quantification of the kinematic differences between spontaneous and visually evoked saccades under natural flight conditions. These measurements served both to establish behavioral baselines and to provide a foundation for subsequent analyses of DN function. Flight turns were categorized based on contextual parameters: maneuvers occurring within the central arena region, away from walls and floor, were classified as "spontaneous" saccades, while turns triggered in response to looming stimuli were designated "escape" saccades. Quantitative analysis revealed two key distinctions between these categories: first, looming-evoked escape saccades exhibited moderately elevated peak angular velocities, averaging approximately 1500°/s compared to 1000°/s for spontaneous saccades; second, escape maneuvers produced significantly broader heading change distributions, centered around 135° versus the more stereotyped 90° turns characteristic of spontaneous saccades, with substantially greater variability in trajectory outcomes.

From a behavioral perspective, these differences align with the purpose of the two turn types. Spontaneous saccades serve primarily as navigational adjustments during exploratory behavior, requiring precise, stereotyped heading changes to maintain efficient search patterns (Reynolds and Frye 2007; Censi et al. 2013). Conversely, escape

saccades prioritize rapid threat avoidance over directional precision, sacrificing stability for speed when confronted with imminent, unexpected collision (Tammero and Dickinson 2002a; 2002b; Muijres et al. 2014). This functional dichotomy suggests potential differences in the underlying neural control mechanisms governing these superficially similar behaviors.

High-resolution free-flight studies have further delineated the aerodynamic distinctions between these maneuver types. Previous studies (Muijres et al. 2014; 2015) employed specialized high-speed videography (7500 fps) to analyze the precise wing kinematics and body dynamics during both spontaneous and escape maneuvers in *Drosophila hydei*. Their measurements revealed that escape responses generate substantially higher peak angular velocities - approximately 5300°/s - compared to the ~1000°/s observed during spontaneous turns. This discrepancy exceeds that documented in my experiments (1500°/s vs. 1000°/s), likely reflecting methodological differences in temporal resolution, as my 100 fps tracking system would inherently smooth peak instantaneous velocities. Nevertheless, both studies converge on the fundamental observation that escape maneuvers exhibit elevated angular velocities relative to spontaneous saccades.

More significantly, Muijres et al. identified fundamental differences in the control strategies underlying these behaviors. While both maneuver types employ banked turns rather than pure yaw rotations as previously assumed (Götz 1964; Hedrick, Cheng, and Deng 2009; Bergou et al. 2010), spontaneous saccades utilize highly stereotyped rotation axes with consistent orientation in the body frame. In contrast, escape maneuvers vary rotation axis orientation based on stimulus direction, and generate negative yaw torque that increases sideslip, requiring subsequent correction and introducing the variability observed in heading change outcomes (Muijres et al. 2014). These mechanistic insights may explain the broader heading distributions I observed in escape saccades.

Saccades in free-flight differ substantially from observations in tethered paradigms, where saccade-like behaviors manifest primarily as rapid fluctuations in yaw torque or asymmetric changes in wing-beat amplitude. In rigidly tethered preparations, these "torque spikes" or “fictive saccades” exhibit significantly lower angular velocities (~500°/s), extended durations (80-100ms), and reduced amplitude (30-60° equivalent heading changes) compared to natural saccades (Heisenberg and Wolf 1979; Mongeau and Frye

2017). While looming stimuli reliably elicit these responses in tethered flies, the kinematic parameters diverge substantially from free-flight equivalents. Magnetically tethered flies, which retain rotational freedom around the yaw axis, produce intermediate kinematic profiles with saccade durations around 80ms and heading changes of approximately 35° (Bender and Dickinson 2006b), bridging the gap between rigid tethering and free flight but still failing to recapitulate natural turn dynamics fully.

These discrepancies between tethered and free-flight behaviors most likely reflect fundamentally altered sensorimotor integration rather than mere mechanical constraints. Tethering eliminates critical mechanosensory feedback, particularly from the halteres, which detect Coriolis forces during body rotation and provide essential input for coordinating flight maneuvers (Dickinson 1999). Without this feedback, the neural circuits generating saccades lack the inhibitory signals necessary to terminate the motor program appropriately, resulting in prolonged, attenuated responses (Bender and Dickinson 2006a). Moreover, tethered paradigms prevent the complex, multi-axis coordination observed in natural saccades, which involve precisely timed adjustments across roll, pitch, and yaw axes through subtle modulations of wing kinematics (Dickinson and Muijres 2016).

The sharp kinematic differences between spontaneous and visually-evoked saccades raise fundamental questions about their underlying neural architecture. Two competing models could explain these observations: either a single descending pathway modulated by context-dependent inputs, or parallel descending pathways mediating different saccade types (Simpson 2024). The single-pathway hypothesis proposes that the same circuit controls both maneuver types, but its activity is modulated by upstream or recurrent circuits integrating visual threat signals. This would allow a common motor network to produce either stereotyped navigational adjustments or rapid evasive maneuvers depending on sensory context. Alternatively, the parallel-pathway model suggests the existence of two dedicated, separated circuits for each saccade type. In the case of spontaneous vs escape saccades, one very similar circuit is the giant fiber (GF) escape pathway (Card and Dickinson 2008). The GF neuron is necessary to elicit a short-mode takeoff escape response to looming stimulus, but another pathway is used (with GF co-activation) to initiate a long-mode takeoff escape (Von Reyn et al. 2017). Similar to the

kinematic differences seen in spontaneous vs escape saccade, the short-mode takeoff trades stabilization for speed, while the long-mode takeoff is more stereotypic and well controlled (Von Reyn et al. 2014; 2017; Ache, Polsky, et al. 2019).

Distinguishing between these models requires examining how specific DNs contribute to different saccade types - precisely the question addressed through optogenetic manipulation of identified DNs during free flight.

4.3. Descending Control of Flight

Optogenetic activation and genetic silencing of a several DNs revealed unique insights - while some neurons showed more “command-like” properties (DNa15, DNp03), leading to sharp changes in flight kinematics and turns, other neurons (DNa05, DNp06, DNg02) showed more moderate and less clear response properties, suggesting they may play a smaller part in a larger control circuit.

I initially chose to start with activation and inhibition experiments of DNa15 - this is due to previous research showing that its activity is highly correlated with wingbeat amplitude changes (fictive saccades) in tethered flight, and artificial activation leads to similar changes in wingbeat amplitude (Schnell, Ros, and Dickinson 2017). In my own experiments, I found evidence to support this - bilateral optogenetic activation led to a strong turning response with a large change in heading during free flight, while genetic inhibition affected mostly the amplitude of heading changes during spontaneous but not looming-elicited saccades. These findings suggest that DNa15 may play a role in the control or initiation of spontaneous saccades specifically, but less so in escape saccades. In comparison, Schnell, Ros, and Dickinson (2017) found that the activity of DNa15 increased both during spontaneous and looming-elicited saccades; however, the fact that it was active when flies performed a looming-elicited saccade does not necessarily mean it was required for the turning behavior - for example, the DNp06 neuron has direct visual input from looming-sensitive VPNs, and it itself projects to motor centers in the VNC; however, its activation showed only modest behavioral responses.

These findings also align with recent work by Ros, Omoto, and Dickinson (2024), who identified this same neuron as DNae014 (which is equivalent to DNaX/DNa15) and characterized it as part of a hypothesized 'saccade-generating unit' (SGU). Their

investigation revealed that DNa15 functions alongside another DN, DNb01, to control saccadic turns. Similar to my silencing experiments, Ros et al. found that genetic ablation of DNa15 reduced but did not eliminate spontaneous saccades, supporting my observation that it contributes to spontaneous turning behavior without being absolutely necessary. Importantly, they confirmed through connectomic analysis that DNa15 is likely cholinergic and forms strong connections with wing steering motor circuits, particularly targeting b2 motor neurons, iii3 motor neurons, and wing contralateral haltere interneurons (w-CHINs) - connections critical for generating rapid turning maneuvers (Lehmann and Bartussek 2017; Lindsay, Sustar, and Dickinson 2017). The hierarchical position of DNa15 in the circuit is further clarified by Ros et al.'s discovery of VES041, a GABAergic neuron that inhibits both DNa15 and DNb01, effectively suppressing saccades when activated. This inhibitory control mechanism may explain how spontaneous saccades are regulated during different behavioral states, such as when flies transition between local search and long-distance dispersal (Ros, Omoto, and Dickinson 2024).

It is also important to note that the split-GAL4 line used for these experiments co-labels another DN, DNa05. Given that co-activation of DNs can lead to different behavioral outputs (Cande et al. 2018), I performed similar optogenetic activation and silencing experiments in a split-GAL4 line labelling DNa05 along with DNp11 (which is known to be related to the GF takeoff circuits; Ache, Namiki, et al. 2019; Dombrovski et al. 2023). These experiments revealed a starkly different result from DNa15: rather than a sharp turn, optogenetic activation caused a transient yet prolonged increase in angular velocity, expressed behaviorally as continuous circling that persisted even after stimulus termination. Both DNa15 and DNa05 exhibit strikingly similar morphological characteristics, with comparable dendritic arborization patterns and axonal projections, which frequently complicated their definitive identification during immunohistochemical analysis. Beyond these anatomical similarities, they also share substantial overlap in their synaptic connectivity. Within the central nervous system, they receive input from many of the same partners (56/187 for DNa15 and 56/140 for DNa05), predominantly from the inferior and superior posterior slope regions (IPS/SPS), although their output connectivity in the CNS is relatively sparse, with downstream connections to just 17 (DNa15) and 3 (DNa05) neurons, primarily within the gnathal ganglia. In the ventral nerve cord, their output profiles show significant convergence, with both neurons targeting many identical

postsynaptic partners (102/171 for DNa15 and 102/225 for DNa05), most notably the wing contralateral haltere interneurons (w-CHINs), which are critical for coordinating wing steering maneuvers. Despite these similarities in connectivity, it remains difficult to mechanistically explain the observed looping behavior based solely on connectome data due to the extraordinary complexity of these circuits and the artificial nature of optogenetic activation. Notably, recent experiments in our lab with an alternative DNa05 split-GAL4 lines demonstrate that this persistent circling behavior is not consistently reproduced, suggesting that co-activation with DNp11 may significantly modulate the behavioral output through currently undefined circuit interactions.

To further understand the circuit architecture governing the different saccade types, I conducted similar experiments with DNp03, which showed complementary functional properties (Buchsbaum and Schnell 2025). Activation of DNp03 led to a strong and sharp turning behavior, characterized by a significant change in heading. Conversely, genetic inhibition led to a distinct dichotomy - while spontaneous saccades were generally not affected, the amplitude of looming-elicited saccades was greatly reduced. This suggests that DNp03, unlike DNa15, has a specific role in the initiation and control of looming-elicited escape saccades, a finding which aligns well with its connectivity patterns. DNp03 receives most of its input from visual neurons such as LPLC1, LPLC4, LC4 and LC22 - all of which are known to be highly sensitive to looming stimuli (Wu et al. 2016; Dombrovski et al. 2023; Moreno-Sanchez et al. 2024). Moreover, in the VNC, DNp03 makes many direct connections to motor neurons, a feature less commonly seen in DNs, most of which make only indirect connections with motor neurons via intrinsic neurons (Cheong, Eichler, et al. 2024). Its connectivity in the VNC is also unique in that it has connections to both steering motor neurons via w-cHINs, and to the wing power muscle neurons, which suggests that it may support concurrent turning with increase in wing power during flight that perhaps aids in evasive maneuvers (Cheong, Eichler, et al. 2024).

The roles of DNa15 and DNp03 neurons can be explained by their hierarchical relationship within the circuit. Connectomic analysis reveals that DNp03 provides substantial input to DNa15 (Dorkenwald et al. 2024; Schlegel et al. 2024), along with connections to other DNs hypothesized to play a part in saccades initiation and control, such as DNa04, DNa05, and DNb01 (Cheong, Eichler, et al. 2024; Ros, Omoto, and Dickinson 2024). This

circuit architecture may explain the clear double dissociation observed in my silencing experiments - where DNp03 inhibition specifically affects looming-elicited saccades while DNa15 inhibition affects spontaneous saccades - as it provides evidence for a shared underlying saccade-generating circuit that is differentially recruited based on behavioral context. Rather than representing completely separate pathways, these neurons may form part of an interconnected network where specific components are activated based on the behavioral context. The connectomic data showing DNp03 providing input to DNa15 supports this interpretation, by suggesting that during looming-elicited responses, DNp03 may activate a hypothesized saccade-generating circuit in a way optimized for looming-driven escape rather than exploration responses. Then, each DN in the network activated by this command-like DN plays a small but critical part in the execution of the behavior; inhibition of a single component does not completely abolish the output, but it does affect its execution. For example, Feng et al. (2020) found that activation of the moonwalker DN (MDN) leads to the activation of a network of other neurons in the VNC, each of which has a different role in the full execution of the behavior. Similarly, Ros, Omoto, and Dickinson (2024) found that genetic ablation of DNa15 does not completely abolish saccades, but rather just reduces their frequency. This hypothesis, however, suggests the existence of a spontaneous-centric command-DN, which activates the same network with parameters optimized for exploration rather than escape.

Furthermore, a similar circuit was recently described by Feng et al. (2024), who identified a circuit in the LAL that can generate both course-correcting and exploratory turns during walking (and perhaps flying) using a common downstream circuit. The two “command” neurons - LAL013 and DNa03 - project to several of the previously described DNs (such as DNa15 and DNb01), receive a major portion of their inputs from the central complex and its associated structures - areas which are known to play critical roles in multisensory integration and motor control, as well as being implicated in more goal-oriented (exploration, food seeking, mating) behaviors (Hulse et al. 2021). The central complex, particularly through its role in maintaining an internal representation of direction, has been demonstrated to transform head direction signals into goal-oriented steering commands (Westeinde et al. 2024). This circuit architecture allows the fly to continuously estimate its current heading and make appropriate corrections to maintain orientation toward remembered goals. Specific cell populations within the central complex (PFL3R, PFL3L,

and PFL2, which also synapse onto LAL014 and DNa03) serve as the interface between allocentric spatial maps and egocentric motor commands, comparing the animal's current head direction vector with a goal vector to generate appropriate steering behaviors. Notably, this system adaptively manages the tradeoff between steering speed and accuracy through specialized neural pathways, with different cell populations recruited depending on whether the animal is oriented close to or far from its goal direction (Westeinde et al. 2024). This transformation mechanism aligns with the central complex's broader role in goal-directed navigation across various behavioral contexts. Thus, both DNa03 and LAL014 represent interesting candidates for spontaneous saccade-specific command neurons within this circuit architecture. To establish their precise roles, however, subsequent investigations should use similar optogenetic activation and genetic silencing protocols employed in our analysis of DNa15 and DNp03. Such targeted manipulations could help elucidate whether these neurons exhibit the predicted complementary double-dissociation pattern - specifically, influencing spontaneous saccades but not looming-elicited responses. This could substantiate the hierarchical circuit model proposed here, wherein parallel command pathways differentially recruit shared downstream neurons based on behavioral context.

Beyond DNa15 and DNp03, I tested the function of two other DNs using optogenetic activation and genetic inhibition studies. DNp06 is a DN receiving direct input from looming-sensitive visual neurons (LPLC2), and it sends projections to motor centers in the VNC. While a previous study suggested it may be involved in the initiation of evasive flight turns (Kim et al. 2023), my own results showed a different behavioral profile. Activation of this neuron during free flight led to only a moderate increase in angular velocity, and these turns showed no preferential heading change direction - meaning, following the activation, the flies had an almost uniform chance of turning to any direction. Silencing experiments had a similar weak effect on both spontaneous and looming-elicited saccades. An in-depth analysis of the neuron’s

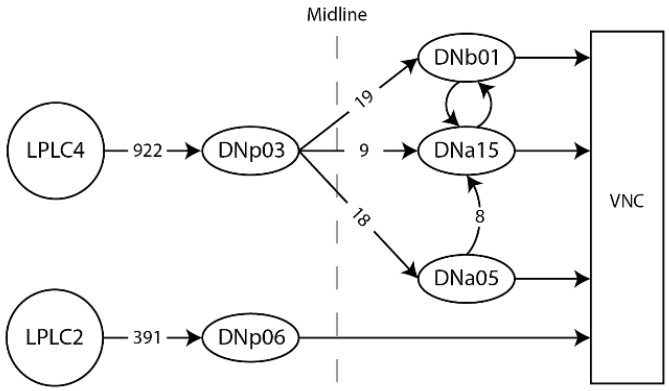

Figure 45. Simplified DN circuit diagram.

connectivity using the latest connectome reconstruction may shed some light on these results - while DNp06 does receive the majority of its input from direction and looming-selective neurons (LPLC1, LPLC2), it lacks connectivity to any of the other saccade-related DNs described here and in other (Schnell, Ros, and Dickinson 2017; Ros, Omoto, and Dickinson 2024; Feng et al. 2024; Cheong, Eichler, et al. 2024), seemingly existing in a parallel circuit. Moreover, when examining its exact synaptic partners in the CNS and VNC, two major findings stand out: first, the majority of its synaptic outputs are onto intrinsic neurons in the leg neuropils and lower tectulum rather than the wing neuropils; and second, it seems to be a major output partner of neurons directly downstream of GF in the CNS, and it has many recurrent connections with the GF neuron in the VNC (Schlegel et al. 2024; Dorkenwald et al. 2024). These observations highly suggest that, rather than initiating or controlling evasive turns in flight, it is much more likely that DNp06 plays a role in the GF takeoff escape circuit. The moderate response seen in both my experiments and in Kim et al. (2023) is most likely as a result of subtle activation of wing-related motor neurons via intrinsic neurons in the intermediate tectulum, an area thought to be involved in the coordination of leg and wing movements (a coordination which is especially important during takeoff maneuvers; Namiki et al. 2018; Asinof and Card 2024). Alternatively, activation of DNp06 may recruit other DNs in the takeoff escape pathways with more connections to the wing neuropils. These findings regarding DNp06 reveal how parallel sensory pathways can be differentially routed to distinct downstream motor circuits based on the behavioral context.

Finally, I examined DNg02, a distinctive class of DNs that differs fundamentally from the previously described DNs. Unlike DNa15 and DNp03, which exist as individual bilateral pairs, DNg02 constitutes a substantial population of approximately 15 cell pairs with nearly identical morphology. Recent research by Namiki et al. (2022) characterized this neuronal population as functioning analogously to a "throttle" mechanism for flight control, demonstrating that the magnitude of bilateral wingbeat amplitude modulation correlates directly with the number of activated DNg02 neurons. Their work established that this population encodes flight power parameters through distributed activity patterns rather than through the binary activation of individual command neurons, representing a clear example of population coding in descending motor control. This computational approach, where behavior is controlled by distributed neuronal activity rather than individual

command neurons, represents a principle that has been underrepresented in DN studies until recently (Simpson 2024). In my own experiments, DNg02 exhibited a moderate (but unique) kinematic profile when activated by optogenetic light - on average, the flies showed a slight increase in angular velocity which was maintained for several seconds, without any clear change in linear velocity or heading direction.

These results are somewhat surprising - given DNg02s suggested role as a population-coded “throttle”, one would hypothesize a similar increase in forward velocity during free flight without a change in angular velocity, both of which I did not observe in my own experiments. I initially hypothesized that the increase in angular velocity might be explained by an imbalance in the activity of the DNg02 population, which is enhanced by the strong optogenetic activation. However, Palmer, Omoto, and Dickinson (2022) provided compelling evidence that challenges this interpretation. In their investigation of DNg02's role in the optomotor response, they performed unilateral activation experiments specifically designed to test whether asymmetric DNg02 activation could drive directional turning. Contrary to expectations, even strictly unilateral activation generated bilaterally symmetric increases in wingbeat amplitude, with equivalent effects on both ipsilateral and contralateral wings. These findings suggested that DNg02 primarily regulates power muscles that operate symmetrically across both wings, rather than directly controlling steering muscles that would produce asymmetric wing kinematics.

The apparent contradiction between Palmer's observations and my free-flight results likely reflects fundamental differences between tethered and naturalistic flight conditions. Tethered preparations predominantly measure simple wingbeat amplitude parameters while constraining the complex multidimensional kinematics of natural flight. The subtle turning behavior I observed may stem from nuanced changes in wing kinematics beyond simple amplitude modulation - such as alterations in wing rotation timing, angle of attack, or stroke trajectory - that remain undetectable in tethered paradigms but manifest as directional biases during free flight. Even small modifications in these parameters can produce significant aerodynamic effects, as demonstrated by Dickson, Straw, and Dickinson (2008) and Muijres et al. (2014), who showed that subtle deformations in wing shape or minor adjustments in stroke timing can substantially impact flight performance and stability.

Furthermore, the comprehensive connectomic analysis by Cheong et al. (2024) provides additional context for understanding DNg02's function. Their work reveals that DNg02 forms a feedforward network with ascending histaminergic neurons (AHNs) and wing power motor neurons, while also providing input to wing-contralateral haltere interneurons (w-CHINs) that coordinate steering control. This intricate connectivity suggests that while DNg02 primarily regulates power output, it simultaneously influences timing circuits that could subtly modulate turning dynamics during natural flight. The anatomical specialization of DNg02 - with bilateral dendritic arborization patterns in the brain but predominantly contralateral axonal projections in the ventral nerve cord - further explains how this population might differentially regulate ipsilateral versus contralateral wing circuits, despite the apparently symmetric activation patterns observed in tethered preparations.

4.4. Integrating Multiple Control Strategies in Descending Motor Systems

My investigation of multiple DNs during free flight has revealed a neural control architecture that transcends the traditional dichotomy between command neuron and population coding frameworks (Simpson 2024). The experimental evidence suggests these mechanisms function not as mutually exclusive control strategies, but rather as complementary components within an integrated system. DNa15 and DNp03 exhibited command-like properties, reliably triggering turning behaviors when activated and showing specific deficits when silenced. In stark contrast, DNg02 demonstrated clear population-coded behavior, where distributed activity across multiple similar neurons collectively regulated flight parameters over a broad dynamic range (Namiki et al. 2022; Palmer, Omoto, and Dickinson 2022)

The most compelling evidence for context-dependent recruitment of descending pathways emerged from the double dissociation observed in silencing experiments: DNa15 inhibition primarily affected spontaneous saccade kinematics while DNp03 silencing specifically reduced the amplitude of looming-evoked escape maneuvers. This finding strongly indicates that these neurons participate in parallel yet interconnected pathways that are differentially recruited based on behavioral context. Such context-dependence appears to be a fundamental property of the DN system rather than an exception. In our own research, I found that DNp03 is only active during flight, suggesting a context-specific

activity pattern (Buchsbaum and Schnell 2025), while the activity of DNa15 is similarly gated by flight state (Schnell, Ros, and Dickinson 2017).

This principle extends beyond flight control circuits to other motor behaviors in *Drosophila*. Previous research has identified neurons that can initiate either running or freezing in a context-dependent manner (Zacarias et al. 2018; Howard et al. 2019), and DNs that trigger either takeoff or landing in response to identical looming stimuli depending on the current behavioral state (Ache, Namiki, et al. 2019). Cande et al. (2018) further demonstrated in a large-scale optogenetic screening that nearly all DNs exhibit both behavioral state dependence and response modifications when co-activated with other DNs.

My findings align with emerging evidence suggesting that descending motor control employs a hybrid architecture where seemingly command-like neurons actually function as entry points or "broadcasters" that recruit specialized downstream networks (Braun et al. 2024). The differential effects observed when manipulating specific DNs likely reflect their distinct positions within this hierarchical yet distributed organization. DNa15 and DNp03, despite their command-like properties, may primarily function by engaging context-appropriate downstream circuits rather than directly encoding all parameters necessary for complex maneuvers. Meanwhile, DNg02's population-based properties demonstrate how distributed neuronal ensembles can implement graded control of flight parameters through collective activity patterns.

This framework helps explain the partial deficits observed in silencing experiments - no single DN entirely controls a behavior, but rather contributes specific components to a distributed network. Such an architecture offers several advantages: it enables rapid initiation through direct pathways while preserving flexibility via distributed control, allows for context-dependent modulation, and provides robustness through partially redundant pathways.

4.5. Methodological Considerations

These findings collectively underscore the importance of examining neural control mechanisms under naturalistic behavioral conditions. The discrepancies between tethered and free-flight paradigms reveal how experimental constraints can obscure the

full complexity of neural control mechanisms. However, my experimental approach encountered several methodological limitations that limited my analysis regarding the exact functional significance of specific DNs.

4.5.1. Technical Challenges in Optogenetic Manipulation

The optogenetic activation paradigm employed in this study introduced significant technical issues that warrant careful consideration when interpreting the results. The use of csChrimson for neuronal activation, while effective for establishing causal relationships, created artificial activity patterns that likely deviate substantially from physiological neural activity. CsChrimson's relatively slow off-kinetics resulted in prolonged and unnatural neuronal activation that at times extends well beyond the light stimulus duration, potentially explaining the sustained behavioral effects observed following brief stimulation (Kim et al. 2015). This sustained activation profile is particularly significant for the study of fast and precise motor outputs such as saccades. Consequently, the artificial prolongation of neural activity likely produced exaggerated behavioral outputs that may not accurately represent the neurons' natural functions.

Furthermore, bilateral activation of DNs through pan-neuronal expression inherently limited my ability to assess their role in directional flight control. Natural flight maneuvers most likely involve asymmetric activation patterns across left and right descending pathways, particularly for steering-related neurons (Schnell, Ros, and Dickinson 2017; Ros, Omoto, and Dickinson 2024; Feng et al. 2024). The simultaneous activation of bilateral neuron pairs limited the possibility of observing how unilateral activity might drive ipsilateral or contralateral turning behaviors - information crucial for understanding the mechanistic basis of directional control.

4.5.2. Limitations of Unilateral Targeting Approaches

To address the limitations of bilateral activation, I attempted to implement stochastic expression systems that would enable unilateral, cell-type specific optogenetic manipulation. The FLP-out recombination approach, which employs heat shock-induced DNA recombination to stochastically express transgenes in subsets of neurons (Nern, Pfeiffer, and Rubin 2015; Fisher et al. 2017), proved significantly more challenging than anticipated. The system's efficacy was remarkably low for DN targeting, with only a small

proportion of flies (approximately 10-15%) showing unilateral expression in the targeted neurons following immunohistochemical validation. Identification of specific expression patterns was further complicated by the marked anatomical similarity between certain DN types - particularly DNa05 and DNa15 - whose dendritic arborizations and axonal trajectories show substantial morphological overlap that frequently confounded definitive classification during later analysis. More troublingly, there was often a disconnect between expression patterns and behavioral outcomes - some flies showed robust light-evoked behaviors despite minimal detectable channelrhodopsin expression, while others exhibited clear expression with no corresponding behavioral response. These inconsistencies likely stem from variable protein expression levels, where stochastic recombination produces a spectrum of outcomes ranging from subthreshold expression (still detectable via immunostaining) to fully functional levels that enable robust optogenetic responses (Golic and Lindquist 1989).

I subsequently implemented the SPARC technique (Isaacman-Beck et al. 2020), which promised more precise control through competitive DNA recombination. While the Dense SPARC variant (SPARC-D) generated strong fluorescence and robust optogenetic responses, it frequently labeled multiple neurons within targeted lines. Conversely, the Intermediate and Sparse SPARC variants, which might have provided more selective labeling, showed negligible expression in DN driver lines. These limitations prevented achievement of the single-cell specificity necessary for rigorous assessment of individual DN contributions. This differential expression pattern likely stems from several potential mechanisms: first, as demonstrated by Isaacman-Beck et al. (2020), the truncated attP sequences used in the Intermediate (38bp) and Sparse (34bp) variants significantly reduce PhiC31-mediated recombination efficiency compared to the Dense variant's 60bp attP sequence. While this reduction enables sparse labeling in populations with high baseline expression levels, it may result in complete lack of expression in very sparse GAL4 lines. Second, the particular GAL4 driver line's expression strength plays a crucial role - the authors primarily validated SPARC using high-expression drivers like T4/T5-GAL4 (~6000 cells) and Mi1-GAL4 (~750 cells), whereas our DN driver lines typically show more restricted expression patterns.

4.5.3. Spatial and Temporal Resolution Constraints

The standard tracking system used for these experiments, while allowing for three-dimensional trajectory reconstruction throughout a relatively large behavioral volume, operated at 100 frames per second - significantly lower temporal resolution than specialized high-speed systems used in previous studies (e.g., Muijres et al., 2014, at 7500 frames per second). This temporal undersampling inevitably smoothed rapid maneuvers, particularly during escape responses, effectively underestimating maximum angular velocities and obscuring their fine kinematic details.

Additionally, the spatial resolution limitations when tracking flies throughout a behaviorally relevant volume constrained our ability to detect subtle postural adjustments or wing kinematic changes that might significantly influence flight dynamics. High-speed video recording later revealed that flight movements initially classified as "saccades" based on trajectory data sometimes represented entirely different maneuvers, highlighting how coarse tracking can obscure critical functional distinctions in neural control mechanisms.

4.5.4. Advancing Methodological Approaches

Several methodological refinements could address these limitations in future investigations. First, employing alternative channelrhodopsin variants with faster kinetics, such as ChrimsonR (Kim et al. 2015), would provide more temporally precise control over neural activation. This improved temporal resolution would better approximate the natural activation dynamics of DNs during flight behaviors. However, ChrimsonR presents its own limitations - it is less commonly used in *Drosophila* neuroscience, has lower photocurrents than csChrimson, and lacks compatible stochastic expression tools (Kim et al. 2015).

Second, optimizing stochastic expression protocols represents an important technical advancement, albeit one beyond the immediate scope of this thesis. Potential approaches include refining heat shock parameters for FLP-out systems to achieve more consistent expression levels, developing improved SPARC variants with enhanced efficiency in sparse driver lines, or implementing alternative intersectional strategies that combine multiple genetic constraints. Given the challenges encountered with current methods, significantly improved throughput would be necessary to generate sufficient numbers of flies with the desired unilateral expression patterns.

Third, I have already begun implementing a high-speed, high-resolution camera system that provides substantially improved kinematic data during free flight. While offering lower spatial and temporal resolution than the similar system used previously for the study of flight kinematics (Muijres et al. 2014; Whitehead et al. 2022), this setup provides an acceptable trade-off between tracking flies as three-dimensional points and performing detailed flight kinematic analysis across a more behaviorally relevant arena volume.

Preliminary experiments with this system have demonstrated promising results - using modern computer vision and deep learning tools focused on animal pose estimation (Mathis et al. 2018; Pereira et al. 2022), it became possible to extract information not visible from the original tracking setup, even with minimal training samples. This approach enables reliable extraction of heading direction separate from movement direction - a distinction not possible with simple 3D tracking - along with measures such as the distance between body and head, which can serve as a proxy for pitching movements. Integration of these advanced tracking capabilities with precisely timed optogenetic manipulation would provide unprecedented insight into how specific DNs influence the component elements of complex flight maneuvers.

The technical advances demonstrated in my work, particularly the integration of real-time three-dimensional tracking with closed-loop optogenetic stimulation, provide a foundation for these future investigations. However, resolving the full complexity of descending control will require continued innovation in both behavioral analysis methodology and cell-type specific targeting strategies. These advances should maintain the naturalistic behavior essential for understanding neural function while providing the experimental precision necessary for causal analysis.

4.6. Conservation of Neural Control Principles Across Insect Species

The hybrid architecture combining command-like and population-coded mechanisms evident in my *Drosophila* work appears to be a widespread organizational principle across insect species. Büschges and Ache (2024) note that despite significant differences in body size and ecological niches, most insect species maintain remarkably consistent numbers of DNs. For example, the cockroach and stick insect possess approximately 285 and 205 pairs of DNs with cell bodies in the CRG, respectively. This numerical consistency across species with vastly different CNS sizes - crickets have roughly ten times the number of

neurons as *Drosophila* but similar DN count - suggests that motor commands are channeled into evolutionarily conserved DN populations rather than scaling proportionally with overall neural capacity.

This dual control architecture is evident across diverse insect taxa. In the cricket, the command-like neuron B-DC-3 can initiate, maintain, and terminate stridulation when activated or inhibited (Hedwig 1992) According to Büschges and Ache (2024), cricket walking is controlled by multiple DN types including ipsilateral descending interneurons (IDINs) and contralateral descending interneurons (CDINs) whose firing rates correlate with walking parameters. These neurons, characterized by Böhm and Schildberger (1992), exhibit population-based control of walking rather than command-like properties. The locust DCMD (descending contralateral movement detector) responds to looming stimuli analogously to *Drosophila*'s GF, but despite forming direct excitatory connections with leg motor neurons, its input alone cannot drive complete escape jumps (Burrows and Fraser Rowell 1973) - suggesting that even apparently command-like neurons function within distributed networks.

Perhaps most illuminating are dragonflies, which despite their phylogenetic distance from flies, have evolved specialized target-selective DNs (TSDNs) that code prey direction via precise population vector coding (Gonzalez-Bellido et al. 2013). This population of eight DN pairs provides wing motor centers with accurate directional information, with each neuron responding to targets in a specific region of visual space - a clear example of population coding that parallels the graded control mechanisms observed in DNg02. As Büschges and Ache (2024) conclude, no single neuron entirely controls a behavior; rather, each contributes specific components to a distributed network. My findings with DNa15, DNp03, and DNg02 in *Drosophila* add to this broader understanding: a fundamental organizational principle combining command-like elements for rapid initiation with distributed population coding for flexible, graded control - a framework that has independently evolved across diverse insect lineages to meet similar computational challenges.

4.7. Conclusions and Future Directions

The simultaneous presence of command-like properties in neurons such as DNa15 and DNp03 alongside the population-coded characteristics of DNg02 within the *Drosophila*

flight control system suggests that evolution has favored neural architectures that integrate multiple coding strategies rather than optimizing for a single control principle. This hybrid approach, where different computational mechanisms coexist within the same behavioral control system, likely represents a fundamental organizational feature of motor circuits that may be conserved across phylogenetically diverse species and behavioral contexts.

The research presented in this thesis has several significant achievements: (1) the establishment of a novel free-flight experimental paradigm that integrates real-time three-dimensional tracking with closed-loop optogenetic manipulation; (2) the characterization of DNs that suggest functional distinctions, with evidence pointing toward context-dependent roles that, while compelling, remain part of an emerging understanding of neural control mechanisms; and (3) evidence supporting a hybrid control architecture that integrates command-like and population-based coding strategies.

The recent release of comprehensive connectome data for *Drosophila*, with detailed synaptic-resolution mapping of the brain and ventral nerve cord (Dorkenwald et al. 2024; Schlegel et al. 2024), represents a transformative resource for investigating descending control circuits. This unprecedented wiring diagram enables precise identification of pre- and postsynaptic partners for each DN, allowing researchers to trace the flow of information from sensory inputs to motor outputs with single-cell resolution. By revealing the complete connectivity patterns between DNs and their upstream and downstream partners, the connectome facilitates hypothesis-driven experiments targeting specific circuit nodes, rather than a more exploratory approach. Integrating this structural connectivity data with functional recordings and optogenetic manipulations could significantly accelerate our understanding of how these descending circuits actually influence behavior, and how they themselves are context-modulated.

The technical advances demonstrated in my work provide a foundation for these future investigations. However, resolving the full complexity of descending control will require continued innovation in both behavioral analysis methodology and cell-type specific targeting strategies. These advances should maintain the naturalistic behavior essential for understanding neural function while providing the experimental precision necessary for causal analysis.

By demonstrating how command-like and population-based mechanisms coexist and complement each other within the descending control system, these findings provide a more nuanced framework for investigating neural circuit function across species. They suggest that the apparent dichotomy between discrete commands and distributed population codes may reflect our analytical approaches rather than fundamental organizational principles of nervous systems.

5. Abstract

Understanding how neural circuits generate complex behaviors remains a fundamental challenge in neuroscience. This thesis investigates the neural basis of flight control in *Drosophila melanogaster*, focusing on how descending neurons (DNs) orchestrate the rapid turning maneuvers known as saccades. Through the development of a novel free-flight experimental paradigm integrating real-time three-dimensional tracking with closed-loop optogenetic manipulation, I examined whether individual DNs function as command neurons capable of triggering complete saccades or if coordinated activity across multiple DNs is required.

Quantitative behavioral analysis revealed distinct kinematic signatures between spontaneous saccades and looming-evoked escape saccades, suggesting potentially different neural control mechanisms. Optogenetic activation and genetic silencing of specific DNs demonstrated their differential contributions to flight control. DNa15 activation triggered sharp turning responses, while it's silencing specifically affected spontaneous saccade kinematics. In contrast, DNp03 activation generated strong turning behaviors, and it's silencing selectively impaired looming-evoked escapes without affecting spontaneous turns—revealing a functional double dissociation. Other neurons exhibited distinct behavioral effects: DNa05 produced persistent circling behaviors, DNp06 evoked modest directionally-unbiased turns, and DNg02 generated gradually developing prolonged turning.

These findings support a hybrid neural architecture where context-appropriate DN pathways are differentially recruited based on behavioral demands. Rather than functioning as isolated command neurons, these DNs appear to operate within an interconnected framework incorporating both command-like and population-coded mechanisms. By bridging the gap between anatomical connectivity and functional roles of DNs during naturalistic behavior, this research advances our understanding of how relatively small populations of neurons orchestrate complex behavioral sequences through specialized yet interconnected functional circuits.

6. List of Figures

7. List of Tables

8. References

Ache, Jan M., Shigehiro Namiki, Allen Lee, Kristin Branson, and Gwyneth M. Card. 2019. “State-Dependent Decoupling of Sensory and Motor Circuits Underlies Behavioral Flexibility in Drosophila.” *Nature Neuroscience* 22 (7): 1132–39. https://doi.org/10.1038/s41593-019-0413-4.

Ache, Jan M., Jason Polsky, Shada Alghailani, Ruchi Parekh, Patrick Breads, Martin Y. Peek, Davi D. Bock, Catherine R. Von Reyn, and Gwyneth M. Card. 2019. “Neural Basis for Looming Size and Velocity Encoding in the Drosophila Giant Fiber Escape Pathway.” *Current Biology* 29 (6): 1073-1081.e4. https://doi.org/10.1016/j.cub.2019.01.079.

Anderson, Marti J. 2001. “A New Method for Non-Parametric Multivariate Analysis of Variance.” *Austral Ecology* 26 (1): 32–46. https://doi.org/10.1111/j.1442-9993.2001.01070.pp.x.

Asinof, Samuel K., and Gwyneth M. Card. 2024. “Neural Control of Naturalistic Behavior Choices.” *Annual Review of Neuroscience* 47 (1): 369–88. https://doi.org/10.1146/annurev-neuro-111020-094019.

Azevedo, Anthony, Ellen Lesser, Jasper S. Phelps, Brandon Mark, Leila Elabbady, Sumiya Kuroda, Anne Sustar, et al. 2024. “Connectomic Reconstruction of a Female Drosophila Ventral Nerve Cord.” *Nature* 631 (8020): 360–68. https://doi.org/10.1038/s41586-024-07389-x.

Baines, Richard A., Jay P. Uhler, Annemarie Thompson, Sean T. Sweeney, and Michael Bate. 2001. “Altered Electrical Properties in *Drosophila* Neurons Developing without Synaptic Transmission.” *The Journal of Neuroscience* 21 (5): 1523–31. https://doi.org/10.1523/JNEUROSCI.21-05-01523.2001.

Bar-Shalom, Yaakov, X. Rong Li, and Thiagalingam Kirubarajan. 2004. *Estimation with Applications to Tracking and Navigation: Theory Algorithms and Software*. John Wiley & Sons.

Bellen, Hugo J., Chao Tong, and Hiroshi Tsuda. 2010. “100 Years of Drosophila Research and Its Impact on Vertebrate Neuroscience: A History Lesson for the Future.” *Nature Reviews Neuroscience* 11 (7): 514–22. https://doi.org/10.1038/nrn2839.

Bender, John A., and Michael H. Dickinson. 2006a. “A Comparison of Visual and Haltere-Mediated Feedback in the Control of Body Saccades in *Drosophila Melanogaster*.” *Journal of Experimental Biology* 209 (23): 4597–4606. https://doi.org/10.1242/jeb.02583.

———. 2006b. “Visual Stimulation of Saccades in Magnetically Tethered *Drosophila*.” *Journal of Experimental Biology* 209 (16): 3170–82. https://doi.org/10.1242/jeb.02369.

Bergou, Attila J., Leif Ristroph, John Guckenheimer, Itai Cohen, and Z. Jane Wang. 2010. “Fruit Flies Modulate Passive Wing Pitching to Generate In-Flight Turns.” *Physical Review Letters* 104 (14): 148101. https://doi.org/10.1103/PhysRevLett.104.148101.

Böhm, Hartmut, and Klaus Schildberger. 1992. “Brain Neurones Involved in the Control of Walking in the Cricket Gryllus Bimaculatus.” *Journal of Experimental Biology* 166 (1): 113–30. https://doi.org/10.1242/jeb.166.1.113.

Borst, A, and J Haag. 2002. “Neural Networks in the Cockpit of the Fly.” *Journal of Comparative Physiology A: Sensory, Neural, and Behavioral Physiology* 188 (6): 419–37. https://doi.org/10.1007/s00359-002-0316-8.

Borst, Alexander, Juergen Haag, and Dierk F. Reiff. 2010. “Fly Motion Vision.” *Annual Review of Neuroscience* 33 (1): 49–70. https://doi.org/10.1146/annurev-neuro-060909-153155.

Boyden, Edward S., Feng Zhang, Ernst Bamberg, Georg Nagel, and Karl Deisseroth. 2005. “Millisecond-Timescale, Genetically Targeted Optical Control of Neural Activity.” *Nature Neuroscience* 8 (9): 1263–68. https://doi.org/10.1038/nn1525.

Brand, Andrea H., and Norbert Perrimon. 1993. “Targeted Gene Expression as a Means of Altering Cell Fates and Generating Dominant Phenotypes.” *Development* 118 (2): 401–15. https://doi.org/10.1242/dev.118.2.401.

Braun, Jonas, Femke Hurtak, Sibo Wang-Chen, and Pavan Ramdya. 2024. “Descending Networks Transform Command Signals into Population Motor Control.” *Nature* 630 (8017): 686–94. https://doi.org/10.1038/s41586-024-07523-9.

Breugel, Floris van, J. Nathan Kutz, and Bingni W. Brunton. 2020. “Numerical Differentiation of Noisy Data: A Unifying Multi-Objective Optimization Framework.” *IEEE Access : Practical Innovations, Open Solutions* 8:196865–77. https://doi.org/10.1109/access.2020.3034077.

Buchsbaum, Elhanan, and Bettina Schnell. 2025. “Activity of a Descending Neuron Associated with Visually Elicited Flight Saccades in Drosophila.” *Current Biology* 35 (3): 665-671.e4. https://doi.org/10.1016/j.cub.2024.12.001.

Burrows, M., and C. H. Fraser Rowell. 1973. “Connections between Descending Visual Interneurons and Metathoracic Motoneurons in the Locust.” *Journal of Comparative Physiology* 85 (3): 221–34. https://doi.org/10.1007/BF00694231.

Büschges, Ansgar, and Jan M. Ache. 2024. “Motor Control on the Move - from Insights in Insects to General Mechanisms.” *Physiological Reviews*, December. https://doi.org/10.1152/physrev.00009.2024.

Cande, Jessica, Shigehiro Namiki, Jirui Qiu, Wyatt Korff, Gwyneth M Card, Joshua W Shaevitz, David L Stern, and Gordon J Berman. 2018. “Optogenetic Dissection of Descending Behavioral Control in Drosophila.” *eLife* 7 (June):e34275. https://doi.org/10.7554/eLife.34275.

Card, Gwyneth, and Michael Dickinson. 2008. “Performance Trade-Offs in the Flight Initiation of Drosophila.” *Journal of Experimental Biology* 211 (3): 341–53. https://doi.org/10.1242/jeb.012682.

Cellini, Benjamin, and Jean-Michel Mongeau. 2020a. “Active Vision Shapes and Coordinates Flight Motor Responses in Flies.” *Proceedings of the National Academy of Sciences* 117 (37): 23085–95. https://doi.org/10.1073/pnas.1920846117.

———. 2020b. “Hybrid Visual Control in Fly Flight: Insights into Gaze Shift via Saccades.” *Current Opinion in Insect Science* 42 (December):23–31. https://doi.org/10.1016/j.cois.2020.08.009.

Censi, Andrea, Andrew D. Straw, Rosalyn W. Sayaman, Richard M. Murray, and Michael H. Dickinson. 2013. “Discriminating External and Internal Causes for Heading Changes in Freely Flying Drosophila.” *PLOS Computational Biology* 9 (2): e1002891. https://doi.org/10.1371/journal.pcbi.1002891.

Cheong, Han SJ, Kaitlyn N. Boone, Marryn M. Bennett, Farzaan Salman, Jacob D. Ralston, Kaleb Hatch, Raven F. Allen, et al. 2024. “Organization of an Ascending Circuit That Conveys Flight Motor State in Drosophila.” *Current Biology* 34 (5): 1059-1075.e5. https://doi.org/10.1016/j.cub.2024.01.071.

Cheong, Han SJ, Katharina Eichler, Tomke Stürner, Samuel K. Asinof, Andrew S. Champion, Elizabeth C. Marin, Tess B. Oram, et al. 2024. “Transforming Descending Input into Behavior: The Organization of Premotor Circuits in the Drosophila Male Adult Nerve Cord Connectome.” *eLife* 13 (March). https://doi.org/10.7554/eLife.96084.1.

Court, Robert, Shigehiro Namiki, J. Douglas Armstrong, Jana Börner, Gwyneth Card, Marta Costa, Michael Dickinson, et al. 2020. “A Systematic Nomenclature for the Drosophila Ventral Nerve Cord.” *Neuron* 107 (6): 1071-1079.e2. https://doi.org/10.1016/j.neuron.2020.08.005.

Currier, Timothy A., and Katherine I. Nagel. 2020. “Multisensory Control of Navigation in the Fruit Fly.” *Current Opinion in Neurobiology*, Systems Neuroscience, 64 (October):10–16. https://doi.org/10.1016/j.conb.2019.11.017.

David, C. T. 1978. “The Relationship between Body Angle and Flight Speed in Free-Flying Drosophila.” *Physiological Entomology* 3 (3): 191–95. https://doi.org/10.1111/j.1365-3032.1978.tb00148.x.

Deora, Tanvi, Namrata Gundiah, and Sanjay P. Sane. 2017. “Mechanics of the Thorax in Flies.” *Journal of Experimental Biology* 220 (8): 1382–95. https://doi.org/10.1242/jeb.128363.

Dickinson, Michael H. 1999. “Haltere–Mediated Equilibrium Reflexes of the Fruit Fly, Drosophila Melanogaster.” Edited by J. L. Van Leeuwen. *Philosophical Transactions of the Royal Society of London. Series B: Biological Sciences* 354 (1385): 903–16. https://doi.org/10.1098/rstb.1999.0442.

Dickinson, Michael H., and Florian T. Muijres. 2016. “The Aerodynamics and Control of Free Flight Manoeuvres in *Drosophila*.” *Philosophical Transactions of the Royal Society B: Biological Sciences* 371 (1704): 20150388. https://doi.org/10.1098/rstb.2015.0388.

Dickinson, Michael H, and Michael S Tu. 1997. “The Function of Dipteran Flight Muscle.” *Comparative Biochemistry and Physiology Part A: Physiology* 116 (3): 223–38. https://doi.org/10.1016/S0300-9629(96)00162-4.

Dickson, William B., Andrew D. Straw, and Michael H. Dickinson. 2008. “Integrative Model of Drosophila Flight.” *AIAA Journal* 46 (9): 2150–64. https://doi.org/10.2514/1.29862.

Dionne, Heather, Karen L Hibbard, Amanda Cavallaro, Jui-Chun Kao, and Gerald M Rubin. 2018. “Genetic Reagents for Making Split-GAL4 Lines in *Drosophila*.” *Genetics* 209 (1): 31–35. https://doi.org/10.1534/genetics.118.300682.

Dombrovski, Mark, Martin Y. Peek, Jin-Yong Park, Andrea Vaccari, Marissa Sumathipala, Carmen Morrow, Patrick Breads, et al. 2023. “Synaptic Gradients Transform Object Location to Action.” *Nature* 613 (7944): 534–42. https://doi.org/10.1038/s41586-022-05562-8.

Dorkenwald, Sven, Arie Matsliah, Amy R. Sterling, Philipp Schlegel, Szi-chieh Yu, Claire E. McKellar, Albert Lin, et al. 2024. “Neuronal Wiring Diagram of an Adult Brain.” *Nature* 634 (8032): 124–38. https://doi.org/10.1038/s41586-024-07558-y.

Feng, Kai, Mariam Khan, Ryo Minegishi, Annika Müller, Matthew N. Van De Poll, Bruno Van Swinderen, and Barry J. Dickson. 2024. “A Central Steering Circuit in *Drosophila*.” Neuroscience. https://doi.org/10.1101/2024.06.27.601106.

Feng, Kai, Rajyashree Sen, Ryo Minegishi, Michael Dübbert, Till Bockemühl, Ansgar Büschges, and Barry J. Dickson. 2020. “Distributed Control of Motor Circuits for

Backward Walking in Drosophila." *Nature Communications* 11 (1): 6166. https://doi.org/10.1038/s41467-020-19936-x.

Fischbach, K. -F., and A. P. M. Dittrich. 1989. "The Optic Lobe of Drosophila Melanogaster. I. A Golgi Analysis of Wild-Type Structure." *Cell and Tissue Research* 258 (3): 441–75. https://doi.org/10.1007/BF00218858.

Fisher, Yvette E, Helen H Yang, Jesse Isaacman-Beck, Marjorie Xie, Daryl M Gohl, and Thomas R Clandinin. 2017. "FlpStop, a Tool for Conditional Gene Control in Drosophila." *eLife* 6 (February):e22279. https://doi.org/10.7554/eLife.22279.

Fry, Steven N., Nicola Rohrseitz, Andrew D. Straw, and Michael H. Dickinson. 2008. "TrackFly: Virtual Reality for a Behavioral System Analysis in Free-Flying Fruit Flies." *Journal of Neuroscience Methods* 171 (1): 110–17. https://doi.org/10.1016/j.jneumeth.2008.02.016.

Fry, Steven N., Rosalyn Sayaman, and Michael H. Dickinson. 2005. "The Aerodynamics of Hovering Flight in *Drosophila*." *Journal of Experimental Biology* 208 (12): 2303–18. https://doi.org/10.1242/jeb.01612.

Frye, Mark A, and Michael H Dickinson. 2004. "Closing the Loop between Neurobiology and Flight Behavior in Drosophila." *Current Opinion in Neurobiology* 14 (6): 729–36. https://doi.org/10.1016/j.conb.2004.10.004.

Gabbiani, Fabrizio, Holger G. Krapp, and Gilles Laurent. 1999. "Computation of Object Approach by a Wide-Field, Motion-Sensitive Neuron." *Journal of Neuroscience* 19 (3): 1122–41. https://doi.org/10.1523/JNEUROSCI.19-03-01122.1999.

Golic, K. G., and S. Lindquist. 1989. "The FLP Recombinase of Yeast Catalyzes Site-Specific Recombination in the Drosophila Genome." *Cell* 59 (3): 499–509. https://doi.org/10.1016/0092-8674(89)90033-0.

Gonzalez-Bellido, Paloma T., Hanchuan Peng, Jinzhu Yang, Apostolos P. Georgopoulos, and Robert M. Olberg. 2013. "Eight Pairs of Descending Visual Neurons in the Dragonfly Give Wing Motor Centers Accurate Population Vector of Prey Direction." *Proceedings of the National Academy of Sciences* 110 (2): 696–701. https://doi.org/10.1073/pnas.1210489109.

Götz, Karl Geokg. 1964. "Optomotorische Untersuchung des visuellen systems einiger Augenmutanten der Fruchtfliege Drosophila." *Kybernetik* 2 (2): 77–92. https://doi.org/10.1007/BF00288561.

Götz, Karl Georg. 1968. "Flight Control in Drosophila by Visual Perception of Motion." *Kybernetik* 4 (6): 199–208. https://doi.org/10.1007/BF00272517.

Haag, J., W. Denk, and A. Borst. 2004. "Fly Motion Vision Is Based on Reichardt Detectors Regardless of the Signal-to-Noise Ratio." *Proceedings of the National Academy of Sciences* 101 (46): 16333–38. https://doi.org/10.1073/pnas.0407368101.

Hales, Karen G, Christopher A Korey, Amanda M Larracuente, and David M Roberts. 2015. "Genetics on the Fly: A Primer on the *Drosophila* Model System." *Genetics* 201 (3): 815–42. https://doi.org/10.1534/genetics.115.183392.

Harris, Charles R., K. Jarrod Millman, Stéfan J. van der Walt, Ralf Gommers, Pauli Virtanen, David Cournapeau, Eric Wieser, et al. 2020. "Array Programming with NumPy." *Nature* 585 (7825): 357–62. https://doi.org/10.1038/s41586-020-2649-2.

Hartley, Richard, and Andrew Zisserman. 2018. *Multiple View Geometry in Computer Vision*. 2. edition, 17.printing. Cambridge: Cambridge Univ. Press.

Hedrick, Tyson L., Bo Cheng, and Xinyan Deng. 2009. "Wingbeat Time and the Scaling of Passive Rotational Damping in Flapping Flight." *Science* 324 (5924): 252–55. https://doi.org/10.1126/science.1168431.

Hedwig, Berthold. 1992. “On the Control of Stridulation in the Acridid Grasshopper Omocestus Viridulus L.” *Journal of Comparative Physiology A* 171 (1): 117–28. https://doi.org/10.1007/BF00195967.

Heisenberg, M, and R Wolf. 1979. “On the Fine Structure of Yaw Torque in Visual Flight Orientation of Drosophilamelanogaster.”

Hodge, James J. L. 2009. “Ion Channels to Inactivate Neurons in Drosophila.” *Frontiers in Molecular Neuroscience* 2. https://doi.org/10.3389/neuro.02.013.2009.

Howard, Clare E., Chin-Lin Chen, Tanya Tabachnik, Rick Hormigo, Pavan Ramdya, and Richard S. Mann. 2019. “Serotonergic Modulation of Walking in Drosophila.” *Current Biology* 29 (24): 4218-4230.e8. https://doi.org/10.1016/j.cub.2019.10.042.

Hsu, Cynthia T., and Vikas Bhandawat. 2016. “Organization of Descending Neurons in Drosophila Melanogaster.” *Scientific Reports* 6 (1): 20259. https://doi.org/10.1038/srep20259.

Hulse, Brad K, Hannah Haberkern, Romain Franconville, Daniel Turner-Evans, Shin-ya Takemura, Tanya Wolff, Marcella Noorman, et al. 2021. “A Connectome of the Drosophila Central Complex Reveals Network Motifs Suitable for Flexible Navigation and Context-Dependent Action Selection.” Edited by Ronald L Calabrese, Stanley Heinze, and Jason Pipkin. *eLife* 10 (October):e66039. https://doi.org/10.7554/eLife.66039.

Inagaki, Hidehiko K., Yonil Jung, Eric D. Hoopfer, Allan M. Wong, Neeli Mishra, John Y. Lin, Roger Y. Tsien, and David J. Anderson. 2014. “Optogenetic Control of Drosophila Using a Red-Shifted Channelrhodopsin Reveals Experience-Dependent Influences on Courtship.” *Nature Methods* 11 (3): 325–32. https://doi.org/10.1038/nmeth.2765.

Isaacman-Beck, Jesse, Kristine C. Paik, Carl F. R. Wienecke, Helen H. Yang, Yvette E. Fisher, Irving E. Wang, Itzel G. Ishida, Gaby Maimon, Rachel I. Wilson, and Thomas R. Clandinin. 2020. “SPARC Enables Genetic Manipulation of Precise Proportions of Cells.” *Nature Neuroscience* 23 (9): 1168–75. https://doi.org/10.1038/s41593-020-0668-9.

Joesch, Maximilian, Bettina Schnell, Shamprasad Varija Raghu, Dierk F. Reiff, and Alexander Borst. 2010. “ON and OFF Pathways in Drosophila Motion Vision.” *Nature* 468 (7321): 300–304. https://doi.org/10.1038/nature09545.

Johns, David C., Ruth Marx, Richard E. Mains, Brian O’Rourke, and Eduardo Marbán. 1999. “Inducible Genetic Suppression of Neuronal Excitability.” *The Journal of Neuroscience* 19 (5): 1691–97. https://doi.org/10.1523/JNEUROSCI.19-05-01691.1999.

Kendroud, Sarah, Ali Asgar Bohra, Philipp A. Kuert, Bao Nguyen, Oriane Guillermin, Simon G. Sprecher, Heinrich Reichert, Krishnaswamy VijayRaghavan, and Volker Hartenstein. 2018. “Structure and Development of the Subesophageal Zone of the Drosophila Brain. II. Sensory Compartments.” *The Journal of Comparative Neurology* 526 (1): 33–58. https://doi.org/10.1002/cne.24316.

Kim, Hyosun, Hayun Park, Joowon Lee, and Anmo J. Kim. 2023. “A Visuomotor Circuit for Evasive Flight Turns in Drosophila.” *Current Biology* 33 (2): 321-335.e6. https://doi.org/10.1016/j.cub.2022.12.014.

Kim, Sung Soo, Romain Franconville, Dan Turner-Evans, and Vivek Jayaraman. 2015. “Optogenetics in Drosophila Melanogaster.” In *New Techniques in Systems Neuroscience*, edited by Adam D. Douglass, 147–76. Cham: Springer International Publishing. https://doi.org/10.1007/978-3-319-12913-6_6.

Klapoetke, Nathan C, Yasunobu Murata, Sung Soo Kim, Stefan R Pulver, Amanda Birdsey-Benson, Yong Ku Cho, Tania K Morimoto, et al. 2014. “Independent Optical Excitation of Distinct Neural Populations.” *Nature Methods* 11 (3): 338–46. https://doi.org/10.1038/nmeth.2836.

Klapoetke, Nathan C., Aljoscha Nern, Martin Y. Peek, Edward M. Rogers, Patrick Breads, Gerald M. Rubin, Michael B. Reiser, and Gwyneth M. Card. 2017. “Ultra-Selective Looming Detection from Radial Motion Opponency.” *Nature* 551 (7679): 237–41. https://doi.org/10.1038/nature24626.

Lehmann, Fritz-Olaf, and Jan Bartussek. 2017. “Neural Control and Precision of Flight Muscle Activation in Drosophila.” *Journal of Comparative Physiology A* 203 (1): 1–14. https://doi.org/10.1007/s00359-016-1133-9.

Li, Feng, Jack W Lindsey, Elizabeth C Marin, Nils Otto, Marisa Dreher, Georgia Dempsey, Ildiko Stark, et al. 2020. “The Connectome of the Adult Drosophila Mushroom Body Provides Insights into Function.” Edited by Leslie C Griffith, Eve Marder, Leslie C Griffith, Jason Pipkin, and Chris Q Doe. *eLife* 9 (December):e62576. https://doi.org/10.7554/eLife.62576.

Lindsay, Theodore, Anne Sustar, and Michael Dickinson. 2017. “The Function and Organization of the Motor System Controlling Flight Maneuvers in Flies.” *Current Biology* 27 (3): 345–58. https://doi.org/10.1016/j.cub.2016.12.018.

Luan, Haojiang, Nathan C. Peabody, Charles R. Vinson, and Benjamin H. White. 2006. “Refined Spatial Manipulation of Neuronal Function by Combinatorial Restriction of Transgene Expression.” *Neuron* 52 (3): 425–36. https://doi.org/10.1016/j.neuron.2006.08.028.

Maisak, Matthew S., Juergen Haag, Georg Ammer, Etienne Serbe, Matthias Meier, Aljoscha Leonhardt, Tabea Schilling, et al. 2013. “A Directional Tuning Map of Drosophila Elementary Motion Detectors.” *Nature* 500 (7461): 212–16. https://doi.org/10.1038/nature12320.

Mamiya, Akira, Pralaksha Gurung, and John C. Tuthill. 2018. “Neural Coding of Leg Proprioception in Drosophila.” *Neuron* 100 (3): 636-650.e6. https://doi.org/10.1016/j.neuron.2018.09.009.

Marshall, Zarion D., Chris C. Wreden, and Ellie S. Heckscher. 2024. “Single-Neuron Labeling in Drosophila Using Multicolor FLP-Out.” *Cold Spring Harbor Protocols*, September. https://doi.org/10.1101/pdb.prot108422.

Martin, Jean-René, Andreas Keller, and Sean T. Sweeney. 2002. “Targeted Expression of Tetanus Toxin: A New Tool to Study the Neurobiology of Behavior*.” In *Advances in Genetics*, edited by Jeffrey C. Hall, Theodore Friedmann, Jay C. Dunlap, and Francesco Giannelli, 47:1–48e. Academic Press. https://doi.org/10.1016/S0065-2660(02)47001-0.

Mathis, Alexander, Pranav Mamidanna, Kevin M. Cury, Taiga Abe, Venkatesh N. Murthy, Mackenzie Weygandt Mathis, and Matthias Bethge. 2018. “DeepLabCut: Markerless Pose Estimation of User-Defined Body Parts with Deep Learning.” *Nature Neuroscience* 21 (9): 1281–89. https://doi.org/10.1038/s41593-018-0209-y.

Matsakis, Nicholas D, and Felix S Klock II. 2014. “The Rust Language.” In *ACM SIGAda Ada Letters*, 34:103–4. ACM.

Maye, Alexander, Chih-hao Hsieh, George Sugihara, and Björn Brembs. 2007. “Order in Spontaneous Behavior.” *PLOS ONE* 2 (5): e443. https://doi.org/10.1371/journal.pone.0000443.

McGugan, Will, ed. 2007. “Introducing Pygame.” In *Beginning Game Development with Python and Pygame: From Novice to Professional*, 41–66. Berkeley, CA: Apress. https://doi.org/10.1007/978-1-4302-0325-4_3.

Meissel, Kane, and Esther S. Yao. 2024. “Using Cliff’s Delta as a Non-Parametric Effect Size Measure: An Accessible Web App and R Tutorial.” *Practical Assessment, Research, and Evaluation* 29 (1). https://doi.org/10.7275/pare.1977.

Mongeau, Jean-Michel, and Mark A. Frye. 2017. “Drosophila Spatiotemporally Integrates Visual Signals to Control Saccades.” *Current Biology* 27 (19): 2901-2914.e2. https://doi.org/10.1016/j.cub.2017.08.035.

Moreno-Sanchez, Anthony, Alexander N Vasserman, HyoJong Jang, Bryce W Hina, Catherine R Von Reyn, and Jessica Ausborn. 2024. “Morphology and Synapse Topography Optimize Linear Encoding of Synapse Numbers in Drosophila Looming Responsive Descending Neurons.” https://doi.org/10.7554/eLife.99277.1.

Mronz, Markus, and Fritz-Olaf Lehmann. 2008. “The Free-Flight Response of *Drosophila* to Motion of the Visual Environment.” *Journal of Experimental Biology* 211 (13): 2026–45. https://doi.org/10.1242/jeb.008268.

Muijres, Florian T., Michael J. Elzinga, Nicole A. Iwasaki, and Michael H. Dickinson. 2015. “Body Saccades of *Drosophila* Consist of Stereotyped Banked Turns.” *Journal of Experimental Biology* 218 (6): 864–75. https://doi.org/10.1242/jeb.114280.

Muijres, Florian T., Michael J. Elzinga, Johan M. Melis, and Michael H. Dickinson. 2014. “Flies Evade Looming Targets by Executing Rapid Visually Directed Banked Turns.” *Science* 344 (6180): 172–77. https://doi.org/10.1126/science.1248955.

Nagel, Georg, Tanjef Szellas, Wolfram Huhn, Suneel Kateriya, Nona Adeishvili, Peter Berthold, Doris Ollig, Peter Hegemann, and Ernst Bamberg. 2003. “Channelrhodopsin-2, a Directly Light-Gated Cation-Selective Membrane Channel.” *Proceedings of the National Academy of Sciences* 100 (24): 13940–45. https://doi.org/10.1073/pnas.1936192100.

Namiki, Shigehiro, Michael H Dickinson, Allan M Wong, Wyatt Korff, and Gwyneth M Card. 2018. “The Functional Organization of Descending Sensory-Motor Pathways in Drosophila.” *eLife* 7 (June):e34272. https://doi.org/10.7554/eLife.34272.

Namiki, Shigehiro, and Ryohei Kanzaki. 2016. “Comparative Neuroanatomy of the Lateral Accessory Lobe in the Insect Brain.” *Frontiers in Physiology* 7 (June). https://doi.org/10.3389/fphys.2016.00244.

Namiki, Shigehiro, Ivo G. Ros, Carmen Morrow, William J. Rowell, Gwyneth M. Card, Wyatt Korff, and Michael H. Dickinson. 2022. “A Population of Descending Neurons That Regulates the Flight Motor of Drosophila.” *Current Biology* 32 (5): 1189-1196.e6. https://doi.org/10.1016/j.cub.2022.01.008.

Nern, Aljoscha, Barret D. Pfeiffer, and Gerald M. Rubin. 2015. “Optimized Tools for Multicolor Stochastic Labeling Reveal Diverse Stereotyped Cell Arrangements in the Fly Visual System.” *Proceedings of the National Academy of Sciences* 112 (22). https://doi.org/10.1073/pnas.1506763112.

Palmer, Emily H., Jaison J. Omoto, and Michael H. Dickinson. 2022. “The Role of a Population of Descending Neurons in the Optomotor Response in Flying Drosophila.” bioRxiv. https://doi.org/10.1101/2022.12.05.519224.

Pereira, Talmo D., Nathaniel Tabris, Arie Matsliah, David M. Turner, Junyu Li, Shruthi Ravindranath, Eleni S. Papadoyannis, et al. 2022. “SLEAP: A Deep Learning System for Multi-Animal Pose Tracking.” *Nature Methods* 19 (4): 486–95. https://doi.org/10.1038/s41592-022-01426-1.

Pfeiffer, Barret D., Teri-T B. Ngo, Karen L. Hibbard, Christine Murphy, Arnim Jenett, James W. Truman, and Gerald M. Rubin. 2010. “Refinement of Tools for Targeted Gene Expression in Drosophila.” *Genetics* 186 (2): 735–55. https://doi.org/10.1534/genetics.110.119917.

Reynolds, Andy M., and Mark A. Frye. 2007. “Free-Flight Odor Tracking in Drosophila Is Consistent with an Optimal Intermittent Scale-Free Search.” *PLOS ONE* 2 (4): e354. https://doi.org/10.1371/journal.pone.0000354.

Ros, Ivo G., Jaison J. Omoto, and Michael H. Dickinson. 2024. “Descending Control and Regulation of Spontaneous Flight Turns in Drosophila.” *Current Biology* 34 (3): 531-540.e5. https://doi.org/10.1016/j.cub.2023.12.047.

Ross, Andrew. 2017. “Insect Evolution: The Origin of Wings.” *Current Biology* 27 (3): R113–15. https://doi.org/10.1016/j.cub.2016.12.014.

Schindelin, Johannes, Ignacio Arganda-Carreras, Erwin Frise, Verena Kaynig, Mark Longair, Tobias Pietzsch, Stephan Preibisch, et al. 2012. “Fiji: An Open-Source Platform for Biological-Image Analysis.” *Nature Methods* 9 (7): 676–82. https://doi.org/10.1038/nmeth.2019.

Schlegel, Philipp, Yijie Yin, Alexander S. Bates, Sven Dorkenwald, Katharina Eichler, Paul Brooks, Daniel S. Han, et al. 2024. “Whole-Brain Annotation and Multi-Connectome Cell Typing of Drosophila.” *Nature* 634 (8032): 139–52. https://doi.org/10.1038/s41586-024-07686-5.

Schnell, B., M. Joesch, F. Forstner, S. V. Raghu, H. Otsuna, K. Ito, A. Borst, and D. F. Reiff. 2010. “Processing of Horizontal Optic Flow in Three Visual Interneurons of the *Drosophila* Brain.” *Journal of Neurophysiology* 103 (3): 1646–57. https://doi.org/10.1152/jn.00950.2009.

Schnell, Bettina, Shamprasad Varija Raghu, Aljoscha Nern, and Alexander Borst. 2012. “Columnar Cells Necessary for Motion Responses of Wide-Field Visual Interneurons in Drosophila.” *Journal of Comparative Physiology A* 198 (5): 389–95. https://doi.org/10.1007/s00359-012-0716-3.

Schnell, Bettina, Ivo G. Ros, and Michael H. Dickinson. 2017. “A Descending Neuron Correlated with the Rapid Steering Maneuvers of Flying Drosophila.” *Current Biology* 27 (8): 1200–1205. https://doi.org/10.1016/j.cub.2017.03.004.

Simpson, Julie H. 2024. “Descending Control of Motor Sequences In.” *Current Opinion in Neurobiology* 84 (February):102822. https://doi.org/10.1016/j.conb.2023.102822.

Stanford Artificial Intelligence Laboratory et al. 2018. “Robotic Operating System.” https://www.ros.org.

Steinbeck, Fabian, Andrea Adden, and Paul Graham. 2020. “Connecting Brain to Behaviour: A Role for General Purpose Steering Circuits in Insect Orientation?” *Journal of Experimental Biology* 223 (5): jeb212332. https://doi.org/10.1242/jeb.212332.

Straw, Andrew D., Kristin Branson, Titus R. Neumann, and Michael H. Dickinson. 2010. “Multi-Camera Real-Time Three-Dimensional Tracking of Multiple Flying Animals.” *Journal of The Royal Society Interface* 8 (56): 395–409. https://doi.org/10.1098/rsif.2010.0230.

Struhl, Gary, and Konrad Basler. 1993. “Organizing Activity of Wingless Protein in Drosophila.” *Cell* 72 (4): 527–40. https://doi.org/10.1016/0092-8674(93)90072-X.

Stürner, Tomke, Paul Brooks, Laia Serratosa Capdevila, Billy J. Morris, Alexandre Javier, Siqi Fang, Marina Gkantia, et al. 2024. “Comparative Connectomics of the Descending and Ascending Neurons of the *Drosophila* Nervous System:

Stereotypy and Sexual Dimorphism." Neuroscience. https://doi.org/10.1101/2024.06.04.596633.

Suver, Marie P., Ainul Huda, Nicole Iwasaki, Steve Safarik, and Michael H. Dickinson. 2016. "An Array of Descending Visual Interneurons Encoding Self-Motion in Drosophila." *Journal of Neuroscience* 36 (46): 11768–80. https://doi.org/10.1523/JNEUROSCI.2277-16.2016.

Sweeney, S. T., K. Broadie, J. Keane, H. Niemann, and C. J. O'Kane. 1995. "Targeted Expression of Tetanus Toxin Light Chain in Drosophila Specifically Eliminates Synaptic Transmission and Causes Behavioral Defects." *Neuron* 14 (2): 341–51. https://doi.org/10.1016/0896-6273(95)90290-2.

Tammero, Lance F., and Michael H. Dickinson. 2002a. "Collision-Avoidance and Landing Responses Are Mediated by Separate Pathways in the Fruit Fly, *Drosophila Melanogaster*." *Journal of Experimental Biology* 205 (18): 2785–98. https://doi.org/10.1242/jeb.205.18.2785.

———. 2002b. "The Influence of Visual Landscape on the Free Flight Behavior of the Fruit Fly *Drosophila Melanogaster*." *Journal of Experimental Biology* 205 (3): 327–43. https://doi.org/10.1242/jeb.205.3.327.

Tuthill, John C., Aljoscha Nern, Stephen L. Holtz, Gerald M. Rubin, and Michael B. Reiser. 2013. "Contributions of the 12 Neuron Classes in the Fly Lamina to Motion Vision." *Neuron* 79 (1): 128–40. https://doi.org/10.1016/j.neuron.2013.05.024.

Tuthill, John C., and Rachel I. Wilson. 2016. "Mechanosensation and Adaptive Motor Control in Insects." *Current Biology* 26 (20): R1022–38. https://doi.org/10.1016/j.cub.2016.06.070.

Virtanen, Pauli, Ralf Gommers, Travis E. Oliphant, Matt Haberland, Tyler Reddy, David Cournapeau, Evgeni Burovski, et al. 2020. "SciPy 1.0: Fundamental Algorithms for Scientific Computing in Python." *Nature Methods* 17 (3): 261–72. https://doi.org/10.1038/s41592-019-0686-2.

Vogel, Steven. 1966. "I. FLIGHT PERFORMANCE OF TETHERED FLIES." *Journal of Experimental Biology*.

Von Reyn, Catherine R, Patrick Breads, Martin Y Peek, Grace Zhiyu Zheng, W Ryan Williamson, Alyson L Yee, Anthony Leonardo, and Gwyneth M Card. 2014. "A Spike-Timing Mechanism for Action Selection." *Nature Neuroscience* 17 (7): 962–70. https://doi.org/10.1038/nn.3741.

Von Reyn, Catherine R., Aljoscha Nern, W. Ryan Williamson, Patrick Breads, Ming Wu, Shigehiro Namiki, and Gwyneth M. Card. 2017. "Feature Integration Drives Probabilistic Behavior in the Drosophila Escape Response." *Neuron* 94 (6): 1190-1204.e6. https://doi.org/10.1016/j.neuron.2017.05.036.

Westeinde, Elena A., Emily Kellogg, Paul M. Dawson, Jenny Lu, Lydia Hamburg, Benjamin Midler, Shaul Druckmann, and Rachel I. Wilson. 2024. "Transforming a Head Direction Signal into a Goal-Oriented Steering Command." *Nature* 626 (8000): 819–26. https://doi.org/10.1038/s41586-024-07039-2.

Whitehead, Samuel C., Sofia Leone, Theodore Lindsay, Matthew R. Meiselman, Noah J. Cowan, Michael H. Dickinson, Nilay Yapici, David L. Stern, Troy Shirangi, and Itai Cohen. 2022. "Neuromuscular Embodiment of Feedback Control Elements in Drosophila Flight." *Science Advances* 8 (50): eabo7461. https://doi.org/10.1126/sciadv.abo7461.

Wu, Ming, Aljoscha Nern, W Ryan Williamson, Mai M Morimoto, Michael B Reiser, Gwyneth M Card, and Gerald M Rubin. 2016. "Visual Projection Neurons in the

Drosophila Lobula Link Feature Detection to Distinct Behavioral Programs." *eLife* 5 (December):e21022. https://doi.org/10.7554/eLife.21022.

Yang, Helen H., Bella E. Brezovec, Laia Serratosa Capdevila, Quinn X. Vanderbeck, Atsuko Adachi, Richard S. Mann, and Rachel I. Wilson. 2024. "Fine-Grained Descending Control of Steering in Walking Drosophila." *Cell* 187 (22): 6290-6308.e27. https://doi.org/10.1016/j.cell.2024.08.033.

Zacarias, Ricardo, Shigehiro Namiki, Gwyneth M. Card, Maria Luisa Vasconcelos, and Marta A. Moita. 2018. "Speed Dependent Descending Control of Freezing Behavior in Drosophila Melanogaster." *Nature Communications* 9 (1): 3697. https://doi.org/10.1038/s41467-018-05875-1.

Zhang, Feng, Li-Ping Wang, Martin Brauner, Jana F. Liewald, Kenneth Kay, Natalie Watzke, Phillip G. Wood, et al. 2007. "Multimodal Fast Optical Interrogation of Neural Circuitry." *Nature* 446 (7136): 633–39. https://doi.org/10.1038/nature05744.

9. Acknowledgements

First and foremost, I extend my sincere gratitude to my supervisor, Dr. Bettina Schnell, for her exceptional guidance, unwavering support, and insightful feedback. Her willingness to embrace my ideas and the freedom she gave me to explore my own research paths have been truly invaluable. Her mentorship has been instrumental in shaping both this research and my development as a scientist.

I am equally thankful to my thesis advisory committee members, Prof. Dr. Heinz Beck, Prof. Dr. Dagmar Wachten, and Prof. Dr. Gaia Tavosanis, whose constructive criticism, diverse perspectives, and thoughtful suggestions have significantly enhanced the quality and scope of this work.

I would like to acknowledge my lab colleagues Yazid Rachad, Chitvan Chandolia and Philippe Fischer, as well as Andres Flores-Valle and Ivan Vishniakou from the Seelig lab for the countless (and probably too long) coffee breaks and mutual support that made even the most challenging days of this journey worthwhile. Their friendship and collaboration have been highlights of my PhD experience.

I would like to thank James Lightfoot for taking the time to review my thesis and providing helpful proofreading and formatting suggestions that improved the final presentation of this work.

Finally, I would like to express my gratitude to my family – my wife Nurit, and my dog Oscar. They have patiently endured my stress (and other nonsense) with unwavering love and support, and their presence has been my anchor throughout this journey.

This research would not have been possible without the generous financial and institutional support from the Max Planck Institute for Neurobiology of Behavior - caesar and the International Max Planck Research School for Brain & Behavior.